

# Lipid Nanoparticle Technologies for Nucleic Acid Delivery: A Nanoarchitectonics Perspective

Abdul Rahim Ferhan, Soohyun Park, Hyeonjin Park, Hyunhyuk Tae, Joshua A. Jackman,\* and Nam-Joon Cho\*

Lipid-based nanoparticles have emerged as a clinically viable platform technology to deliver nucleic acids for a wide range of healthcare applications. Within this scope, one of the most exciting areas of recent progress and future innovation potential lies in the material science of lipid-based nanoparticles, both to refine existing nanoparticle strategies and to develop new ones. Herein, the latest efforts to develop next-generation lipid-based nanoparticles are covered by taking a nanoarchitectonics perspective and the design, nucleic acid encapsulation methods, scalable production, and application prospects are critically analyzed for three classes of lipid-based nanoparticles: 1) traditional lipid nanoparticles (LNPs); 2) lipoplexes; and 3) bicelles. Particular focus is placed on rationalizing how molecular self-assembly principles enable advanced functionalities along with comparing and contrasting the different nanoarchitectures. The current development status of each class of lipid-based nanoparticle is also evaluated and possible future directions in terms of overcoming clinical translation challenges and realizing new application opportunities are suggested.

possibilities have enabled rapid development and deployment of mRNA vaccines for coronavirus disease-2019 (COVID-19) prevention, for example.<sup>[9]</sup> Ongoing advances in the field related to issues like nucleic acid engineering, nanoparticle stability improvement, and immune safety considerations along with application trends have been extensively covered in the past two years.<sup>[10]</sup> However, the architectural design principles of lipid-based nanoparticles have been relatively less covered, especially from a material science perspective that takes into account the latest concepts and trends.

One emerging concept to rationally control the structure and function of nanoscale objects is called nanoarchitectonics and has been used to design advanced nanomaterials for biomedical, energy, and environmental applications.<sup>[11]</sup> Nanoarchitectonics

## 1. Introduction


Lipid-based nanoparticles are enabling new possibilities for nucleic acid medicine across various dimensions such as infectious disease vaccines and gene editing.<sup>[1]</sup> These capabilities are broadly applicable to various types of nucleic acids, including deoxyribonucleic acid (DNA)<sup>[2]</sup> and ribonucleic acid (RNA),<sup>[3]</sup> and some of the most promising types are messenger RNA (mRNA),<sup>[4]</sup> small interfering RNA (siRNA),<sup>[5]</sup> transfer RNA (tRNA),<sup>[6]</sup> and self-amplifying RNA (saRNA).<sup>[7]</sup> One of the greatest benefits of lipid-based nanoparticle technology is the platform aspect whereby one nucleic acid molecule can be swapped out with another one, while utilizing the same nanoparticle design principles and manufacturing route.<sup>[8]</sup> Such

refers to the fusion of nanotechnology with organic chemistry, supramolecular chemistry, and biology and involves combining molecular-level manipulation with self-assembly and nanofabrication.<sup>[12]</sup> It is thus ideally suited to serve as a conceptual framework to evaluate design trends and to suggest future directions for the development of lipid-based nanoparticles for nucleic acid delivery applications, especially as the field grows to include not only traditional lipid nanoparticles (LNPs) but also lipoplexes and bicelles among various possibilities (Scheme 1). The molecular design and self-assembly properties of natural and synthetic lipids underlies the core nanoparticle technology and understanding how to modulate the coassembly of lipids by themselves and in combination with nucleic acids can lead to new types of lipid nanoarchitectures and support future innovation.

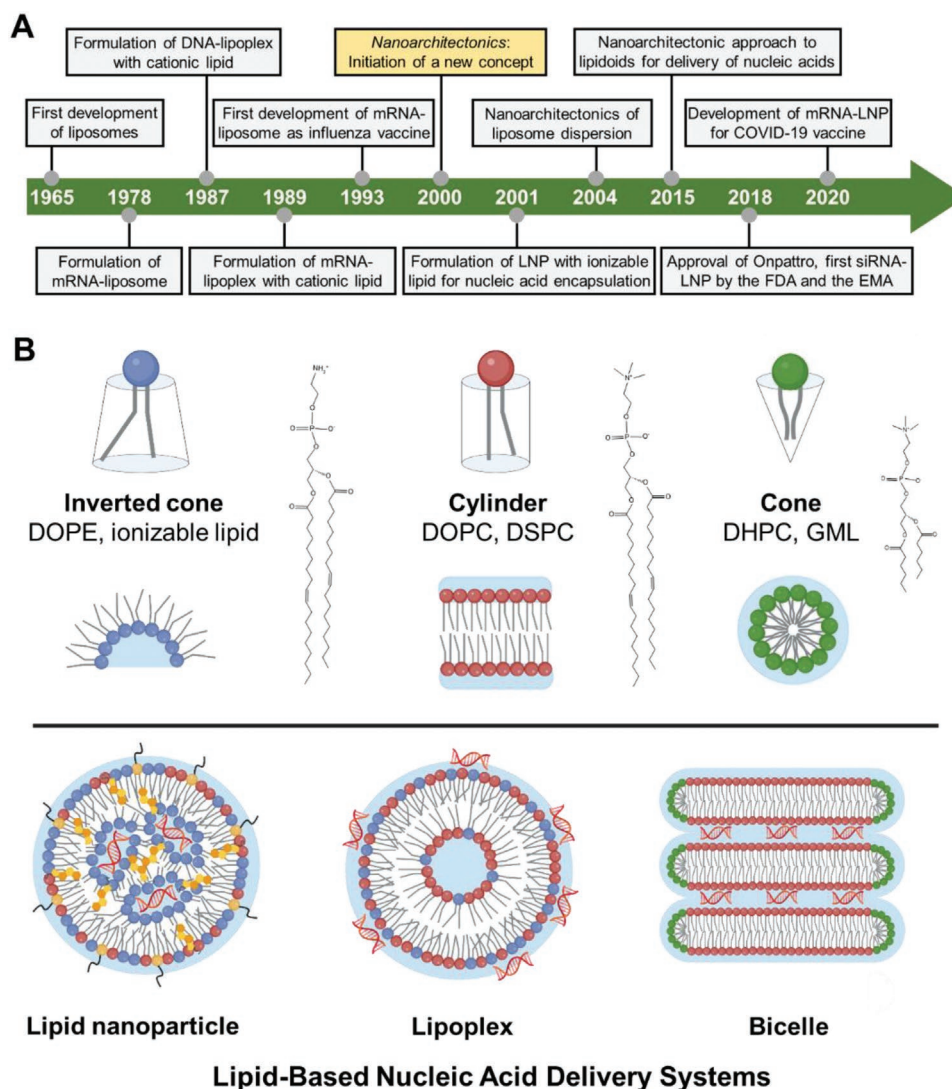
In this review, we cover the latest efforts to develop next-generation lipid-based nanoparticles for nucleic acid delivery applications by taking a nanoarchitectonics perspective and critically analyze the design, production, and application prospects for three classes of lipid-based nanoparticles as follows: 1) traditional LNPs; 2) lipoplexes; and 3) bicelles. The nucleic acid encapsulation strategies for each nanoparticle type are introduced and help to rationalize how different lipid nanoarchitectures can be useful depending on the delivery objective and application scope. While the main focus is on distilling molecular self-assembly principles to build advanced lipid-based nanoparticle systems, we also discuss pertinent issues related to overcoming clinical translation challenges and enabling scaled-up manufacture that can help to realize new application opportunities.

A. R. Ferhan, S. Park, H. Park, H. Tae, N.-J. Cho  
School of Materials Science and Engineering  
Nanyang Technological University  
Singapore 639798, Singapore  
E-mail: njcho@ntu.edu.sg

H. Park, J. A. Jackman  
School of Chemical Engineering and Translational Nanobioscience  
Research Center  
Sungkyunkwan University  
Suwon 16419, Republic of Korea  
E-mail: jjackman@skku.edu

 The ORCID identification number(s) for the author(s) of this article can be found under <https://doi.org/10.1002/adfm.202203669>.

DOI: 10.1002/adfm.202203669



**Scheme 1.** Applying the nanoarchitectonics concept to support innovation of lipid-based nanoparticle technology for nucleic acid delivery. A) Timeline of lipid-based nanoparticle technology progress and conceptual advances in the nanoarchitectonics field. B) Schematic representations of different lipid-based nanoparticle types, including (1) traditional lipid nanoparticles (LNPs), (2) lipoplexes, and (3) bicelles. The nanoparticles are enabled by the combination of controlling molecular self-assembly with various-shape lipids and using different nanofabrication strategies, highlighting how a nanoarchitectonics perspective can be useful to support future innovation. FDA, United States Food and Drug Administration; EMA, European Medicines Agency; DOPE, 1,2-dioleoyl-*sn*-glycero-3-phosphoethanolamine; DOPC, 1,2-dioleoyl-*sn*-glycero-3-phosphocholine; DSPC, 1,2-distearoyl-*sn*-glycero-3-phosphocholine; DHPC, 1,2-dihexanoyl-*sn*-glycero-3-phosphocholine; GML, glycerol monolaurate.

## 2. Lipid Nanoparticles

Lipid nanoparticles (LNPs) represent the most clinically advanced non-viral vector for the delivery of ribonucleic acids (RNAs).<sup>[13]</sup> LNPs have been widely used for encapsulating and delivering small interfering RNA (siRNA) in RNA interference (RNAi) therapy (see ref. [14]) and, more recently, have gained widespread attention by enabling the rapid development of messenger RNA (mRNA)-based vaccines to prevent COVID-19 infection.<sup>[15]</sup> The remarkable success of LNPs in the clinical setting can be attributed to a few major technological milestones with respect to lipid design and scalable methods of production. In particular, the utilization of ionizable lipids has

led to tremendous improvements in LNP functional performance, especially transfection efficiency.<sup>[16]</sup>

At the same time, the shift from bulk preparation methods such as batch extrusion to microfluidic-based production strategies has allowed more precise control over the physicochemical properties and overall quality of LNPs along with scalable manufacturing capabilities.<sup>[17]</sup> This enabled systematic studies to be conducted to understand the relationship between the physicochemical properties of LNPs, which depend on the nanoarchitectonic design strategy and production methods, and in vivo delivery performance. Finally, advances in microfluidic mixing technologies have facilitated scale-up through parallelization, which paved the way for large-scale manufacturing

of high-quality RNA-encapsulated LNPs.<sup>[18]</sup> This ultimately accelerated the translation of RNA-based LNP therapeutic solutions from the benchtop to the clinical setting. Nevertheless, efforts to continually improve the performance of LNPs in delivering different types of nucleic acid payloads are still ongoing. Along this line, it is crucial to understand the influence of different physicochemical parameters on the performance of LNPs, and how specific design characteristics can be incorporated to overcome limitations particularly associated with the transport of nucleic acids across biological barriers. In this section, we will review the evolution of LNPs as delivery systems for nucleic acids, especially RNAs, based on their design principles and production platforms and shed light on how nanoarchitectonic concepts are relevant to the design of LNPs.

### 2.1. General Design Rules from Biological Inspiration

Within the context of nucleic acid delivery using lipid-based systems, a series of works have taken inspiration from the delivery of native nucleic acids by lipoproteins.<sup>[19]</sup> In biological systems, native nucleic acids such as microRNAs are delivered to target cells by lipoproteins such as high-density lipoproteins (HDLs).<sup>[20]</sup> This occurs via binding of apolipoprotein A-I (ApoA-I), which is a major structural protein of HDLs, to specific scavenger receptors, such as SR-B1 that are present on target cell membranes.<sup>[20a]</sup> While HDLs are most popularly known for their role in reverse cholesterol transport (RCT)<sup>[21]</sup> in which case they remove excess cholesterol from peripheral tissues and transport it to the liver for biliary excretion, they have also been found to play critical roles in the transport of other biomolecules (e.g., signaling lipids, proteins, and nucleic acids).<sup>[22]</sup> Endogenous HDL particles are relatively small ( $\approx 7\text{--}13$  nm in diameter) and are highly dynamic in terms of physicochemical properties. Notably, they transition from a discoidal shape (i.e., in their nascent form) to a spherical shape (i.e., in their mature form) and undergo changes in lipid composition during RCT (i.e., due to the adsorption, accumulation, and subsequent release of cholesterol). Such morphological transitions offer insights into key design criteria related to multiple aspects of nucleic acid delivery, namely loading efficiency, physiological stability, and cell targeting and uptake efficiency.<sup>[23]</sup> Consequently, HDL particles represent excellent natural model systems for the formulation of lipid-based nanoparticle drug delivery vehicles<sup>[24]</sup> and significant work has been performed to develop synthetic lipid and lipoprotein nucleic acid delivery vehicles that are inspired by these systems and follow a few general design principles as described below.<sup>[23,25]</sup>

With regard to nucleic acid loading, the shape and size transition of HDL particles upon cholesterol adsorption during RCT demonstrate how shape and size constraints may limit the number of nucleic acid molecules that can be loaded and transported per particle, with spherical particles offering higher loading capacities than discoidal particles of the same diameter. As such, the diameter of the particles needs to be carefully considered to maximize loading without compromising particle distribution, particle stability, or cell uptake efficiency. In addition, the amount of loading is also

influenced by the loading method. While passive loading is generally more convenient, the loaded molecules can diffuse or leak out during circulation even before the delivery vehicle reaches target cells. On the other hand, loaded molecules that are covalently bound to the delivery particle are retained until reaching target cells. However, an active release mechanism needs to be implemented to ensure that the molecules in that case can be effectively unloaded once the delivery vehicle reaches a target cell. Practically, this issue highlights how careful consideration of the noncovalent intermolecular forces in the delivery system is warranted in order to ensure that the delivery is optimally suited to enable both nucleic acid encapsulation and eventual release. In some cases, stimuli-responsive systems that are sensitive to environmental conditions such as solution pH have proven useful to achieve these performance objectives.

To further enable systemic circulation and attain a long circulation half-life, the particles should first be physically robust under flow conditions at physiological temperature (i.e., maintain structural integrity and not degrade or destabilize under shear stress).<sup>[26]</sup> In addition, the particles should avoid binding with blood components, which could lead to interparticle aggregation and uptake by the mononuclear phagocyte system (MPS). MPS evasion is traditionally achieved through the introduction of hydrophilic moieties or the attachment of non-fouling polymers (e.g., polyethylene glycol or PEG) to the outer surface of the particles.<sup>[27]</sup> In terms of size, the particles should not be too small (i.e., not less than  $\approx 8$  nm) to avoid kidney clearance.<sup>[28]</sup> Along this line, lipid conjugation strategies have been explored to obtain lipidated therapeutic nucleic acids that boast higher circulation times and are less prone to degradation.<sup>[29]</sup> Ultimately, such protection improves the overall biodistribution of the nucleic acids and ensures that the nucleic acids effectively reach target cells.<sup>[30]</sup> Besides providing protection from nuclease degradation, the conjugation of lipids to nucleic acids has also led to new functionalities. For example, lipidated nucleic acids can be designed to assemble into pre-programmed shapes with precise control over geometrical dimensions.<sup>[31]</sup> This offers greater flexibility in terms of architectural design and more faithfully mimics natural delivery systems.

Finally, cell targeting and nucleic acid uptake in the cytoplasm represent two closely related critical considerations in the development of targeted delivery vehicles. Inspired by the ability of HDL particles to achieve targeted delivery via binding of ApoA-I to specific scavenger receptors, cell targeting in synthetic delivery vehicles can likewise be accomplished either through opsonization by apolipoprotein A or E (ApoA or ApoE) when the delivery vehicles are injected into the systemic circulation or by functionalizing the delivery vehicles with natural targeting molecules (e.g., ApoA or ApoE) or synthetic ligands.<sup>[32]</sup> Once the delivery vehicle reaches the target cell, the uptake mechanism is also influenced by the targeting strategy. While most lipid-based delivery systems rely on endocytosis, delivery vehicles that undergo opsonization are internalized by cells through phagocytosis.<sup>[33]</sup> In addition, the mechanism of uptake also depends on the surface charge, shape, size, and surface chemistry of the delivery vehicle.

## 2.2. LNP Design Principles

In addition to the general design rules inspired by biological nanoparticle examples such as HDL particles described above, the design principles behind the formulation of LNPs also expand on the early designs of synthetic liposome-based carriers, which consist of a neutral unilamellar lipid bilayer with an aqueous core, encapsulating short-stranded nucleic acid molecules (i.e., oligonucleotides).<sup>[34]</sup> While liposomes can serve as carriers for a variety of therapeutic molecules, their simple structure and the use of largely neutral lipids for the delivery of oligonucleotides posed several challenges.<sup>[35]</sup> Firstly, weak interactions between the lipids and negatively charged nucleic acids hampered efficient entrapment during production. Secondly, when introduced into biological systems, liposomes are prone to clearance by the reticuloendothelial system (RES), opsonization and destabilization, leading to reduced circulation time.

Over the years, the design has significantly evolved to achieve lipid-based delivery systems that overcome these limitations through employing a combination of different types of phospholipids. Within the context of nucleic acid delivery, it is vital to 1) ensure that the phospholipid carrier can efficiently interact with, condense, and entrap the nucleic acids, in a process collectively known as encapsulation and 2) effectively deliver the encapsulated nucleic acids to the cells with minimal biological interference during circulation. Encapsulation serves not only to spatially entrap the nucleic acids within the delivery vehicle, but to also isolate them from the external environment while protecting their structure and function. Initially, permanently cationic lipids were largely used to improve the interaction between positively charged lipid membrane interfaces and negatively charged nucleic acids.

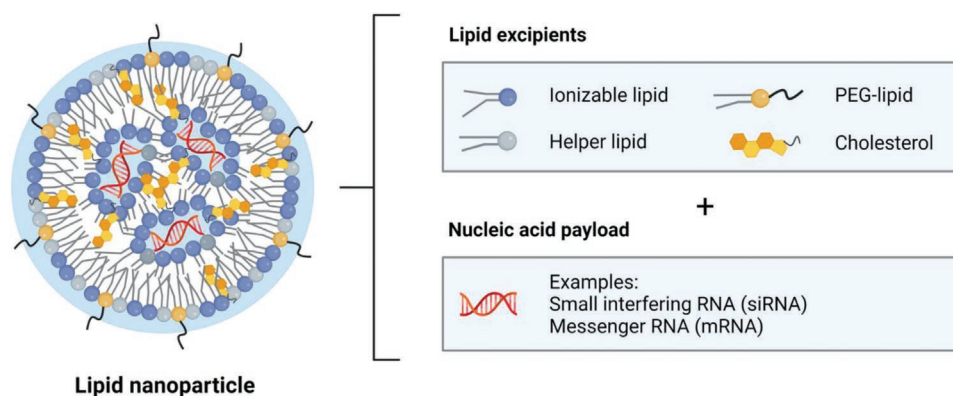
While it was successful in increasing the encapsulation efficiency, the use of permanently cationic lipids attracted nonspecific biological interactions and suffers from problems associated with triggering the innate immune response (e.g., arising from the activation of the complement system) and cytotoxicity (i.e., arising from the activation of proapoptotic and proinflammatory cascades), thus failing to provide a sustainable solution to issues related to reduced systemic circulation times. Early efforts to mitigate these issues focused on utilizing cationic lipids with delocalized charge while the issues were eventually

tackled through the design of a unique class of lipids with switchable charge known as ionizable lipids, which achieved significant improvements in encapsulation efficiency by being positively charged at low pH during production and avoided nonspecific biological interactions by remaining neutral at physiological pH during circulation. A careful balance of head-group and tail properties further enabled control over membrane biophysics to guide the development of tailored LNPs with heightened functionalities.

When combined with PEG lipid, helper lipid, and cholesterol, the delivery system becomes distinct from a traditional liposomal carrier in terms of structure, morphology, and lipid composition, and is therefore referred to as an LNP. Architecturally, LNPs are characterized by a phospholipid bilayer surrounding an electron-dense core in which ionizable lipid-encapsulated nucleic acid payloads are densely packed in the interior<sup>[36]</sup> (**Scheme 2**). Compared to liposomes, which consist of phospholipid bilayers and cholesterol with distinct phase transitions from ordered gel phase to liquid crystalline phase, Larson et al. reported that cationic mRNA–LNPs transition from an inverse hexagonal phase at pH values below the  $pK_a$  of the cationic lipid, to a lamellar phase above the  $pK_a$ .<sup>[37]</sup> Likewise, such phase changes also occur when the temperature is increased, indicating that the inverted hexagonal phase is more thermodynamically favorable. Based on these developments, it becomes clear that the most critical aspects of LNP formulation are nanoarchitecture design and lipid composition. By varying the lipid composition, the interaction with the nucleic acid payload can be carefully tuned. This directly impacts the encapsulation efficiency and influences the particle morphology and overall charge, which taken together will determine the overall performance of the delivery system. Conversely, the choice of lipids also depends on the nature of the nucleic acid payload. In the following subsections, we elaborate on the rationale behind the choice of lipid compositions, as well as the considerations for different payloads, in designing RNA–LNP delivery systems.

### 2.2.1. Lipid Composition

The formulation of LNPs is uniquely characterized by the utilization of four different lipid excipients namely: 1) ionizable



**Scheme 2.** Lipid nanoparticle architecture. Structural configuration and key components of a lipid nanoparticle with nucleic acid payload, highlighting how each component contributes to the overall structure and function.

lipids, 2) helper phospholipids, 3) cholesterol, and 4) PEG lipid. Each one of these excipients plays specific roles in ensuring the overall effectiveness of LNP as a nucleic acid delivery vehicle. Recently, Siegwart Daniel and co-workers developed selective organ targeting (SORT) nanoparticles, which enable the delivery of mRNA and gene editing systems to non-liver tissues.<sup>[38]</sup> SORT nanoparticles include a supplemental molecule whereby the chemical structure determines the LNP's tissue-specific activity. Their work demonstrates how a "fifth excipient" can further enhance the physicochemical properties and targeted delivery performance of LNPs. In all cases, the key to designing LNPs with high delivery efficacy lies in achieving an optimal balance between particle stability, sustained systemic circulation, and the ability to release the payload in a controlled manner inside the target cell, all of which rely on the proper selection of the different lipid excipients as described below.

**Ionizable Lipids:** Ionizable lipids are positively charged at acidic pH and neutral at physiological pH. During LNP production, they specifically serve to condense and entrap negatively charged nucleic acids (e.g., siRNA, mRNA, pDNA) through electrostatic interactions under acidic conditions. However, when the LNPs are introduced to the physiological environment, the ionizable lipids will switch to being neutral<sup>[13b]</sup> (Figure 1A). Compared to permanently charged cationic lipids, the use of ionizable lipids with neutral surface charge in the physiological system is especially beneficial in preventing the adsorption of negatively charged biomolecules onto the LNP and preventing rapid sequestration by immune cells during systemic circulation.

Once the LNP reaches the endosome, which typically presents an acidic environment, the ionizable lipids will revert to being positively charged. This leads to electrostatic interactions with the anionic endosomal membrane, resulting in the formation of a nonbilayer hexagonal phase that momentarily destabilizes the endosomal membrane and thereby facilitates the release of the nucleic acid to the cytosol<sup>[39]</sup> (Figure 1B).

There are three major classes of ionizable lipids depending on the tail structure of lipids, namely conventional two-tail, multi-tail, and branched-tail ones (Figure 2). While the number/structure of the tail region largely affects the overall geometry of the lipid self-assembly (i.e., a bulkier tail group promotes a more cone-shaped structure), another important factor to consider is tail saturation. Unsaturated ionizable lipids generally increase fluidity and a tendency to form a nonbilayer phase, which facilitates membrane disruption and payload release.<sup>[40]</sup> One of the most widely used two-tail, unsaturated ionizable lipids is DLin-MC3-DMA, which is incorporated in the FDA-approved siRNA-LNP drug (ONPATTRO). Multi-tail ionizable lipids have three or more tails, which can result in a more cone-shaped geometry to enhance endosome disruption.<sup>[41]</sup> Along this line, branched-tail ionizable lipids have also been developed, which may present methacrylate, acrylate, or ester chains that extend either as a 1C branch near the head or a 1C branch at the end. This can promote endosomal escape arising from stronger protonation of spaced ionizable lipids at endosomal pH and the increased cross-section of lipid tails, allowing for the formation of a more cone-shaped geometry.<sup>[42]</sup>

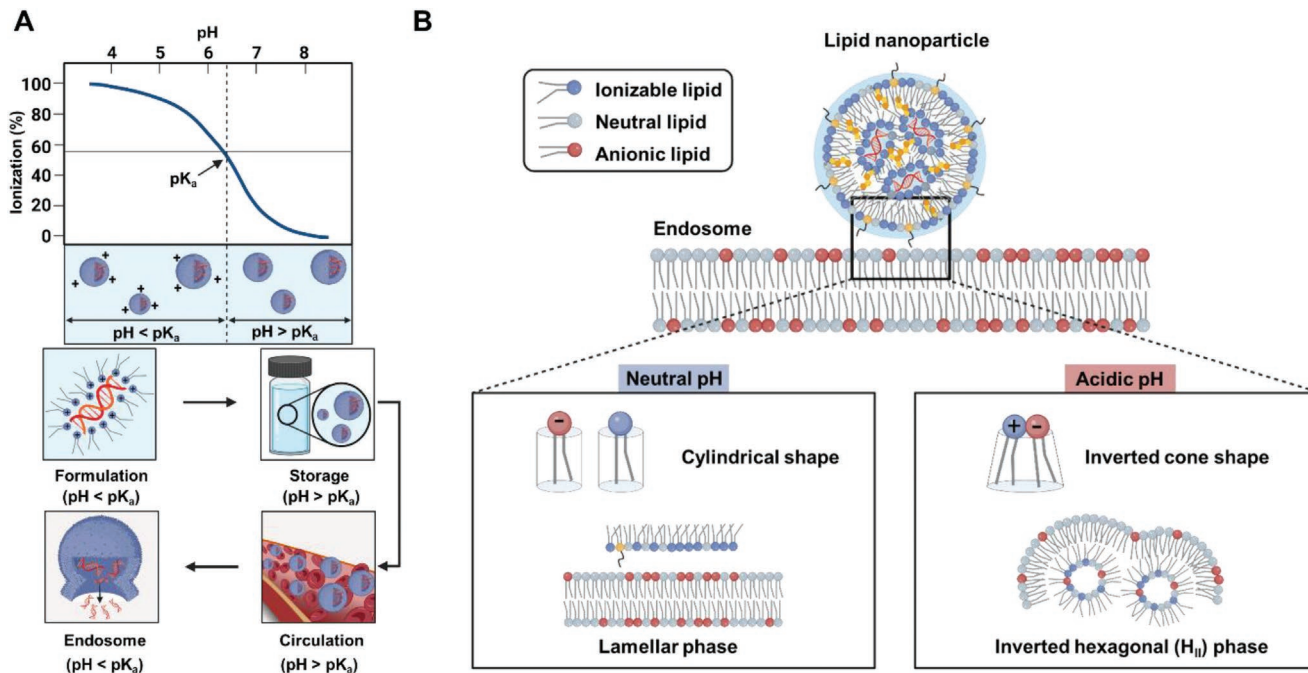


**Figure 1.** Illustration of the pH-dependent behavior of lipid nanoparticles due to ionizable lipids. A) Principle of the mechanism of ionizable lipids. During formulation, the ionizable lipids present a positive charge at low pH (below its  $pK_a$ ) to promote favorable interactions with negatively charged nucleic acids and facilitate nucleic acid encapsulation. During storage and in circulation under physiological pH (above its  $pK_a$ ), the ionizable lipids will switch to being neutral and remain stable. Once the LNP reaches the endosome, which typically presents an acidic environment (below its  $pK_a$ ), the ionizable lipids will become protonated again and resume a positive charge. B) Schematic representation of LNP interaction with the endosome, leading to a change in lipid geometry due to the formation of ion pairs. Protonated ionizable lipids interact with anionic lipids adopting an inverted cone geometry, which promotes the formation of the inverted hexagonal ( $H_{II}$ ) phase associated with membrane fusion.

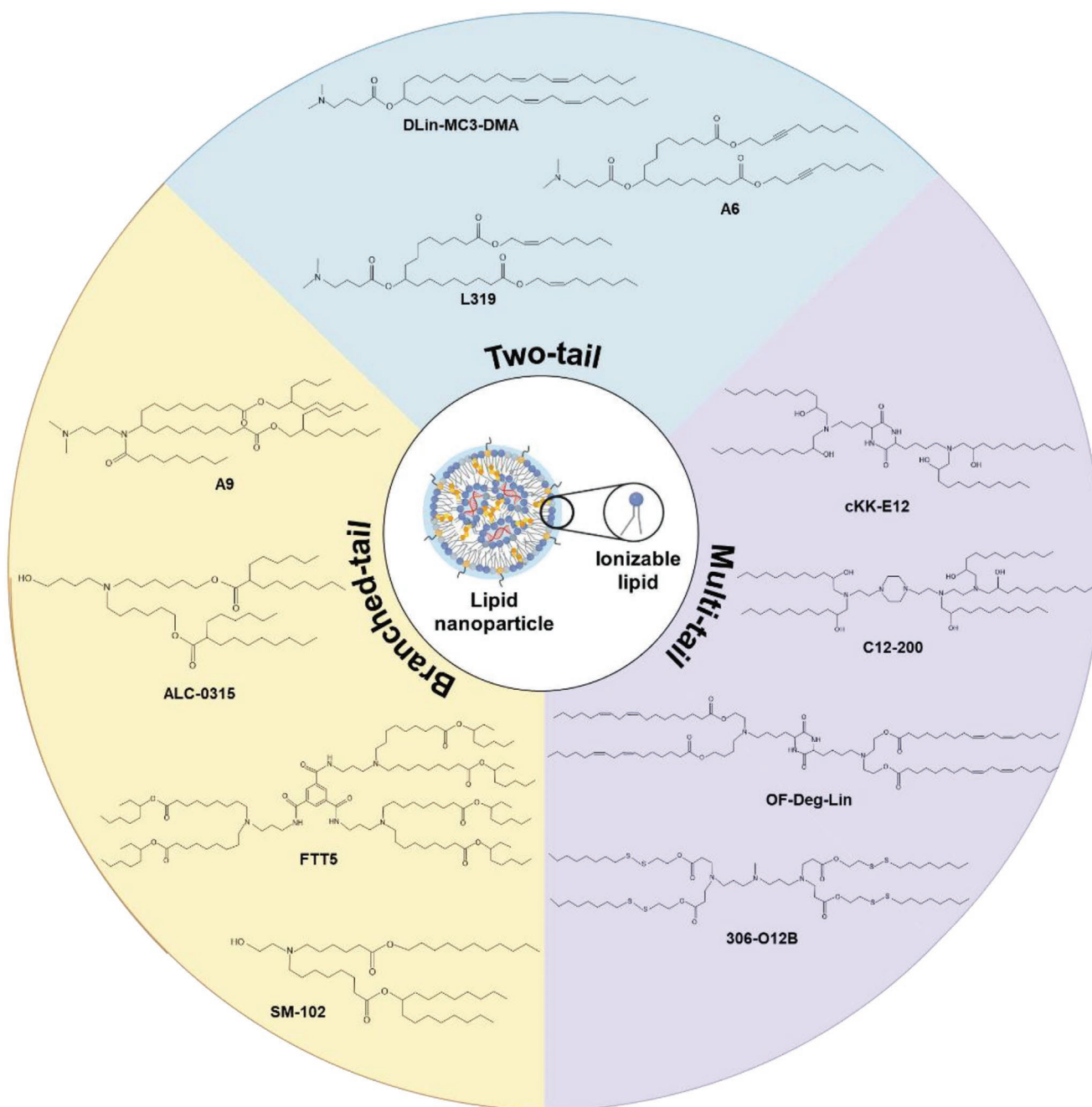


**Figure 2.** Structural classes of ionizable lipids. Three major classes of ionizable lipids depending on the tail structure, namely two-tail, multi-tail, and branched-tail.

Biodegradability can be improved by incorporating ester bonds to promote degradation into nontoxic metabolites after intracellular delivery.<sup>[43]</sup> This is critical to reduce systemic accumulation and eliminate potential side effects. Finally, since chain branching increases the cross-section of phospholipid tails (i.e., reduces chain packing) and results in the formation of phospholipids with cone-shaped geometry that promote spontaneous negative curvature to the membrane (i.e., due to the inversion of cone-shaped structures), it generally leads to better fusogenicity.

As a critical factor in the nucleic acid delivery process, it is important to understand the structure-function relationship between the molecular structure of ionizable lipids to the transfection efficiency of the LNPs, and how this in turn will determine the therapeutic efficiencies of LNPs.<sup>[44]</sup> For example, it has been found that lipid tail saturation, as well as the type of linker between the lipid tail and the headgroup can significantly influence transfection efficiency.<sup>[40c,45]</sup> More interestingly, small structural variations such as those arising from differences in the double bond positions of unsaturated lipid tails

or branching positions, are sufficient to produce significant variations in delivery performance.<sup>[45,46]</sup> Following this line, it is anticipated that ionizable lipids with novel structures will continue to emerge, which will facilitate the rational optimization of LNP lipid composition. Such developments may also be guided by the need for improvements in biodegradability, which is a key feature for clinical translation, as well as the promising opportunity of fine tuning the lipid geometry through adjustments in tail branching (i.e., in terms of extent and position), tail length, and number of tails.

**Helper Phospholipids:** The roles of helper phospholipids are various, ranging from facilitating membrane fusion, which contributes to higher transfection efficiencies, and increasing bilayer stability.<sup>[47]</sup> Helper phospholipids can have different molecular structures and geometry. For example, 1,2-dioleoyl-*sn*-glycero-3-phosphoethanolamine (DOPE), which is widely regarded as a fusogenic lipid, has a small phosphoethanolamine head (i.e., comprising of a primary amine and a phosphoric acid moiety), and two bulky and unsaturated oleoyl chains, resulting in a cone-shaped geometry. It is suggested that such geometry has the capability to stabilize the non-bilayer inverted hexagonal (H<sub>II</sub>) phase, which transiently forms during membrane fusion. Hence, the addition of DOPE as helper lipids enhances fusogenicity, effectively increasing the amount of LNP accumulation in target cells leading to higher transfection efficiencies. On the other hand, phosphatidylcholines (PCs), such as 1,2-distearoyl-*sn*-glycero-3-phosphocholine (DSPC) and 1,2-dioleoyl-*sn*-glycero-3-phosphocholine (DOPC) form a cylindrical geometry and provide greater bilayer stability relative to DOPE. In particular, the high melting temperature ( $T_m$ ) of DSPC, which is a saturated PC, leads to highly stable bilayers at physiological temperatures. However, such high stabilities will hamper endosomal release and reduce the efficiency of payload delivery. In comparison, DOPC, which is an unsaturated PC, has a lower  $T_m$  and exists in the fluid phase at physiological temperatures. As a result, they contribute to lower bilayer stability while allowing better efficiencies in payload delivery compared to DSPC. Taken together, DSPC offers the highest bilayer stability, followed by DOPC and DOPE. In other words, DOPC represents a good intermediate choice as a helper lipid and the balance between bilayer stability and transfection efficiency is often achieved through the introduction of cholesterol.

**Cholesterol:** The introduction of cholesterol can affect the degree of lipid packing, which influences membrane fluidity and permeability of the bilayer of the LNP.<sup>[4]</sup> Structurally, cholesterol comprises of three domains namely the head, body, and tail.<sup>[48]</sup> The head is a hydroxyl group positioned in a tilted configuration above one of the cyclohexane or cyclohexene rings of the body. The body comprises of a fused four-ring system containing three cyclohexane or cyclohexene rings and one cyclopentane ring, while the tail is a saturated alkyl side chain of the cyclopentane ring. It is suggested that the flexibility of cholesterol arises from the lack of functional groups in the tail and saturated nature of the alkyl chain. As a result, cholesterol molecules can fill gaps between other phospholipid molecules, through the interaction of the hydroxyl head groups with the aqueous phase of the phospholipid membrane (i.e., via polar interactions and hydrogen bonding). Together, the body and

tail of the cholesterol molecule promote orderly arrangement of the hydrophobic portion of the bilayer, leading to tighter lipid packing of the membrane. Consequently, this reduces membrane permeability and increases the overall structural integrity of the LNPs. In addition, cholesterol can traverse lipid bilayers and offer the possibility of equilibration across a concentration gradient should the need arise. During circulation, cholesterol also helps to prevent the diffusion of the other lipid excipients of the LNPs into high-density lipoproteins (HDL)-endogenous lipids thereby improving the LNP stability in vivo.

**Poly(ethylene glycol) PEG Lipid:** The introduction of PEG lipid serves to protect the LNP surface from opsonization, reticuloendothelial clearance, and destabilization during systemic circulation.<sup>[27a,49]</sup> This is achieved through a combination of steric repulsion and the formation of a hydration layer arising from the extension of hydrophilic PEG chains from the LNP surface. Based on the same mechanism, PEG-lipids also prevent the aggregation of LNPs during production, storage, and in circulation. Taken together, the structure of PEG extending from the LNP surface increases the overall stability of LNPs, which is largely advantageous. However, the prevention of non-specific molecular adsorption on the LNP surface offered by PEG lipids comes with a caveat as it also implies a significant reduction in the adsorption of apolipoprotein E (ApoE), ApoE is an extracellular protein that plays a key role in influencing the systemic circulation time of LNPs. The binding of ApoE has been found to trigger a redistribution of lipids at the shell and the core and plays a critical role in fusogenicity. In particular, it facilitates the cellular uptake of LNPs through receptor-mediated cellular entry.<sup>[50]</sup> Hence, it is vital to strike an optimal balance when deciding on the appropriate amount of PEG to be introduced to LNPs to ensure good protection against opsonization and reticuloendothelial clearance without compromising fusogenicity and cellular uptake. The adjustment of PEG density also allows the tuning of LNP pharmacokinetics for different applications.

While there are obvious benefits of including PEG lipids in LNPs, it is worthy to note that PEG is widely known to trigger immune responses and hypersensitivity reactions by activating the complement system. In addition, it can also suffer from accelerated blood clearance (ABC) (i.e., following the binding of anti-PEG antibodies). This has been intensively discussed, most recently during the development, and ongoing evaluation of COVID-19 vaccines, in which the potential of PEG lipids to cause anaphylaxis especially among patients with PEG allergy represents a significant concern.<sup>[51]</sup> In fact, there is evidence that highlights the importance of the form of PEG; specifically suggesting that PEG conjugated with lipids, not PEG alone, is more likely to cause allergic reactions.<sup>[52]</sup> Along this line, it is also important to note that PEG-lipids have the tendency to desorb and therefore escape the LNP architecture to circulate freely, increasing the likelihood of triggering immune responses. Considering these issues, several natural (e.g., polyaminoacids, glucosaminoglycans) and synthetic (e.g., polyacrylamide, polysulfobetaine methacrylates) polymers have been investigated as alternatives to PEG.

**Cell-Specific Targeting:** In addition to their primary roles in encapsulation, maintaining particle stability, and supporting systemic circulation, the lipid excipients can also play a critical

role in achieving cell-specific targeting as well as in modulating biodistribution and uptake mechanisms. For example, it has been established that ApoE adsorption is largely responsible for LNP accumulation in the liver since lipid-associated ApoE binds to low-density lipoprotein (LDL) receptors in the liver.<sup>[53]</sup> Along this line, several works have explored the possibility of varying the helper lipid composition to modulate the LNP interaction with ApoE.<sup>[46,47c,50]</sup> It has been observed that LNPs containing DOPE helper lipid interact more favorably with ApoE, therefore resulting in increased levels of accumulation in the liver.<sup>[47c]</sup> On the other hand, LNPs containing DSPC helper lipid exhibited weaker interactions with ApoE, leading to accumulation in the spleen. This was attributed to the unsaturated nature of DOPE, which leads to higher membrane fluidity; greater membrane fluidity has been previously observed to increase protein adsorption.<sup>[54]</sup>

Based on this rationale, lipid compositions can therefore be tuned to modulate the uptake mechanism for LNPs in line with controlling protein adsorption. In the most common scenario in which the cell uptake of LNPs occurs via the endocytic pathway,<sup>[55]</sup> the collective role of helper lipids and PEG lipids is to reduce protein adsorption and prevent corona formation. In the case of receptor-mediated endocytosis of ligand-targeting LNPs, lipids can be conjugated with antibodies or aptamers. It is worthy to note that for uptake via endocytosis, the ionizability of the lipids represents another crucial factor that enables the LNPs to withstand pH changes throughout the process, achieve endolysosomal escape, and eventual release of the nucleic acid cargo. Alternatively, the cell uptake of LNPs can also occur via phagocytosis.<sup>[56]</sup> In this case, lipid compositions should preferably be tuned to induce protein adsorption and trigger opsonization involving apolipoproteins (e.g., ApoA-I and ApoE), which would lead to phagocytosis. Furthermore, the concept of decorating pre-synthesized LNPs with native or synthetic biomolecules for the purpose of modulating biodistribution and cell uptake can be extended to improve cell targeting. Recently, SORT nanoparticles developed by Siegwart Daniel and co-workers demonstrated the ability to deliver mRNA with increased cell-targeting capabilities (i.e., to non-liver tissues) by endowing LNPs with an additional molecule that exhibits tissue-specific activity.<sup>[38]</sup>

## 2.2.2. Payload Considerations

LNPs were initially developed and optimized for the delivery of siRNAs. Although similar lipid compositions can theoretically encapsulate other types of nucleic acids, it may be challenging to apply the same formulation across the board considering the differences in molecular size, net charge, and conformational structure.<sup>[57]</sup> For example, small activating RNAs (saRNAs), and microRNAs (miRNAs), both of which are also involved in the RNA interference pathway like siRNAs, are double-stranded and with lengths between 20 and 24 base pairs. On the other hand, single-stranded mRNAs can and double-stranded plasmid DNAs (pDNAs), can vary from several hundred to several hundred thousand nucleotides. Since the negative charge of nucleic acids arises from the phosphate backbone, their net charge is directly correlated to the number of nucleotides and whether they are single- or double stranded. In addition, nucleic acids

such as pDNAs and transfer RNAs (tRNAs) have well-defined conformational structures; pDNAs are circular and tRNAs have a distinctive three-leafed clover structure comprising of three hairpin loops. As such, adjustments to the lipid composition are often required to accommodate different nucleic acids. Specifically, the ratio between the four lipid excipients, as well as the ratio of ionizable lipid to RNA has been found to significantly affect the delivery efficacy both in vitro and in vivo.<sup>[58]</sup>

*siRNA versus mRNA:* In order to exemplify the importance of considering the different characteristics of nucleic acid payloads on the efficacy of LNP delivery systems, we examine two types of RNAs, namely siRNA and mRNA, that are most commonly encapsulated by LNPs. It is well known that siRNA and mRNA structurally differ based on size and effective charge. While siRNA has a short and well-defined structure (i.e., double-stranded with a typical length of between 20–24 base pairs<sup>[59]</sup>), mRNA has a relatively less defined structure with variable lengths (i.e., threadlike, single-stranded with lengths in the range of several hundred to a thousand bases<sup>[60]</sup>)—as a reference, the SARS-CoV-2 single-stranded genomic RNA is approximately 30 kilobases in length.<sup>[61]</sup> These differences potentially lead to variations in lipid packing and the overall LNP configuration and size. For example, it was found that while siRNA molecules in siRNA–LNPs are largely confined within multilamellar nanostructures (i.e., consisting of siRNA molecules sandwiched between tightly packed concentric lipid bilayers of ionizable lipids with PEG lipids on the outermost layer), mRNAs, due to their larger size, can rearrange the compartmental organization within the internal core of the mRNA–LNPs and form inverted hexagonal nanostructures instead.<sup>[62]</sup> In this configuration, mRNA molecules are encapsulated within an aqueous environment surrounded by a monolayer of ionizable lipids with their headgroups facing inwards. These individual compartments are in turn densely packed and contained within a nonpolar environment bounded by a phospholipid monolayer containing a mixture of ionizable lipids, helper lipids, and PEG lipids with their headgroups facing the external aqueous environment. Based on these arguments, it becomes clear that the chemical, as well as architectural, requirements of the lipid formulation would greatly depend on size and structure of the intended encapsulated material. For example, a smaller payload (e.g., siRNA) with well-defined structure would result in a denser, well-packed arrangement of encapsulated nucleic acids in the interior of the LNPs and potentially a smaller overall LNP. Conversely, a larger payload (e.g., mRNA) with a less ordered structure would result in a less dense arrangement within the LNPs and possibly a larger overall LNP. Indeed, previous works have shown that siRNA and mRNA are most effectively delivered in differentiated LNP formulations.<sup>[44a]</sup>

Besides adjusting the ratio between the four lipid excipients, various proprietary ionizable lipids with new structures and functionalities have emerged driven by the need to enhance the efficacy of mRNA–LNPs. In a noteworthy development, Ball et al. explored the possibility of codelivery of siRNA and mRNA using a single LNP formulation.<sup>[58]</sup> To achieve this, they employed a formulation comprising of an ionizable and biodegradable amine-containing lipidoid, cholesterol, DSPC, DOPE, and PEG lipid. They began with two previously reported LNP



formulations that were found to be potent for siRNA and mRNA delivery and systematically varied the lipidoid-to-RNA ratio, as well as the percentage of lipidoid in relation to the helper lipid, cholesterol, and PEG lipid. They also gradually changed the composition of helper lipids from a blend containing majority DSPC to DOPE, and introduced a negatively charged helper polymer in the form of poly(sodium 4-styrenesulfonate) (PSS) to enhance the efficacy. Surprisingly, they found that coformulation of siRNA and mRNA in the same LNP was not only possible but enhanced the efficacy of both drugs in vitro and in vivo. It was suggested that since DSPC has two saturated aliphatic tails while DOPE has a cis-double bond in each of its two aliphatic tails, the packing of nucleic acids within the internal core of the LNP can be carefully optimized by varying the ratio of DSPC to DOPE to accommodate the significant structural differences of both siRNA and mRNA. Furthermore, the additional negative charge of PSS promotes electrostatic attraction in the particle and increased overall particle stability. Separately, Hejdankova et al.

recently developed a novel structural class of ionizable adamantane-based lipidoids named XMaNs, which overcomes issues related to tedious optimization of LNP components for a wide range of nucleic acids.<sup>[63]</sup> Briefly, XMaN LNPs were formulated with DMG-PEG<sub>2000</sub>, cholesterol, the helper lipid DOPE, XMaN lipidoids (**Figure 3A**), and combined with diverse types of nucleic acids (mRNA, siRNA, pDNA, 2',3'-cGAMP) (**Figure 3B**) in a microfluidic device. Nucleic acid-loaded XMaN LNPs have an intricate architecture (**Figure 3C**) and the microfluidic production has allowed the fabrication of XMaN LNPs with good sizes and excellent size distribution (**Figure 3D**). Using the best performing member of the XMaN family, they were successful in entrapping and delivering siRNA, mRNA, plasmid DNA as well as a cyclic dinucleotide. Taken together, these works highlight that the delivery of different nucleic acid payloads, whether isolated or in combination, is highly achievable and can be significantly enhanced through a series of systematic and efficient formulation optimization.

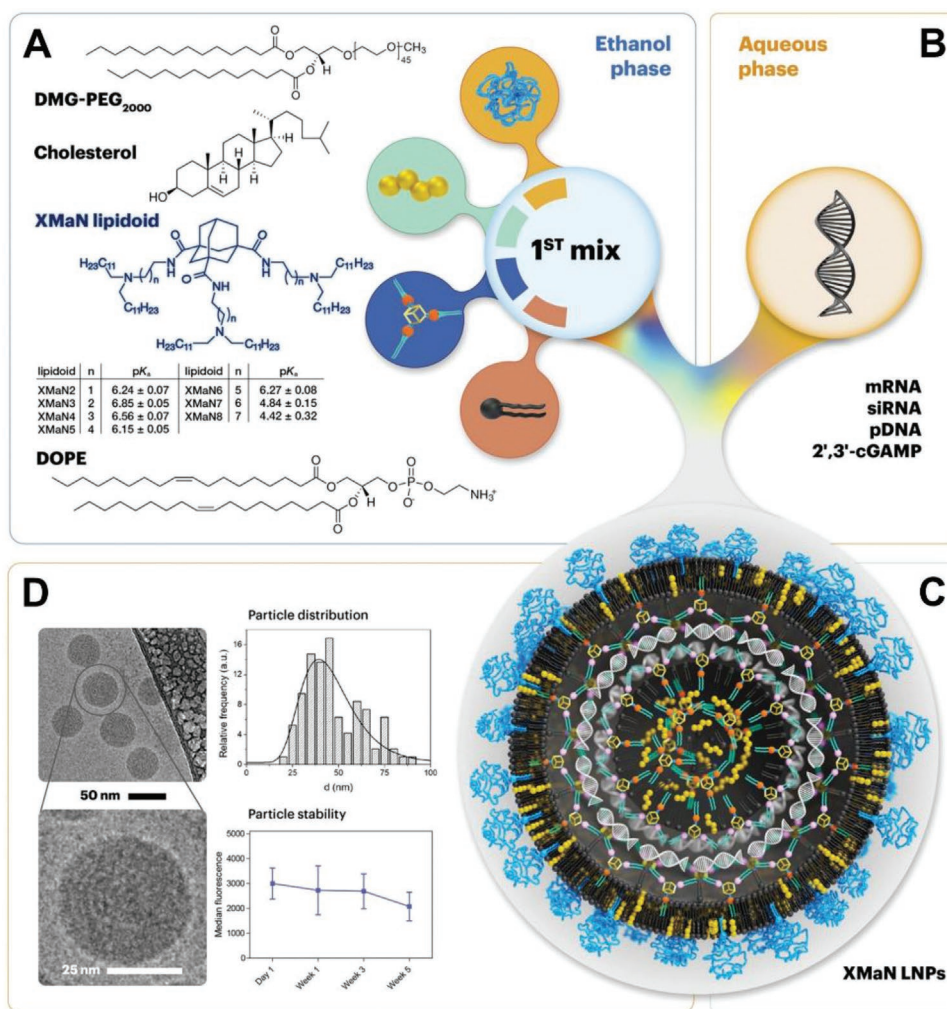


**Figure 3.** General overview of the approach to obtain LNPs incorporating XMaN lipidoids to achieve the delivery of different types of nucleic acids. A) Four lipid excipients, including XMaN lipidoids, are first mixed in ethanol, before they are combined, using a microfluidic platform, with B) a wide range of nucleic acid payloads that are dissolved in an aqueous buffer. C) A representation of a possible architectural configuration of nucleic acid-encapsulating XMaN LNPs. D) Cryo-TEM images of mRNA-loaded XMaN LNPs, their size distribution and evaluation of their functional stability after prolonged storage (i.e., up to five weeks) at 4 °C. Adapted with permission.<sup>[63]</sup> Copyright 2021, Wiley-VCH.

*Formulation Optimization:* The evolution of LNPs from encapsulating siRNA to mRNA highlights the need to optimize the lipid formulation for each type of nucleic acid payload since the formulations are not interchangeable. To achieve the most ideal LNP formulation for the delivery of different nucleic acid payloads, most works rely either on the one-factor-at-a-time (OFAT) approach or the design-of-experiment (DoE) approach. In the OFAT approach, one lipid is varied systematically while keeping all other factors constant. While this method is advantageous to reveal the direct correlation between the varied parameter to the overall physicochemical property of the LNP, it does not consider higher order interactions between the different lipid excipients. Consequently, a possible optimal formulation arising from second or third order interactions between the lipids could be missed. The method is also time consuming and could lead to wastage of precious reagents, especially when it involves optimizing lipid parameters for different nucleic acids. The DoE approach, on the other hand, gains maximum insights about the effect of varying several parameters to the overall property of the LNPs through minimal number of experiments.

Generally, it involves a screening design paired with response surface methodology (RSM). Screening design first identifies potential significant variables (e.g., choice of ionizable lipid, helper lipid, amount of cholesterol, ratio of lipid to nucleic acid payload, etc.) while RSM determines the critical degree of adjustment that should be applied to the most important variable.<sup>[64]</sup> The DoE approach provides information on the interaction between several parameters, leading to more accurate conclusions compared to the OFAT approach. More importantly, it streamlines the formulation optimization process. This was clearly demonstrated by Love et al., where the formulation of LNPs containing erythropoietin (EPO)-mRNA and C12-200 phospholipid was optimized from a previous formulation designed for siRNA-LNP.<sup>[65]</sup> The study identified the choice of helper phospholipid as the most important parameter for effective delivery EPO-mRNA; the use of DOPE was favorable over DSPC, which was initially used in the formulation of siRNA-LNP. The weight ratio of C12-200 phospholipid to mRNA was also identified as another important parameter. Notably, second-order interactions (e.g., between C12-200 mol% and C12-200-to-mRNA weight ratio) were detected, highlighting the advantage of the DoE approach over the OFAT approach. Such capability to detect higher-order interactions is especially vital when performing formulation optimization involving ionizable lipids with novel functionalities, of which multiple layers of interdependencies with other parameters could be difficult to resolve.

In a separate demonstration, Dahlman and co-workers described a cluster-based screening approach, which was inspired by statistical DoE methodologies, to optimize the formulation of mRNA-LNPs for the delivery of nebulized therapeutic mRNA.<sup>[64b]</sup> The cluster-based approach involves, firstly, the identification of LNP chemical traits that influence the in vivo delivery of nebulized LNPs (e.g., the amount of PEG added to the LNP, the structure of the lipid-PEG, the charge of the phospholipid and the presence or absence of cholesterol). A hypothesis relating to the effect of varying each of these traits is assigned as an axis in an N-dimensional chemical space and

a small group of LNPs (e.g., around 8 to 12) are then formulated at the extreme of each axis. Within these “extreme groups,” a selection process is further applied to determine whether 1) the LNPs meet size and stability requirements, 2) the stability remains unchanged when LNPs are pooled together, and 3) the pooled LNPs functionally deliver mRNA following nebulization. Promising groups that pass this selection process are then expanded and combined by formulating LNPs near the intersection of these groups, with newly formulated LNPs also subject to the same selection process. All these data, including from groups that initially failed, were considered to design subsequent LNPs. Through this regimented process, they were able to efficiently scan a diverse LNP chemical space, and manipulate several pertinent parameters that influence in vivo delivery, iteratively.

### 2.2.3. Physicochemical Parameters

The size and surface charge of the resultant LNPs have been identified as critical parameters that affect not only the amount of nucleic acid payload that can be packaged within the internal core but also the in vivo behavior of LNPs.<sup>[66]</sup> These parameters influence the pharmacokinetic profile of LNPs. For example, smaller particles are observed to exhibit longer systemic circulation times and slower clearance from the blood stream. More importantly, it has been observed that particle size affects cell uptake since the endocytic pathway varies with particle size, which has implications on the intracellular processing and overall efficacy of the LNPs.<sup>[67]</sup> For instance, it was found that the endocytosis of 40 nm diameter LNPs is based on a dynamin-dependent pathway while the endocytosis of LNPs larger than 98 nm in diameter is based on a clathrin-dependent pathway.<sup>[68]</sup> More recently, Hasset et al. evaluated the effect of LNP size on mRNA vaccine immunogenicity on mice. They systematically changed the LNP diameter at a fixed lipid composition and found that LNPs with smaller diameter did not lead to a significant immune response in mice. However, significant immune responses were observed in non-human primates regardless of the LNP diameter.<sup>[69]</sup> In a separate study, Chen et al. also found that the hepatic gene silencing of FVII in mice was significantly influenced by the size of the siRNA-LNPs.<sup>[70]</sup> Specifically, gene silencing was far more efficient using LNPs with an optimal size of 38–78 nm in diameter compared to smaller (i.e., 27 nm in diameter) and larger (i.e., 117 nm in diameter) particles. The observation was attributed to the inability of large LNPs to infiltrate the fenestrations in the liver vasculature and the instability of smaller LNPs in serum. In addition, the ionizable lipids also tend to dissociate more rapidly from smaller LNPs leading to lower transfection efficiencies. Aside from demonstrating the effect of size on the efficacy of LNPs, these studies also highlight the importance of producing LNPs with high monodispersity without overlapping size distributions. Likewise, the phospholipid charge not only affects the interaction between the lipid excipients and the nucleic acid payload, which determines the encapsulation efficiency but also determines the overall surface charge and zeta potential of the LNPs, which strongly influences interactions with biological components in vivo. While the uptake pathway is influenced by particle size,

the degree of initial adsorption of the LNP on the cell membrane is governed by its zeta potential. It is therefore essential to achieve precise control over these parameters.

### 2.3. Platform Development

As evidenced by the previous section, the key to the success of LNPs as nucleic acid delivery systems lies in a solid understanding of the structure–function relationship. Clearly, the molecular structures define the resultant geometry of the lipid components, affect their interaction with the nucleic acids, and influence the overall morphology and physicochemical properties of the LNP (i.e., the concept of nanoarchitectonics<sup>[71]</sup>), all of which in turn determine the behavior of LNPs in vivo, and ultimately the performance of the LNPs within the context of a nucleic acid delivery system.<sup>[72]</sup>

While the design principles are built upon these correlations, they would not have been realized without proper and consistent control over the LNP fabrication process, which has allowed systematic studies to be conducted in a reproducible manner. At the same time, reproducibility and scalability represent key prerequisites for the clinical development of LNPs. Along this line, efforts have been continually made to improve the production methods of LNPs. The development of production platforms serves two overarching objectives. Firstly, it aims to achieve controlled and reproducible production of LNPs so that fundamental investigations looking into the structure–function relationship can be performed reliably thereby facilitating formulation optimization of LNPs. Second, it promotes scalable manufacturing, which paves the way for the entry of LNPs to the clinic. In the following subsections, we will elaborate on how the production platforms have evolved over recent years, particularly through the advent of microfluidics technologies.

#### 2.3.1. Bulk Mixing Methods

Early production of liposome- and LNP-based delivery systems relies on bulk mixing methods. Liposome-based carriers, particularly those containing siRNA, have been commonly prepared through lipid film hydration followed by extrusion, or using the sonication and homogenization methods. Extrusion involves passing the solution containing the lipid mixtures through a series of filters to attain liposomes with the desired size. The intended payload is encapsulated through the sonication or homogenization steps.

Besides extrusion, liposomes can be fabricated following the ethanol injection method. In this method, lipid mixtures in ethanolic solution are injected into a large volume of aqueous solution under continuous stirring. The ethanol is then removed via evaporation leading to the spontaneous formation of vesicles. This method has several advantages over the film hydration method. Firstly, the method is relatively straightforward as it does not involve any intermediate processing steps. Secondly, the method does not involve any sonication steps, avoiding unnecessary damage to the phospholipid molecules. Most importantly, it produces unilamellar vesicles with smaller diameters and better monodispersity. While the film hydration

and ethanol injection methods can be easily adopted and performed at the laboratory scale, they are labor-intensive and lack scalability. The crossflow injection method was then developed by Wagner et al. to streamline the process and execution of the ethanol injection method.<sup>[73]</sup> In the crossflow injection method, the setup comprises of two stainless steel tubes welded perpendicular to one another with a small injection hole at the intersection between the tubes. Through this injection hole, lipid mixtures in ethanol are injected into a stream of aqueous buffer leading to the spontaneous self-assembly of lipids to form liposomes. It was found that the introduction of high lipid concentrations under high injection pressures leads to liposomes with a narrow size distribution. It was suggested that unlike the lipid film hydration and ethanol injection methods, the crossflow injection method was suitable for continuous and scalable manufacturing of liposomes. Overall, these bulk preparation methods establish the guiding principles behind LNP production and provide the basis for the development of more advanced production platforms that are aimed to improve the physicochemical properties of the LNPs.

#### 2.3.2. Advent of Microfluidics

Microfluidics refers to the control and manipulation of fluids within channels, cavities, and structural features with dimensions in the micrometer range.<sup>[74]</sup> Microfluidics have found relevance in a wide variety of biomedical applications, including in the preparation of gene and drug delivery vehicles.<sup>[75]</sup> It allows greater consistency in the preparation process since the flow is well controlled by means of optimizing and fixing the flow channel dimensions and flow rates of the introduced fluids, thus leading to improved reproducibility. Besides, microfluidics also increases throughput and opens the possibility of integration with digital automation.<sup>[76]</sup> Within the context of LNP production, microfluidics overcome challenges related to manual experimental execution and batch processes. For example, microfluidics allows controlled mixing of lipids in organic solvent and nucleic acids in aqueous buffer under continuous flow, with minimal operator intervention. This contrasts with the lipid injection method, which, although principally similar in terms of solvent mixing, is a batch process that requires continuous stirring and subsequent removal of the ethanol via an evaporation step.

Motivated by the growing promise of nanoparticles as an alternative to viral vectors for the delivery of nucleic acids into specific types of cells for gene therapy, Wang et al. designed a rapid developmental pathway for generating nanoparticle-based vectors for highly efficient delivery of a variety of nucleic acid payloads for gene therapy applications.<sup>[77]</sup> It relied on a combinatorial synthetic approach based on supramolecular assembly executed within a custom-designed digital microreactor to achieve a convenient, flexible, and modular method for generating DNA-encapsulated supramolecular nanoparticles. The employment of controlled microfluidic formulation for the rapid discovery of potent siRNA-containing LNPs was later reported by Anderson and co-workers.<sup>[70]</sup> The method involved the production of large amounts of siRNA–LNPs on a microliter scale through stepwise ethanol dilution. Briefly,

an ethanolic solution containing the lipid excipients was first rapidly mixed with an equal volume of aqueous solution containing siRNA. This leads to lipid self-assembly into LNPs while encapsulating the siRNA through electrostatic interactions. The siRNA–LNPs were then further diluted with aqueous buffer to prevent LNP aggregation. These steps were performed within a polydimethylsiloxane (PDMS) microfluidic channel, with periodic trenches and ridges on the floor of the channel to promote mixing. Around the same time, the group of Langer developed a pattern-tunable microvortex platform for the mass production and size control of lipid-polymer hybrid nanoparticles.<sup>[78]</sup> The platform involves the formation of symmetric microvortices at the intersection of three inlets (i.e., two flanking inlets introducing lipid and lipid-PEG dissolved in 4% ethanol/water, and one central inlet introducing PLGA dissolved in acetonitrile). These microvortices promote the rapid mixing of the lipid excipients with PLGA, followed by nanoprecipitation and the formation of the nanoparticles. The microvortex formation was regulated through careful prediction and manipulation of the 3D fluid flow patterns. Using this approach, they reported that the resultant nanoparticle size can be controlled with high productivity and low polydispersity by adjusting the flow rates, particularly by varying the Reynolds number between 30 and 150. In a subsequent development, Valencia et al. developed a fully integrated microfluidic platform with a multi-inlet micromixer for programmable and systematic mixing of large quantities of precursors to make nanoparticles.<sup>[79]</sup> The platform was successful in synthesizing nanoparticles with a wide range of properties by combining 15 different precursors in different ratios, achieving 45 different formulations with different sizes and surface compositions. Taken together, the obvious advantages of flow-based platforms offered by microfluidics within the context of preparing nanoparticle-based delivery systems have led to the realization of the importance of rapid mixing, and further development of microfluidic mixing technologies thus followed suit to expand its capabilities.<sup>[80]</sup>

### 2.3.3. Microfluidic Mixing Architectures

Due to their nonpolar tails, lipids readily dissolve in ethanol but not in aqueous solvent. The addition of lipids dissolved in ethanol to an aqueous buffer containing nucleic acids results in the formation lipid bilayer structures upon hydration, which subsequently interact with the nucleic acids to form small multilamellar liposomes with nucleic acids sandwiched between the bilayers. Based on this principle, LNPs are formed when there is a rapid increase in polarity within the bulk environment when two miscible phases combine (e.g., when lipids dissolved in an organic solvent are rapidly introduced to an aqueous buffer). This occurs through the supersaturation of lipid molecules, which leads to their self-assembly to form LNPs<sup>[81]</sup> (Figure 4A). Along this line, it is important to note that in order for the multilamellar bilayers to efficiently trap the nucleic acids, the ethanol concentration must be near the region of breakdown of the liposomal structure.<sup>[16c]</sup> In other words, while increasing the concentration of ethanol leads to higher nucleic acid entrapment, it also leads to a higher degree of membrane destabilization. Hence it has been found that

dilution of the ethanol/buffer mixture to around 25% ethanol is typically ideal for the formation of LNPs with good encapsulation efficiency and sufficient stability.

In microfluidic channels, the Reynolds (Re) number is usually smaller than 1, which means that the concentration of lipids in the organic solvent is dominated by molecular diffusion. Based on this principle, microfluidic mixing architectures have been developed with the aim of enhancing the mixing efficiency and attain a uniform population of LNPs while achieving excellent entrapment of the nucleic acid payload.<sup>[18c,82]</sup> Microfluidic mixing can be broadly categorized into passive and active mixing; passive mixers solely rely on the geometry of the microfluidic channels while active mixers control the flow of sample solutions by electrohydrodynamic disturbances. Within the context of LNP fabrication, most micromixers can be categorized as passive mixers. Some examples of advanced passive micromixers used for LNP production include the T-junction mixer, staggered herringbone micromixer (SHM), hydrodynamic flow focuser (HFF), bifurcating and baffle mixers (Figure 4B). These micromixers differ in their 3D structure and induce rapid mixing between the organic and aqueous phases in a controlled environment through different mechanisms.

**T-junction Mixer:** T-junction mixing is a rapid mixing method where input streams are introduced directly opposite to each other at very high flow rates (i.e., 40–60 mL min<sup>-1</sup>), with a perpendicular output.<sup>[83]</sup> When the aqueous phase containing nucleic acids and organic phase containing lipids are introduced as inputs, the collision of the input flows results in turbulent mixing, resulting in the formation of nucleic acid–LNPs. It has been found that the particle size can be reduced by increasing the flow rates. Likewise, increasing the flow rates also resulted in significant improvements in the polydispersity index (PDI), which is an indication of the size distribution.<sup>[83a]</sup> However, as T-junction mixing is operated at high flow rates, it is not a preferred method especially in the laboratory where the reagents for high throughput screening need to be conserved. Hence, T-junction mixing is favored for large-scale production of siRNA–LNPs.

**Staggered Herringbone Micromixer (SHM):** The staggered herringbone micromixer architecture was introduced by Stroock et al. as a passive mixing method for steady pressure-driven flows in microchannels at low Reynolds number.<sup>[84]</sup> It comprises a series of asymmetric protrusions, which mix solvents based on chaotic advection. Within the context of LNP production, the characteristic diffusion length between the organic lipid and nucleic acid–aqueous streams is significantly reduced. This allows controllable mixing to occur faster (i.e., in the millisecond scale) than the characteristic timescale for lipids to aggregate, hence producing LNPs with uniform sizes. Unlike T-junction mixing, microfluidic devices with SHM are suitable for mixing small quantities of input solutions, hence making them ideal for screening applications in the laboratory. Nevertheless, scale-up can be achieved through parallelization of microfluidic chips.<sup>[85]</sup> For example, high production rates of LNPs up to 72 mL min<sup>-1</sup> have been achieved by incorporating six sets of SHM in a single microfluidic device.<sup>[86]</sup> Most notably, SHM devices were commercialized by Precision NanoSystems in their first-generation NanoAssemblr platform.

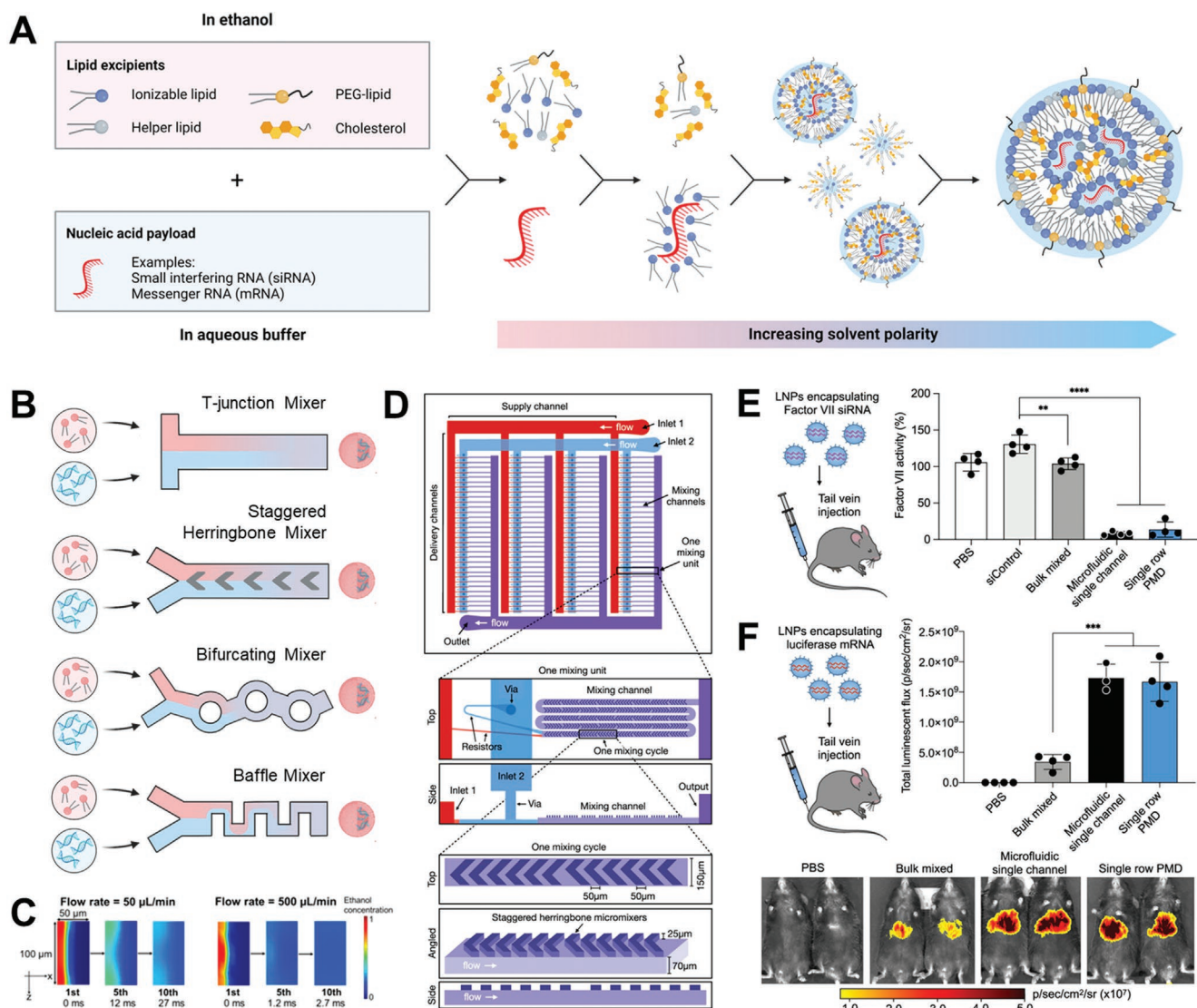


**Figure 4.** Self-assembly process of LNPs within microfluidic systems. A) The self-assembly process of nucleic acid–LNPs in a microfluidic mixer begins when lipid excipients (i.e., ionizable lipid, PEG lipid, helper lipid, and cholesterol) dissolved in ethanol are rapidly mixed with the nucleic acid payload (e.g., siRNA, mRNA, etc.) dissolved in an aqueous buffer. This initially occurs at a low buffer pH whereby the ionizable lipid will assume a protonated form and bind, via electrostatic interactions, to the negatively charged backbone of the nucleic acid. Concurrently, the increasingly polar environment drives the formation of vesicles and the encapsulation of the nucleic acid. As the mixing progresses, and with increasing buffer pH, the ionizable lipid becomes increasingly neutral, leading to the fusion of adjacent vesicles to form the interior core of the LNP. The extent of vesicle fusion is influenced by the amount of PEG lipid added due to its hydrophilicity as well as steric effects. Adapted with permission.<sup>[81]</sup> Copyright 2021, MDPI Publishing. B) Major microfluidic mixing architectures for LNP formulation (top to bottom): T-junction mixer, staggered herringbone micromixer, bifurcating mixer, and baffle mixer. C) The effect of varying flow rate on the mixing profile of ethanol (red) and water (blue) within a baffle mixer, visualized through a computational fluid dynamics simulation. Adapted with permission.<sup>[89]</sup> Copyright 2018, American Chemical Society. D) A diagrammatic representation of microfluidics parallelization, showing (from top to bottom) the arrangement of mixing channels, each mixing unit, and each mixing cycle within a parallelized microfluidics device, which adopts the staggered herringbone architecture. Evaluation of the in vivo delivery performance of E) siRNA–LNPs and F) mRNA–LNPs obtained using the parallelized device compared to bulk mixing. The evaluation was performed by means of administering to mice. The mRNA encodes for luciferase and the in vivo delivery performance was evaluated by directly visualizing the luminescence from selected regions of the mice. The results clearly show that the in vivo delivery performance of nucleic acid–LNPs obtained via microfluidic mixing is superior to those obtained via bulk mixing. D–F) Adapted with permission.<sup>[85]</sup> Copyright 2021, American Chemical Society.

*Hydrodynamic Flow Focuser (HFF):* Hydrodynamic flow focusing (HFF) was first reported by Jahn et al. and involves the continuous-flow hydrodynamic focusing of the organic phase (i.e., lipids dissolved in organic solvent) by the aqueous phase.<sup>[87]</sup> Typically, a central stream introduces the organic

phase, which is pinched by two aqueous streams. These flows are laminar, which results in a well-defined interface between the two phases where interfacial forces can be carefully tuned by adjusting the operating parameters. Two main operating parameters are the total flow rate (TFR) of the two phases and

the flow rate ratio (FRR) between the two phases. Both parameters influence the width of the central stream, which is representative of the degree of hydrodynamic focusing. Since LNP formation is based on a reduction in lipid solubility at the interface between the two phases, the size and size distribution of the resultant LNP are dependent on diffusion, which is influenced by the degree of hydrodynamic focusing. Specifically, it was found that increasing the FRR can reduce the LNP size while attaining narrower size distribution, and higher TFRs resulted in larger LNPs only at low FRRs.

*Bifurcating and Baffle Mixers:* Motivated by the commercial success of SHM devices for the production of LNPs, Precision NanoSystems later introduced the NxGen, which is a micro-mixing architecture consisting of a sequence of bifurcating mixers for scalable, nonturbulent mixing.<sup>[88]</sup> Briefly, the organic and aqueous phases containing lipids and nucleic acids, respectively, are introduced from two pronged inlets that merge into a single flow. Downstream, a series of toroidal mixers promote chaotic advection to the merged stream. The stream initially splits upon entry into the first toroidal mixer and travels different path lengths before merging again. This process, which induces rapid mixing in a single layer by centrifugal force, is repeated a few more times leading to the formation of nucleic acid–LNPs with higher encapsulation efficiency and reproducibility compared to SHM. More importantly, it allows production rates to be increased by up to 25-fold. A similar architecture that operates based on a similar principle is the baffle mixer. In baffle mixers, the organic and aqueous phases are also introduced from two pronged inlets that merge into a single flow. However, instead of having a series circular, toroidal mixtures, it comprises sharp perpendicular turns to induce chaotic advection. Baffle mixers can produce LNPs with controllable sizes in the range of 20–100 nm, by varying the TFR, FRR, and device dimensions (Figure 4C).<sup>[89]</sup> Taken together, both bifurcating and baffle mixers are single-layer mixing architectures, which serve as excellent alternatives to SHM and HFF for LNP production.

Each of the abovementioned approaches has their advantages and limitations. For example, while the conventional method of lipid film hydration followed by extrusion is easy to perform, it is a time-consuming multistep production process with relatively low encapsulation efficiencies ( $\approx 40\text{--}60\%$ ). The crossflow injection method is highly suitable and is already in use for large-scale production in the industry but is less suited for laboratory-scale research. On the other hand, microfluidic-based approaches allow controlled mixing and generally result in relatively high encapsulation efficiencies. For example, the T-junction and HFF methods can produce uniform LNPs, has broad solvent compatibility and can achieve high encapsulation efficiencies ( $\approx 70\%$ ). The SHM method can produce highly uniformed particles with a polydispersity index of less than 0.1. In addition, the encapsulation efficiency of the SHM method is very high ( $>95\%$ ). However, due to the architecture of the mixture, SHM is prone to clogging within the channel. All microfluidic approaches require parallelization for scale-up (Figure 4D). Nevertheless, parallelization has shown to improve in vivo delivery for siRNA (Figure 4E) and mRNA (Figure 4F). In conclusion, compared to conventional preparation methods, the advent of microfluidics especially with the development of microfluidic mixing architectures has offered better control

over the production process of LNPs leading to LNPs with greatly improved physicochemical properties and encapsulation efficiencies. More importantly, microfluidics has paved the way for more rapid screening of LNP formulations and scale-up manufacturing, as well as the prospect of automated LNP synthesis.<sup>[90]</sup>

## 2.4. Applications

A better understanding of the structure–function relationship, as well as improvements in the design principles and platform development has enabled the exploration of LNPs for use in different clinical applications. Conversely, the promise of LNPs as delivery systems in certain applications has driven the refinement of their design principles and platform development. In the following subsections, we will review how two main applications, namely RNAi therapy and mRNA-based vaccines for COVID-19, have led to the progress of LNPs.

### 2.4.1. RNAi Therapy

The development of LNPs was originally motivated by RNA interference (RNAi) therapy.<sup>[91]</sup> RNAi refers to a fundamental cellular mechanism for silencing gene expression, which can be harnessed for reducing the expression of pathological proteins and therefore exploited as a novel therapeutic approach.<sup>[92]</sup> In brief, it relies on the specific binding and silencing of therapeutic targets by means of introducing siRNA molecules.<sup>[93]</sup> While the therapeutic mechanism is very promising since the approach can reversibly silence any gene, the effective delivery of siRNA proved to be challenging.<sup>[83b,94]</sup>

LNPs were developed as an alternative to viral vectors and represent the most advanced non-viral vector for gene delivery.<sup>[55c,95]</sup> Nevertheless, formulation optimization had to be conducted rigorously to achieve maximum siRNA encapsulation and transfection efficiencies.<sup>[55b,96]</sup> These studies had been largely facilitated by the advent of microfluidics.<sup>[17b,85,95,97]</sup> For example, Chen et al. demonstrated the utilization of controlled microfluidic formulation leading to the rapid discovery of potent siRNA–LNPs.<sup>[70]</sup> In the industry, the success of RNAi can be attributed to T-junction mixing, which enabled the production of stable siRNA–LNPs that are capable of potent knock-down of Apolipoprotein B (ApoB) in non-human primates.<sup>[83b]</sup> This is a prominent study as it represents one of the earliest reports highlighting the effectiveness of RNAi in a large animal study, revealing the significant reduction of ApoB mRNA and protein even beyond 10 days. Separately, Merck & Co. also adopted a similar approach by employing T-junction mixing to produce siRNA–LNPs targeting the murine gene Ssb.<sup>[83a]</sup> Likewise, they were successful in reducing the target mRNA levels in vivo by over 80%. Undoubtedly, microfluidic devices have proven beneficial for formulation optimization within the context of siRNA–LNPs, as they allow mixing of small amounts of reagents, which is ideal for screening lipid structures with minimal wastage. In addition, LNPs produced using microfluidic devices are typically smaller, and more uniform, than those produced via bulk preparation techniques. This has led

to the discovery of novel lipid structures for potent hepatic gene silencing *in vivo*. In addition, with the ability to carefully tune the mixing rates between the organic phase containing the lipids and the aqueous phase containing the nucleic acids, the size of the LNPs can be better controlled to understand the effect of LNP size to gene silencing performance. For example, the use of high flow rates to produce small LNPs corresponded to better gene silencing capability compared to the use of low flow rates, which produced large LNPs. All these advances are critical in the effort to overcome outstanding challenges in the delivery of LNPs. For example, while an siRNA–LNP formulation has been established and developed into an FDA-approved prescription medicine (i.e., known as patisiran and marketed as ONPATTRO, NCT02939820) to treat polyneuropathy in people with hereditary transthyretin-mediated amyloidosis, clinical trials led by Roche/Ionis Pharmaceuticals (NCT03761849) and WAVE Life Sciences/Takeda (NCT04617847 and NCT04617860) to explore similar approaches with LNP candidates for treating Huntington’s disease are ongoing.

#### 2.4.2. mRNA Vaccine for COVID-19

The translation of mRNA–LNPs to the clinic had been recently realized in the form of mRNA vaccines against COVID-19.<sup>[10a,36a,98]</sup> This development not only highlights the benefits of mRNA-based vaccines but also establishes the biocompatibility of LNPs as a delivery vehicle.<sup>[99]</sup> While the success accelerated by the COVID-19 pandemic was unprecedented considering there had been only one FDA-approved LNP-based siRNA drug (i.e., ONPATTRO) prior to that,<sup>[100]</sup> it was not entirely surprising considering an extensive amount of effort has been put in to understand the structure–function relationship and improve the performance of LNPs over the last decade. Such collective efforts have facilitated the quick adoption of LNPs, which was initially largely developed for siRNA, to incorporate mRNA payloads instead. As discussed in the previous sections, the evolution of design principles and platform development play critical roles in incrementally improving the design and manufacturing of potent LNPs, culminating in the maturity of the LNP-based delivery systems that meet the requirements of good manufacturing practice and safety. Key milestones that contributed to the realization of LNP-based mRNA vaccine include the introduction of ionizable lipids as well as the development of microfluidics and advanced micromixing architectures. In particular, microfluidic platforms that offer high degrees of parallelization for large-scale manufacturing (e.g., Precision NanoSystems’ NanoAssemblr platform) have played a pivotal role in ensuring the clinical success of mRNA–LNPs. In addition to the available COVID-19 vaccines (NCT04470427, NCT04368728, etc.), other LNP–mRNA vaccines against influenza (NCT03076385 and NCT03345043), Zika virus (NCT04064905), rabies virus (NCT03713086), and multiple other viruses are currently undergoing human clinical trials.

With the establishment of such platforms, LNPs containing mRNA as well as other types of nucleic acids continue to be explored for other therapeutic applications and following other routes of administration.<sup>[101]</sup> For example, Dahlman and co-workers recently optimized the formulation of LNPs so that

mRNA can be delivered to the lungs in the form of nebulized aerosols.<sup>[64b]</sup> Based on all the data gathered via a cluster-based screening approach, they found that PEG lipids are critical in attaining stable LNPs. Furthermore, nebulized mRNA delivery can be improved with the use of cationic helper lipids and a higher molar fraction of PEG, and more PEG is needed for formulations with cationic helper lipids than those with neutral lipids. The resultant LNPs optimized following their approach exhibited greater structural stability after nebulization, as opposed to LNPs designed for systemic delivery. In essence, their work demonstrated the possibility of adopting nucleic acid-based LNP delivery systems for developing therapeutic application following different routes of administration, at the same time revealed that formulations developed for systemic delivery cannot be simply adopted for inhalation, which underscores that the importance of formulation optimization.

### 3. Lipoplex

While LNPs are fabricated by direct coassembly of ionizable lipids, helper lipids, PEGylated lipids, sterols, and nucleic acids during solvent mixing, another intriguing lipid nanoarchitecture for delivery applications involves the aqueous-phase mixing of preformed liposomes with nucleic acids, termed “lipoplexes.” The lipoplex strategy evolved from early efforts<sup>[102]</sup> to encapsulate nucleic acids into liposomes composed of anionic and zwitterionic lipids through passive loading, which faced challenges such as low efficiency in terms of nucleic acid entrapment and delivery.<sup>[34a,103]</sup> Although negatively charged liposomes may reduce the leakage of contents with increased stability and protection, inefficient entrapment (ranging 2%–50% with the highest efficiency obtained by the freeze/thawing procedure<sup>[34a]</sup>) due to the repulsion between the membrane and nucleic acid was the major concern of encapsulation method.<sup>[104]</sup> To enhance interactions between liposomes and nucleic acids, cationic lipids have been utilized in order to facilitate electrostatic attraction with negatively charged nucleic acid molecules.<sup>[105]</sup> As a result, passive loading of nucleic acids into liposomal interiors is not required, and instead electrostatic interactions between liposome surfaces and nucleic acids spontaneously drive lipoplex self-assembly. The first lipoplex demonstrations utilized liposomes composed of cationic and zwitterionic lipids that were mixed with pDNA<sup>[106]</sup> or mRNA<sup>[107]</sup> and exhibited superior transfection efficiency (especially with RNA transfection yielding 100- to 1000-fold more) with less cytotoxicity compared to a polymer-based delivery vehicle, a diethylaminoethyl (DEAE)-dextran complex, that was tested in parallel.

Motivated by these pioneering studies, lipoplexes have emerged as a powerful platform technology that can potentially take a single liposome formulation and mix it with different, customizable nucleic acids to create distinct lipoplex options for various applications. Indeed, while LNPs incorporating ionizable lipids have demonstrated high practical utility for mRNA vaccine applications, lipoplexes have reached human clinical trials for applications such as cancer therapy.<sup>[108]</sup> Even so, there continue to be key issues related to the cationic lipid design along with paired neutral lipid choice, processing parameters,

and the corresponding influence on the nanoparticle's architecture and delivery functionality. In this section, we cover these design points and also discuss selected cases that directly compare the performance of LNPs and lipoplexes.

### 3.1. Nanoarchitecture Design Principles

#### 3.1.1. Lipid Composition

The composition of a lipoplex is defined by two lipid types: 1) cationic lipid and 2) neutral (helper) lipid. As with LNPs, in lipoplexes, cationic lipids mainly interact with nucleic acids while neutral lipids influence self-assembly properties and assist with conferring particle stability. A noteworthy distinction is that the majority of cationic lipids used in lipoplex formation are permanently charged, meaning that  $pK_a$  is larger than 8 (or without  $pK_a$ ), while a few cases feature slightly ionizable lipid-like characteristics (e.g., DC-Chol, DODMA, multivalent cationic lipids, etc. that are discussed below). Hence, the stability and efficiency of the complex are highly dependent on the neutral lipid choice and molar charge ratio (N/P, cationic lipid-to-nucleic acid ratio). It is also worthy to note that the transfection efficiency might vary depending on the cell types, and there are several comprehensive studies comparing commercially available transfection reagents such as Lipofectamine, RNAiMAX, and Lipofectin.<sup>[109]</sup>

**Cationic Lipid:** Cationic lipids incorporated in lipoplexes should be able to capture the nucleic acid, maintain stability before entry, facilitate cellular entry (via fusion or destabilization), and subsequently release nucleic acids in the target cell.<sup>[110]</sup> Lipid structures can be divided into three functional units consisting of a hydrophilic headgroup, hydrophobic tail, and linker, connecting the former two moieties. Modifying

each element can affect the stability (compaction with nucleic acid), disassembly, and phase behavior of the lipoplex, which have been extensively discussed.<sup>[111]</sup> Depending on the tail group, cationic lipids can be categorized into aliphatic chains or cholesterol-based derivatives while the majority of headgroups are composed of permanently positively charged, quaternary ammonium or amines and their derivatives (Figure 5).

The first cationic lipid used to form a DNA lipoplex was 1,2-di-*O*-octadecenyl-3-trimethylammonium propane (DOTMA), which is a double-chain quaternary ammonium with ether bonds. One of the major commercial transfection reagents, Lipofectin, is based on DOTMA/DOPE (1/1 mol%) composition and is recommended to deliver nucleic acids to endothelial cells.<sup>[112]</sup> Since then, several other related compounds with aliphatic chains were developed to improve transfection efficiency and reduce cytotoxicity. 1,2-dioleoyl-3-trimethylammonium-propane (DOTAP) with ester bonds,<sup>[113]</sup> dimethyldioctadecyl ammonium bromide (DDAB), and single-chain lipid, cetyltrimethyl ammonium bromide (CTAB), were subsequently utilized to fabricate lipoplexes while the most widely used cationic lipids have remained DOTMA and DOTAP.

Based on these lipids, various derivatives were also developed by replacing the methyl group with the hydroxyethyl group, leading to lipids such as 1,2-dioleoyl-3-dimethyl-hydroxyethyl ammonium bromide (DORIE) and 1,2-dioleoyloxypropyl-3-dimethyl-hydroxyethyl ammonium chloride (DORI) that demonstrated enhanced compaction of nucleic acids with lipids.<sup>[110b,111b]</sup> Aside from dioleoyl derivatives, dimyristoyl compounds were recognized later to display higher transfection efficiency, leading to the development of another commonly used cationic lipid, 1,2-dimyristyloxypropyl-3-dimethyl-hydroxyethyl ammonium bromide (DMRIE), which is currently used in clinical-stage lipoplex formulations together with DOTAP and DOTMA.<sup>[114]</sup>

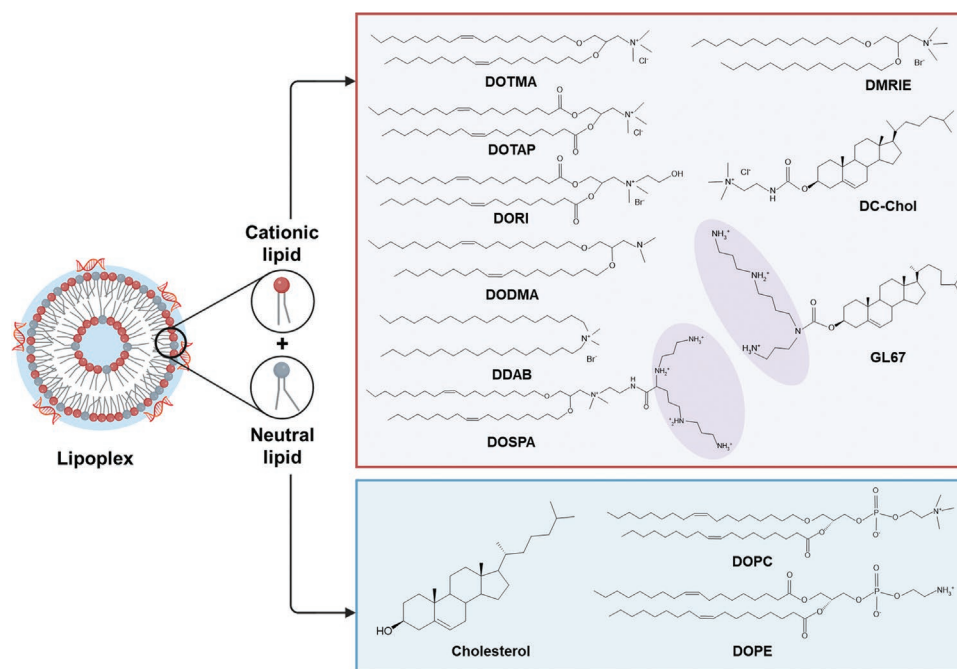


**Figure 5.** Lipoplex components and nanoarchitecture organization. Schematic illustration of the lipoplex and molecular structures of the cationic lipids and neutral lipids.



Furthermore, multivalent cationic lipids have gained attention by showing higher transfection efficiencies due to their ability to condense nucleic acids more tightly and to partially ionize to act as a buffer to better protect the nucleic acid from degradation compared to their monovalent counterparts.<sup>[115]</sup> For example, another widely used transfection agent, Lipofectamine, is based on polycationic 2,3-dioleyloxy-N-[2(sperminecarboxamido)ethyl]-N,N-dimethyl-1-propanaminium trifluoroacetate (DOSPA) and DOPE at a  $\approx 2.2:1$  molar ratio and is often considered a benchmark composition for evaluating transfection efficiency.<sup>[116]</sup> Another advantage multivalent lipids might confer is their high efficiency to capture nucleic acid with a lower amount of lipid (lower N/P) compared to the monovalent ones.<sup>[117]</sup>

On the other hand, cholesterol derivatives such as 3 $\beta$ -[N-(N',N'-dimethylaminoethane)carbamoyl]-cholesterol hydrochloride (DC-Chol) are another popular class of cationic lipids used in lipoplexes.<sup>[118]</sup> As cholesterol itself is commonly used as a neutral, helper lipid in lipoplex formation to increase membrane packing by embedding its bulky steroid moiety between hydrophobic tails of neighboring lipids, the addition of a cationic moiety in cholesterol derivatives was found to exhibit superior performance, enabling delivery of nucleic acids into various cell types in vitro and in vivo.<sup>[59b,119]</sup> Also, DC-Chol contains a carbamate linker and a tertiary amine with a relatively low pK<sub>a</sub> value (50% charged in buffer<sup>[120]</sup>) compared to other permanently charged lipids, providing higher biodegradability and aiding the efficient release of nucleic acid.<sup>[121]</sup> Due to these advantages, a DC-Chol and pDNA lipoplex formulation has been shown to exhibit low toxicity upon local or systemic administration and has entered clinical trials for the treatment of genetic disorders and cancer along with its multivalent derivative with spermine, N<sup>4</sup>-cholesteryl-Spermine (Genzyme lipid 67, GL67).<sup>[114b,122]</sup>

Typically, ionizable lipids used in lipid nanoparticle formulation possess apparent pK<sub>a</sub> less than 7 in order to exhibit positive surface charges at acidic (endosomal) pH while neutral charges at physiological pH. Abovementioned DC-Chol and 2-dioleyloxy-N,N-dimethyl-3-aminopropane (DODMA) possess pK<sub>a</sub> value around 8, offering pH-dependent nucleic acid and lipid interactions.<sup>[121,123]</sup> For example, DODMA molecules rearrange toward the hydrophobic region of the bilayer at high pH, offering an increased flip-flop rate that might affect the fusion process.<sup>[123]</sup> As ionizable lipids may offer more efficient endosomal escape by membrane rearrangement upon contact with anionic lipid membrane, there were several efforts to discover efficient ionizable lipids that can be used without a neutral lipid, leading to a development of a series of aminoglycoside derivatives that exhibit higher stability and smaller mean diameters compared to cationic lipid-based lipoplexes.<sup>[124]</sup> Other efforts include an ionizable lipid based on vitamin E-scaffolds<sup>[125]</sup> and  $\alpha$ -amino-lipophosphonates to target dendritic cells.<sup>[126]</sup>

**Neutral Lipid:** Neutral lipids have many useful functions as part of lipoplex compositions, including assisting with formation-related phase changes and reducing interparticle aggregation. While certain cationic lipids forming lipoplexes without neutral lipids can be functional to deliver nucleic acids, appropriate inclusion of neutral lipids such as DOPE and/or cholesterol can significantly improve the stability and the transfection

activity of lipoplex.<sup>[127]</sup> Thus, neutral lipids in lipoplex are also called “co-lipids,” functioning similarly to “helper lipids” in LNP excipients. Interestingly, the choice of neutral lipids might significantly enhance or hamper the transfection efficiency. For example, DOTMA,<sup>[106,110b]</sup> DOTAP,<sup>[128]</sup> and DC-Chol<sup>[129]</sup> have shown that the incorporation of DOPE largely augmented transfection efficiency whereas DOPC hampered the nucleic acid delivery both in vitro and in vivo.<sup>[130]</sup> These propensities are closely related to the geometry of lipids and in turn, the architectural configuration of lipoplex that will be more discussed in the next Section 3.1.2.

Cholesterol is another widely used neutral lipid<sup>[131]</sup> aiding colloidal stability of lipoplex and participating in membrane fusion by promoting contact sites for lipid mixing and expanding the pore induced by fusion.<sup>[132]</sup> Also, its inclusion in lipoplex has shown higher resistance to serum-induced aggregation and protein binding, which may explain enhanced transfection.<sup>[133]</sup> Indeed, a quantitative analysis performed by replacing DOTAP lipids with cholesterol (or DOPE) showed reduced affinity of negatively charged plasma proteins that might be responsible for protein corona formation.<sup>[134]</sup> Interestingly, the choice between cholesterol and DOPE may vary depending on the tail group of cationic lipid.<sup>[135]</sup> When various chain lengths of lipids were tested with an equimolar ratio of either cholesterol or DOPE inclusion, the highest effects were observed with saturated 14 carbon or 12 carbon chains, respectively, while both neutral lipids boosted the transfection efficiency compared to cationic lipid alone.<sup>[136]</sup> Therefore, it should be noted that the selection and optimum mole fraction of cationic and neutral lipid depend on the lipid types, possibly N/P charge ratio, types of nucleic acid, and cells.

### 3.1.2. Architectural Configuration

The architectural configuration of lipoplex is closely related to the phase behavior governed by several factors such as types of lipids, the composition of cationic lipids, and N/P charge ratio. Despite recent clinical achievements, the structure–activity relationship of lipoplex continues to be unraveled and functional optimization is often based on empirical approaches. To improve clinical performances, it is vital to understand the physicochemical properties affected by different parameters. The supramolecular structure of lipoplexes depends on the participating components' intrinsic properties such as their geometry and other environmental (extrinsic) factors as well as the balance between electrostatic interaction (headgroup) and repulsive force driven by hydrophobic domain upon the addition of nucleic acid.<sup>[137]</sup>

The most common structures are lamellar phase ( $L_c^c$ ) and inverted hexagonal phase ( $H_{II}^c$ ), which can also be referred to external and internal model, respectively, depending on the relative orientations of nucleic acid (**Figure 6A**).<sup>[138]</sup> Safinya pioneered early studies (and continue to explore more) of supramolecular structures of lipoplexes.<sup>[139]</sup> Initiated by applying the small-angle X-ray scattering (SAXS) technique to a mixture of two cylindrical-shaped lipids, DOTAP/DOPC lipoplex, a lamellar phase composed of multiple sheets of bilayers was discovered (**Figure 6B**).<sup>[140]</sup> SAXS measurements show that

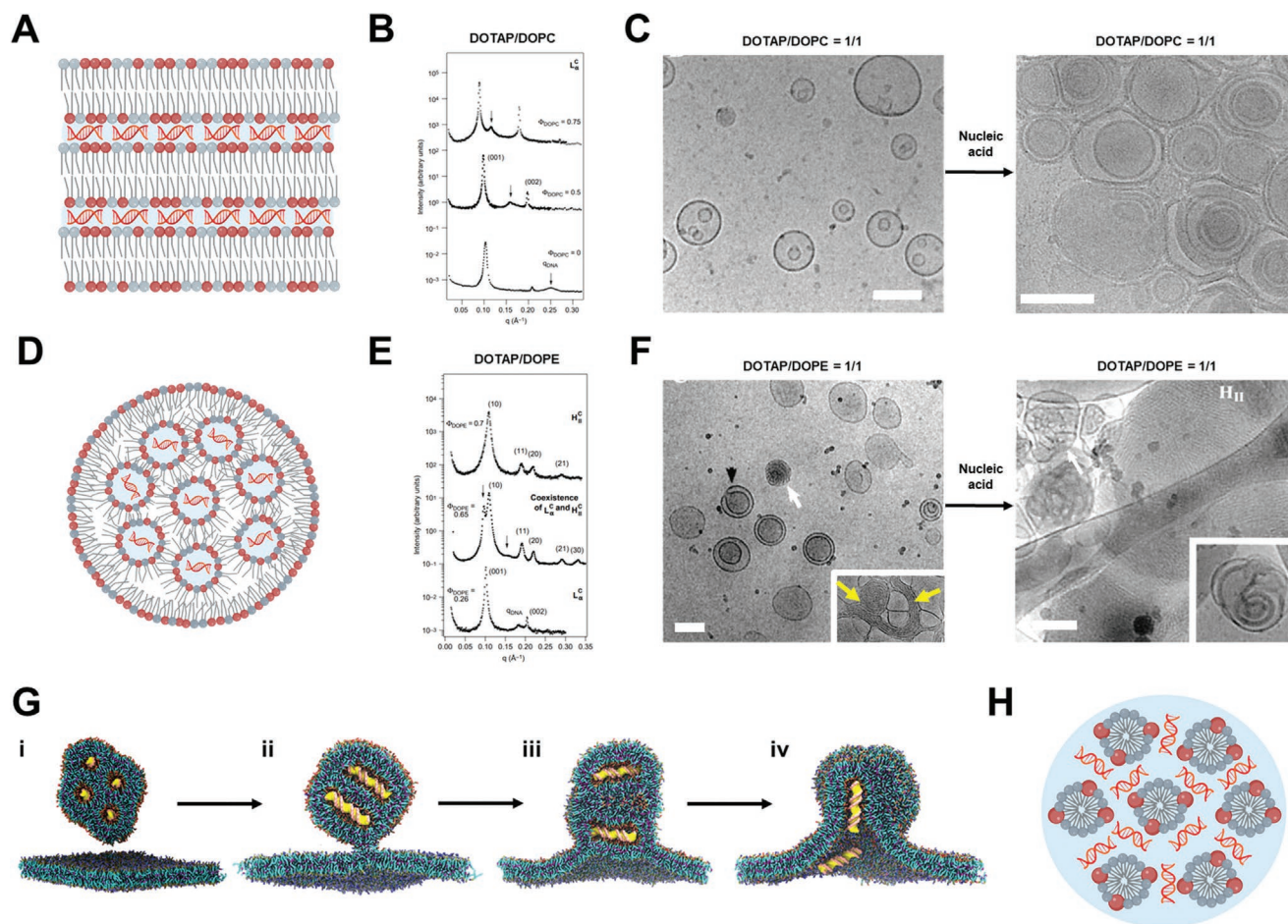


**Figure 6.** Architectural configuration of lipoplexes. A) Schematic of the lamellar phase ( $L_{\alpha}^C$ ) of DOTAP/DOPC lipoplex. B) SAXS scans of lipoplex at constant N/P charge ratio of 2.2 with increasing DOPC ratio. The arrows indicate the DNA peaks, whereby the spacing between DNA increase as the membrane charge density decreased. C) Cryo-EM images of DOTAP/DOPC lipoplex without/with nucleic acids. D) Schematic of the inverted hexagonal phase ( $H_{II}^C$ ) of DOTAP/DOPE lipoplex. E) SAXS patterns of the  $L_{\alpha}^C$  and  $H_{II}^C$  of lipoplexes with increasing DOPE ratio. F) Cryo-EM images of DOTAP/DOPE lipoplex without/with nucleic acids. G) Coarse-grained molecular dynamics simulations to visualize the fusion mechanism between lipoplexes and endosomal membrane: i) free lipoplex complexed with dsDNAs approaches the endosomal bilayer; ii) stalk formation upon initial contact; iii) hemifusion diaphragm; iv) membrane fusion with successful delivery of nucleic acids. H) Schematic of the hexagonal phase ( $H_{II}^C$ ) of lipoplex. B,E) Adapted with permission.<sup>[139]</sup> Copyright 2001, Elsevier. C,F) Adapted with permission.<sup>[130]</sup> Copyright 2001, American Society for Biochemistry and Molecular Biology. G) Adapted with permission.<sup>[146]</sup> Copyright 2020, eLife Sciences Publications Ltd.

the DNA monolayers are sandwiched between cationic membranes with an interlayer spacing of 6.4 nm ( $\approx 4$  nm of bilayer and  $\approx 2.4$  nm of water spacing with intercalated DNA) in an equimolar fraction case, and the spacing varied with the molar fraction of lipid molecules as the bilayer thickness changed due to the different length between DOPC and DOTAP.<sup>[139]</sup> Interestingly, the spacing between DNA was relevant to the membrane charge density as indicated by the arrows: the spacing increased as the membrane charge density decreased (increasing DOPC fraction). A cryo-EM image in the absence of DNA shows enclosed liposomes with an equimolar composition of DOTAP/DOPC (Figure 6C).<sup>[130]</sup> When the nucleic acid is added, these liposomes transform into a layered structure to accommodate nucleic acid molecules.<sup>[130]</sup>

Soon after verifying lamellar phase, the same group also identified inverted hexagonal phase ( $H_{II}^C$ ) when the inverted cone-shaped DOPE was included (Figure 6D).<sup>[141]</sup> With

increasing DOPE mole fraction in DOTAP/DOPE lipoplex from 0.26 to 0.70, SAXS scans showed that the internal structure of the DOTAP/DOPE lipoplex changes from  $L_{\alpha}^C$  to something else, which was defined as  $H_{II}^C$  with a diameter of  $\approx 2.8$  nm embedding DNA within a lipid monolayer arranged in a hexagonal lattice (Figure 6E).<sup>[139]</sup> Of note, when much smaller-sized siRNA is entrapped instead of DNA, the peaks in SAXS may appear less obvious (meaning less orientation) because of the higher disordered phase.<sup>[117]</sup> Cryo-EM analysis also showed that the distinct feature of equimolar DOTAP/DOPE with the coexistence of  $L_{\alpha}^C$  and  $H_{II}^C$  (Figure 6F).<sup>[130]</sup>

Although it is well known that particular  $H_{II}^C$  complexes (DOTAP/DOPE = 0.69) successfully delivered DNA, whereas similarly high fraction of DOPC-based lipoplex failed to deliver nucleic acids,<sup>[142]</sup> it should be noted that the architectural configuration of lipoplex and biological functionality cannot be directly correlated.<sup>[106]</sup> In other words, lipoplexes with  $H_{II}^C$  do

not always show higher transfection efficiency compared to the ones with  $L_{\alpha}^C$ , thus the phase is not a universal parameter to predict transfection efficiencies.<sup>[143]</sup> Also, the existence of serum can affect the outcome, in which membrane fusion is not a dominant factor, and lipoplexes with  $L_{\alpha}^C$  phase outperformed the others.<sup>[144]</sup> Some studies have reported that the morphological changes or phase transitions from  $L_{\alpha}^C$  to  $H_{II}^C$  upon lipoplex–cell membrane contact trigger better transfection efficiency, and a series of studies have attempted to optimize the cationic lipids by tuning their molecular structures.<sup>[145]</sup>

More recently, the interaction of lipoplex and negatively charged endosomal membrane has been computationally simulated, interrogating key parameters such as lipid types (different headgroups and the extent of chain length and saturation), endosomal membrane composition, and sizes of lipoplex.<sup>[146]</sup> By using this approach, two alternative fusion pathways were suggested (Figure 6G, perpendicular and parallel) with a possible endosomal membrane composition dependency. Also, an unsaturated chain in a cationic lipid was found to be necessary for effective membrane fusion. It was also simulated that larger lipoplexes ( $\approx 30$  nm) confer more thermodynamically stable self-assembled structures than smaller ones ( $\approx 20$  nm). For example, the highest amount of nucleic acid delivery was achieved for the unsaturated DOTAP/DOPE lipoplex compared to its saturated counterparts, which can be explained by the decreased bending modulus of unsaturated lipids to favor the fusion.

About a decade after the  $H_{II}^C$  report, continuous efforts revealed another representative phase called hexagonal ( $H^C$ ) structure based on dendritic cationic lipid/DOPC lipoplex that was highly efficient in in vitro transfection (Figure 6H).<sup>[147]</sup> Due to highly charged (16+) bulky headgroups of dendritic lipid, the complex forms long micelle-like structure to surround the nucleic acid. The improved efficiency was ascribed to the efficient packing of nucleic acid within lipoplex that can facilitate easier release of nucleic acid in cells. More recently, a concept of cuboplex has emerged, utilizing bicontinuous cubic phases (cubosome) made of glycerol monooleate (GMO), DOTAP, and GMO-PEG (97/2/1 mol%).<sup>[148]</sup> As marginal amount of cationic lipid inclusion suggests, the endosomal membrane interactions of cuboplex is not governed by electrostatics but by elasticity energetics, and possess intrinsic fusogenic properties to aid endosomal escape. Although cuboplex is largely different from conventional lipoplex composition, the development and structural characterization of this novel vehicle provide valuable insights how nanoarchitectonic approach can contribute to the advancement of lipid-based gene delivery technologies.

## 3.2. Platform Development

### 3.2.1. Lipoplex Manufacturing Considerations

One of the biggest advantages of lipoplex comes from the simplicity and flexibility of its fabrication, which takes two steps: 1) formation of cationic liposomes and 2) complexation with nucleic acid (Figure 7A). Liposomes can be prepared via traditionally known liposome production methods, ranging from simple rehydration of lipids, sonication, or ethanol injection; sophisticated monodisperse ones can be formulated by

extrusion and microfluidics. In this section, a few considerations while fabricating lipoplex (cationic liposome fabrication followed by nucleic acid complexation), their effects on functional activities, and the importance of N/P charge ratio are critically discussed.

### 3.2.2. Liposome Fabrication

Liposomes are sphere-shaped lipid vesicles consisting of one (unilamellar) or more (multilamellar) lipid bilayers. When amphipathic lipids are hydrated, hydrophilic headgroups face aqueous phase whereas hydrophobic tail groups orient or aggregate towards each other to form thermodynamically favored self-assembly structure. Therefore, the simplest liposomes can be fabricated by mechanically dispersing the lipid suspension in aqueous medium, which can be done by shaking or vortexing.

Largely, the preparation of methods can be divided into mechanical and organic solvent-assisted methods. Most of mechanical preparations start from lipid thin-film hydration as mentioned above, then subjected to further processing including sonication, freeze-thawing, and/or extrusion. Among them, sonication is the most used method to prepare liposomes for lipoplex formation even though its size distribution can be relatively larger than other processing methods.<sup>[149]</sup> From the first reported lipoplex fabrication to recent optimization studies, sonication has been widely used and proven effective even compared to other methods.<sup>[106,145b,150]</sup> For more homogenous and smaller unilamellar liposome production, freeze-thaw and/or extrusion can be applied after lipid hydration or after mild sonication. Freeze-thawing is adopted commonly to improve the encapsulation efficiency of molecules by expanding the inner water phase by ice crystal formation, which result in high population of unilamellar vesicles while physically disrupting the lamellar structure.<sup>[151]</sup> Extrusion can be accompanied to yield more homogenous particles, often using 200 nm filter to produce cationic liposomes. Ethanol injection is another widely used method to fabricate liposomes, which can be versatile and easy to scale up. In this method, the lipid–ethanol solution is injected into the aqueous phase (or vice versa), then ethanol is removed by rotary evaporation or dialysis to produce concentrated liposome suspensions.<sup>[152]</sup> The microfluidic method is a sophisticated improvement of ethanol injection that the mixing of organic and aqueous phases can be controlled by the interfacial diffusion of narrow microchannel, which has been described in the previous section. In lipoplex formation, microfluidics can be used in either fabricating initial liposomes or mixing nucleic acid with liposomes, which will be discussed in the next section.

Multiple studies have compared the transfection efficiency of lipoplex formulated from different methods, whereby the reason of one's performance is debatable whether it is due to the particle size and/or lamellarity, or other factors. Early studies have reported that the transfection efficiency is higher in large multilamellar liposomes (300–700 nm) formed by vortexing rather than in relatively smaller sized liposomes (<100 nm) formed by sonication (Figure 7B).<sup>[110b,120,153]</sup> Similar conclusion was drawn when the transfection efficiency of lipoplex was tested with or without serum as well.<sup>[154]</sup> On the other

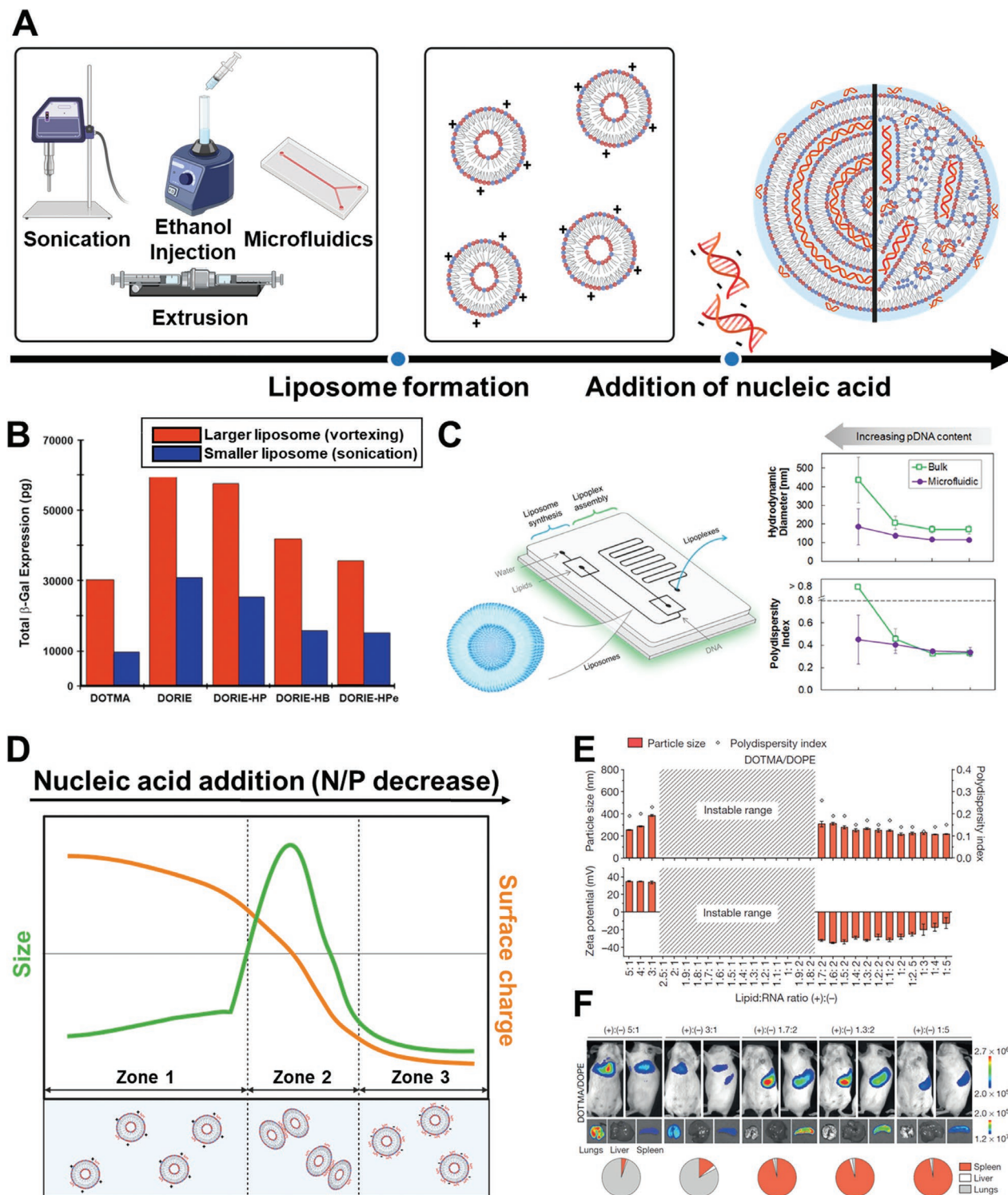


**Figure 7.** Platform development of lipoplex. A) Schematic illustrations of lipoplex formulation from cationic liposome formation to addition of nucleic acids. B) Comparison of transfection efficiency depending on the liposome preparation method. Vortexing and sonication were used to produce dominantly large multilamellar (red) and smaller (blue) liposomes, respectively. C) One-step formation of lipoplex assisted by a microfluidic device. The graph (right) shows the hydrodynamic diameter and polydispersity index of microfluidic-obtained and bulk mixing-prepared lipoplexes. D) Schematic representation to show that the N/P charge ratio largely affects the colloidal stability of lipoplexes, which can be presumed by their particle size (green line) and net surface charge (orange line). E) Lipoplexes formulated at various N/P ratios display a distinct instable range around N/P = 1, whereby the zeta potential is close to neutral. F) Bioluminescence imaging of BALB/c mice after intravenous administration of Luc-RNA-lipoplexes from panel E) at various N/P charge ratios. B) Adapted with permission.<sup>[135]</sup> Copyright 2010, Springer Nature. Panel C schematic is adapted with permission.<sup>[173]</sup> Copyright 2017 Elsevier. Panel C graph is adapted with permission.<sup>[165b]</sup> Copyright 2016 American Chemical Society. E,F) Adapted with permission.<sup>[169]</sup> Copyright 2016, Springer Nature.

hand, ethanol injection method was reported to be equally or more effective than the dry-film method<sup>[155]</sup> and its efficiency proven in human clinical studies.<sup>[99d,156]</sup>

### 3.2.3. Nucleic Acid Complexation

During the formation of lipid-nucleic acid complex, the nucleic acid electrostatically binds to the cationic lipid by fast exothermic process, then subsequently rearrange/fuse into lipoplex by slower endothermic reaction.<sup>[157]</sup> While the first fast regime occurs instantly when the lipid and nucleic acid contact, the kinetics of slow rearrangement and fusion-induced growth of lipoplexes largely depend on the mixing protocol. The mode of mixing can vary by the sequence of adding components and whether the addition is bulk (one-step mixing by pipetting or vortexing) or titration (more than two steps). In permanently charged cationic lipid, the complexation solution conditions are generally maintained at physiological pH or in deionized water to facilitate strong electrostatic interactions between nucleic acid and lipids. Whereas excess electrolytes can shield and decrease the driving force of self-assembly of lipoplex when there was significant differences (1.5 M and 0.15 M),<sup>[158]</sup> a direct link between transfection efficiency and solution conditions during the formation of lipoplex (mild salt concentrations or deionized water) remains controversial.<sup>[114b]</sup> However, in the cases of pH-responsive lipids such as DC-Chol and DODMA, slightly acidic or neutral buffer solution is preferred over deionized water to increase the payload and transfection efficiency.<sup>[159]</sup>

One of the first studies comparing the order of addition of nucleic acid and lipids was reported by Zelphati et al. that the small, stable lipoplexes could be formed at high N/P charge ratio (which will be explained in the next section) by bulk-adding the nucleic acids into the excess of liposomes while the opposite order produces large aggregates.<sup>[160]</sup> At low N/P charge ratio, the trend was reversed such that the addition of liposomes to the excess of nucleic acid could produce stable lipoplexes. This observation could be explained by titration approach.<sup>[161]</sup> During the nucleic acid addition into liposomes (in excess), nucleic acids come into contact with multiple liposomes, associating at the interface of two (or more) liposomes at once. This interaction may generate asymmetrical stresses, leading to rupture and aggregation of the lipoplex. In the opposite case when the liposome is added, the excess nucleic acids rapidly bind and wrap the surface of the cationic liposomes, forming a relatively stable complex until a critical point where liposomes bind to other ones that are already coated with nucleic acid. Then, the aggregates start to form, and the generated stress drives the rupture and growth of the particles. The former case might produce too large particle that can limit the transfection efficiency, but the latter case could inhibit the intimate lipid mixing and necessary structural rearrangements.<sup>[111a,162]</sup> Likewise, small variations in each step can result in largely different self-assembled structure, thus care should be taken during formulation and optimization of lipoplex preparation. Of note, an optimal mixing method might vary depending on the nucleic acid types and concentration as well. For example, vortex-mixing resulted in better transfection efficiency than spontaneous mixing

when the siRNA concentration was higher than a certain point whereas the opposite was true when N/P charge ratio was high.<sup>[163]</sup>

After presenting that the order of mixing can be a critical parameter influencing the complex behavior, Zelphati et al. from the same study proposed a controlled mixing method to mix both components simultaneously at a fixed ratio/speed with the aid of a syringe pump.<sup>[160]</sup> The optimal mixing rate was higher for the smaller liposomes, whereby the results were reproducible and more homogenous lipoplexes could be formed. This controlled mixing was further developed recently via microfluidics to formulate the liposome as well as to complex with nucleic acids.<sup>[164]</sup> This method has demonstrated potential for controlling physical properties of liposomes including size distribution and lamellarity in precisely confined microenvironment. Compared to the bulk mixing method, microfluidics generated lipoplexes with more homogenous and smaller sizes (Figure 7C).<sup>[145a,165]</sup> This feature might explain higher transfection efficiency in some cases, whereby about half number of stacked bilayers were needed (reduced amount of cationic lipid) to incorporate the same amount of nucleic acid.<sup>[165b]</sup>

Lastly, it is worthy to note that generalizing the effect of lipoplex size by comparing different literature should be avoided because multiple parameters involve in the final resulting aggregates such as lipid compositions, N/P charge ratio, nucleic acid, and reported transfection efficiency might vary a lot depending on the cell lines as mentioned above.<sup>[109c]</sup> Nevertheless, large lipoplexes (up to a certain extent) feature wide range of contact area with cells and tend to form large intracellular vesicles after endocytosis, which are more susceptible to release the nucleic acid.<sup>[144,166]</sup> Consequently, the transfection efficiency also depends on whether a particular cell dominantly uptake particles by endocytosis.<sup>[144]</sup> While most of the mentioned studies were conducted in vitro, the physicochemical properties of lipoplex might be more pronounced in the in vivo experiments because cellular uptake of nanoparticles is strongly dependent on their size and surface charge.<sup>[167]</sup> Generally, the mean diameter of lipoplex particles that have entered clinical trials ranged 100–500 nm.<sup>[114b]</sup>

### 3.2.4. Charge Ratio (N/P)

The charge ratio (N/P) denotes the molar ratio between cationic moieties, such as protonatable nitrogen (N) atoms of the lipid headgroup, and the anionic charges brought by the phosphate (P) groups of the nucleic acids. Theoretically, N/P = 1/1 will result in the net charge of 0 but usually this point can be achieved empirically by a slight excess of either negative (nucleic acid) or positive charges (cationic lipid) due to steric hindrance and/or other geometrical constraints.<sup>[168]</sup> As N/P is the most easily tunable and dominant factor that directly affects the colloidal stability of the complex, examining its effect on colloidal stability is a prerequisite to optimize lipoplex formula.

From a functional perspective, too low N/P increases uncomplexed nucleic acid,<sup>[169]</sup> but too high N/P leads to increased cytotoxicity due to excess cationic lipids as mentioned above. With respect to stability, there are three main regimes depending on the N/P (Figure 7D,E). Starting from higher N/P (low amount

of nucleic acid), most particles are positively charged and repel each other because the population is dominantly cationic with a small part of lipoplexes. Upon adding more nucleic acid, lipoplexes become near to neutral surface charge (see zeta potential measurement) such that they start to aggregate because of colloidal instability.<sup>[160]</sup> With increasing nucleic acid, the lipoplex reaches again colloidal stable structure that is negatively charged with some uncomplexed or not sufficiently condensed nucleic acid molecules surrounding the particle.

The optimal N/P charge ratio might vary depending on the lipid choices and respective applications, ranging from >10 for monovalent cationic lipids such as DOTMA to less than 1 for multivalent GL67 or several DNA-complexed cases.<sup>[114b,170]</sup> Although negatively charged regime is often regarded as less effective considering the anionic cell membrane,<sup>[131a]</sup> in vivo studies have reported that Luc expression was predominant in the lungs of mice when the particle is positively charged whereas the gradual increase of nucleic acid can shift the targeted organ to the spleens (Figure 7F).<sup>[169,171]</sup> Interestingly, not only the lead composition of DOTMA/DOPE, but also other combinations of lipids including cholesterol and DOTAP have led to exclusive targeting of spleen when the lipoplex was negatively charged, prompting the selection of N/P = 0.65 condition for clinical testing.

To conclude the manufacturing considerations with perspective of scalable production, lipoplex-based gene delivery features a simple preparation step for liposome and a flexible choice of nucleic acid that can be complexed without aids of sophisticated devices or specific skills. All liposome production methods have been established in depth, and fabrication methods except for microfluidics are quite straightforward and widely available, allowing us to scale-up the liposome manufacturing and to easily combine with commercially established protocols for nucleic acid production. Therefore, the flexibility regarding nucleic acid choice comes as a major advantage in utilizing lipoplex in “on demand” situations such as imminent viral outbreaks or personalized production of gene delivery vehicle.<sup>[168a]</sup> Furthermore, the qualities of liposome and nucleic acid can be separately screened prior to complex formation, which can minimize the contamination and enhance the batch-to-batch reproducibility with lower cost.<sup>[172]</sup>

### 3.3. Current Applications and Future Possibilities

#### 3.3.1. Cancer Vaccines

There has been intense interest in developing lipoplex as a vaccine that stimulates targeted immune response to treat cancer. Toward this goal, antigen-presenting cells such as dendritic cells (DCs) are ideal targets of lipoplexes to boost the immune response. Among the pioneering works, intravenously administered nonfunctionalized DOTAP/DOPE lipoplex has been developed for systematic targeting of DCs.<sup>[168a,169]</sup> The administration of lipoplex induced both adaptive and innate immune responses via antigen-encoding RNA.<sup>[169]</sup> Importantly, this study highlights that surface charge-dependent organ-targeting is achievable by simply tuning the N/P charge ratio. The site-specific RNA expression from lungs to spleen was achieved

when the N/P was 5–3 and 0.85–0.2, respectively (Figure 7F),<sup>[169]</sup> which is distinguishable from targeting function of neutral LNP mainly to hepatocytes.<sup>[174]</sup>

Additionally, lipoplex has been used as a vaccine specifically for treating melanoma with various nucleic acids such as pDNA or RNA.<sup>[99d,122b,175]</sup> For example, multiple nonmutated, tumor-associated antigens were targeted by intravenously administered melanoma FixVac (BNT111-mRNA)-DOTMA/DOPE lipoplex, leading to the elevated cytokines such as IFN- $\alpha$ ,  $\gamma$ , IL-6 with ex vivo CD8<sup>+</sup> T-cell responses across different cancer types.<sup>[108]</sup> On the other hand, OVA-encoding mRNA-DOTAP/DOPE lipoplex induced a potent type I IFN response upon subcutaneous, intradermal, and intranodal injection, interfering with the generation of potent cytolytic T-cell responses.<sup>[176]</sup> When the antitumor effect of mRNA-DOTAP/DOPE lipoplex was compared with pDNA-lipoplex, mRNA-lipoplex showed higher lipofection efficiency than pDNA one.<sup>[177]</sup> Thus, mRNA-DOTAP/DOPE lipoplexes demonstrate great potential to treat cancer including melanoma in the context of cancer immunotherapy, gene, and vaccine therapy. Indeed, several human clinical studies are ongoing with lipoplex vaccines to treat melanoma (NCT02410733, NCT03897881, and NCT03480152), breast cancer (NCT02316457), advanced esophageal cancer and (non-small cell) lung cancer (NCT03908671), or multiple tumors including pancreatic, colorectal and lung cancers (NCT03948763), whereby the lipoplex carriers include DOTAP/DOPE or DOTMA/DOPE compositions or a proprietary RNAiMAX composition. Both intravenous and subcutaneous administration routes have been utilized for lipoplex administration while emerging evidence shows that the administration route can critically determine whether mRNA-lipoplexes stimulate or inhibit type I interferon (IFN) immune responses based on a recent in vivo mouse study.<sup>[178]</sup> Promoting strong immune responses should also be balanced with safety considerations, highlighting the potential of lipoplexes along with important translational needs for refining vaccination regimens and advancing mechanistic understanding of how administration route and dosing relate to immune responses.

#### 3.3.2. Infectious Disease Vaccines

Likewise, lipoplexes can be utilized as a vaccine for infectious disease such as immunodeficiency syndrome caused by human immunodeficiency virus (HIV). Similar to the immunotherapy for cancer, DOTAP/DOPE lipoplex carrying mRNA encoding Gag protein modulated DCs to stimulate HIV-specific immune responses.<sup>[179]</sup> The same lipoplex system with HIV-1 antigen Gag-encoding mRNA produced antigen-specific functional T cells in spleens and lymph nodes, together with the immune-activation characterized by the release of type I IFN.<sup>[180]</sup> Another inspiring example includes the parallel evaluation of lipoplex and LNP entrapping HIV-1 Env-encoding saRNA to compare the transfection efficiency in vitro (Figure 8A) and in vivo.<sup>[172]</sup> Strikingly, immunogenicity comparison of both formulations resulted in a distinctive trend that the cationic lipid-based lipoplexes (DDAB rather than DOTAP) achieved the maximum response of HIV IgG titers after a single dose whereas all LNPs showed the enhanced antibody response only after the second

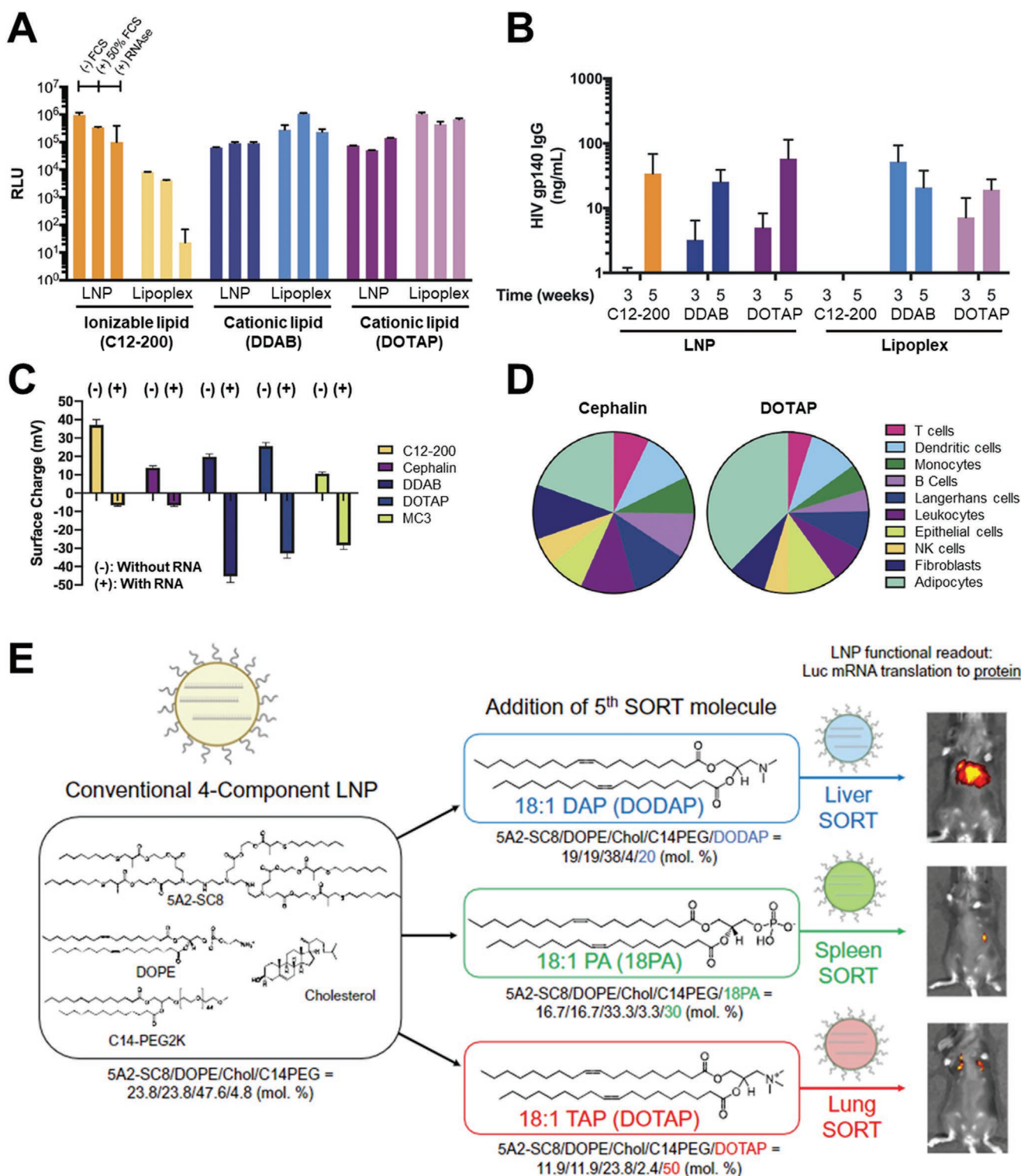


**Figure 8.** Possibilities of tuning the lipid compositions in conventional lipoplex or LNP compositions. A) Transfection efficiency of Luc-saRNA delivered by LNP/lipoplex under standard conditions without FCS (–) FCS), with FCS (+) 50% FCS), or with RNAse (+) RNAse). B) Immunogenicity measured by antibody titers after IM injection of HIV-1 Env saRNA complexed to the LNP/lipoplex. C) Zeta potential measurements of mRNA lipoplexes with varying complexing lipids. D) Total protein expression mediated by C) lipoplexes within different cell subtype. E) Schematic representation showing selective organ targeting (SORT) strategy for tissue-specific nucleic acid delivery by adding different net charged lipid molecules to aim specific biodistribution. A,B) Adapted with permission.<sup>[172]</sup> Copyright 2019, Springer Nature. C,D) Adapted with permission.<sup>[185]</sup> Copyright 2021, Elsevier. E) Adapted with permission.<sup>[38]</sup> Copyright 2021, National Academy of Sciences.

injection (Figure 8B). This proof-of-concept study highlights the potential usage of cationic lipids with adjuvant properties such as enhancing humoral immune response and immunostimulatory effects *in vivo*.<sup>[181]</sup>

Recently, DNA-lipoplex vaccine was also developed for the treatment of SARS-CoV-2 utilizing saturated neutral lipid (DOTAP/DOPE/DPPC = 1/1/2 mol%) and low N/P charge ratio of 0.25 with highly negative net charge.<sup>[170a]</sup> The study selected intramuscular (IM) injection method and has proven its effective spike protein expression, neutralizing antibody responses, and T-cell activation comparable to the parallelly tested gold standard, intramuscular electroporation method. Similar trend was reported in the efforts to develop malaria surface protein-encoded pDNA-lipoplex vaccine (equimolar DOTAP/cholesterol), whereby the N/P of 0.33 (anionic) lipoplex performed higher immunogenicity in mice compared to the N/P of 3.33 (cationic) one when it was administered IM.<sup>[170b]</sup> In both cases with DNA-lipoplex, higher N/P triggered increased cytotoxicity while lower N/P displayed higher transfection, presumably because of the more efficient release of DNA from negatively charged lipoplexes (lower N/P) compared to the higher ones. Considering that DNA-based drugs can be stored at 2–8 °C for a few years and room temperature for 1 year,<sup>[182]</sup> efficient entrapment of DNA using lipoplex can improve the availability of the vaccine, avoiding costly frozen-state supply chain for existing mRNA vaccines.<sup>[183]</sup>

### 3.3.3. Lipid Nanoparticles versus Lipoplexes: Which One Is Better?

As the formulation and concept of LNP and lipoplex are distinctive, it is an immediate point of inquiry to consider which one works better and under what conditions. However, there have been a few direct comparison studies to address this point. In one example, Kubota et al. evaluated cationic lipid-based LNP and lipoplex in conventional LNP composition (DODMA/DSPC/cholesterol/PEG-lipid = 50/10/38.5/1.5), using ethanol mixing and extrusion (50 nm-filtered), respectively, to compare their physicochemical properties as well as biological functionalities including particle characterization, transfection efficiency, and inflammatory cytokine response.<sup>[184]</sup> While both particles showed the maximum size at N/P = 5, lipoplexes were only slightly larger than LNP with ≈15 nm margin (117 and 100 nm, respectively), which was probably attributed to the addition of PEG lipid and DODMA with low  $pK_a$  that could be verified again by unilamellar structure of lipoplexes observed by cryo-EM images. While cellular uptake efficiency and inflammatory cytokine responses indicated LNP is more compatible with the given cell line, it should be noted that the selected composition was ideal for LNP formulation and not for lipoplexes as the entrapment mechanism of the latter one is mainly governed by electrostatic attraction on surface.

On the other hand, Blakney et al. have fabricated both ionizable and cationic lipid-based LNP and lipoplex with a conventional lipoplex formula (complexing/neutral lipid = 35/65 mol%) to characterize physicochemical properties and biological activities.<sup>[172]</sup> Although both liposomes and LNPs were produced by microfluidics, all resulted particle sizes ranged 100–200 nm, which are quite larger than typical LNPs,

postulating that the self-assembled structure of LNPs formed here is different from the one from classical composition with PEG lipids. Only ionizable lipid-based lipoplex showed negative surface charge, reflecting incompletely coupled saRNA due to the ionization of the lipid at physiological pH on surface, which later significantly affected the susceptibility to degradation, and lower transfection *in vitro* as well as *in vivo* (Figure 8A). Conclusively, the overall functionality was the highest from ionizable lipid (C12-200) and cationic lipid (DDAB rather than DOTAP in this case) in LNP and lipoplex, respectively, confirming that the optimization strategy of entrapping nucleic acid should be distinguished between LNP and lipoplex platform.

For further study, the same group has formulated lipoplexes by varying complexing lipids from cationic to zwitterionic or ionizable lipids (complexing/neutral lipid = 1/1 mol%) to intradermally deliver mRNA in human skin explants and evaluated the effects of complexing lipids on cellular uptake and expression.<sup>[185]</sup> Intriguingly, the combinations with zwitterionic (cephalin) and ionizable lipids (C12-200 and MC3) could also successfully entrap nucleic acid (complexation efficiency > 80%) with varied extent of negative zeta potentials (Figure 8C). Surprisingly, the differences in the surface charge after forming lipoplex were strongly correlated with the pattern of nucleic acid uptake and expression among cell types (Figure 8D), not the inherent lipid types classified (i.e., cationic/zwitterionic/ionizable lipids). For instance, cellular uptake depending on the cell types shared similarities among moderately charged cephalin and DDAB lipoplexes, whereas highly charged DOTAP and MC3 lipoplexes were expressed in different distributions of cells within skin explants.

Another example includes recent efforts on developing selective organ targeting (SORT) lipid nanoparticles designed to deliver nucleic acid to specific organs such as lungs, spleens, and livers by tuning the membrane charge of the composition.<sup>[38,171]</sup> Based on conventional LNP composition (ionizable lipid/DOPE/cholesterol/PEG-lipid = 5/5/10/1 mol%), ionizable (cationic) lipids, anionic lipids, and permanently charged cationic lipids were supplemented, and the result clearly indicated that the respective inclusion of particles delivered mRNA to the liver, spleen, and lungs after IV injection (Figure 8E).<sup>[38]</sup> This distinctive tissue-targeting property was derived from the recognition, affinity, and adsorption of specific serum proteins toward particle's surface charge/composition.<sup>[38]</sup> These findings strongly support the nanoarchitectonic design strategy of lipid self-assemblies that can be adopted to engineer optimized lipid-based nucleic acid delivery vehicles.

## 4. Lipid Bicelles

While lipid bicelles were originally invented as suitable membrane-mimetic environments to reconstitute membrane proteins for structural biology studies,<sup>[186]</sup> they have also emerged as promising tools for biotechnology applications such as drug delivery,<sup>[187]</sup> antibacterial medicine,<sup>[188]</sup> and lipid bilayer coatings.<sup>[189]</sup> To date, LNPs and lipoplexes are the most advanced types of lipid-based nanoparticles for nucleic acid delivery applications, but there is growing attention to lipid bicelles. Compared to the typical spherical geometry of LNPs and lipoplexes,



bicelles have a wider range of possible geometries, including a disk-like shape in some cases that can be advantageous for tissue penetration and cellular uptake. As such, lipid bicelles represent a promising frontier for lipid-based nanoparticles for nucleic acid delivery applications and are covered in this part.

#### 4.1. Nanoarchitecture Design Principles

Bicelle morphology depends on a wide range of factors and controlling pertinent parameters such as lipid concentration, molar ratios, and temperature can enable rational control over nanoarchitecture features. In this section, we begin by introducing the self-assembly principles of bicelles and relevant considerations related to morphology and lipid geometry, before expanding our coverage to more advanced functionalization concepts that enhance bicelle stability.

##### 4.1.1. Self-Assembly Principles

It is widely appreciated that long-chain phospholipids self-assemble to form liposomes in aqueous solution whereas detergents self-assemble into micelles.<sup>[190]</sup> Interestingly, new morphological phases emerge when long-chain phospholipids and detergents are mixed together and this original discovery gave rise to the “bicelle” concept.<sup>[191]</sup> Practical utilization of bicelles was further advanced by recognizing that short-chain phospholipids can behave as detergent-like molecules and hence it is possible to form bicelles using phospholipids only.<sup>[192]</sup> The molar ratio of long-chain phospholipids to short-chain phospholipids is defined as the *q*-ratio and strongly influences bicellar phase properties.<sup>[193]</sup> Depending on the lipid

composition and *q*-ratio, bicelles can form a wide range of morphologies, including multilamellar vesicles, toroidal pore complexes, extended lamellae, chiral nematic ribbons, disk-shaped nanostructures, and spherical micelles<sup>[194]</sup> (Figure 9A).

While the phase properties of bicelles are complex and depend on various parameters such as lipid concentration, ionic strength, and temperature, it is possible to control them, and we turn our attention to the case of disk-like bicelles that form in certain conditions. The self-assembly of bicelle disks can be rationalized by considering the geometrical properties of the different lipid components, as depicted in Figure 9B,C. In general, lipid molecules have a hydrophilic headgroup and one or more hydrophobic alkyl chains. For short-chain phospholipids, the headgroup is relatively large compared to the two short chains and hence the geometry is cone-like. A similar conical geometry is also found for typical detergent molecules. As such, short-chain phospholipid and detergent molecules tend to pack in high-curvature regions. On the other hand, long-chain phospholipids usually have a more cylindrical appearance because the headgroup and two long chains are more similar shape wise. It is therefore more energetically favorable for long-chain phospholipids to reside in planar regions. For these reasons, upon mixing of lipid molecules in bicelle compositions, the overall self-assembly process is driven by hydrophobic interactions and the different types of lipids are preferentially organized into distinct bicelle regions. Indeed, due to the curvature-related energetic preferences, short-chain phospholipids and detergents have low miscibility with long-chain phospholipids<sup>[195]</sup> and the cone-like and cylinder-like molecules tend to self-assemble into the disk edges and central planar region, respectively.<sup>[196]</sup> An interesting case concerns the use of headgroup-functionalized, long-chain phospholipids such as PEGylated lipids. Due to the increased size of the headgroup

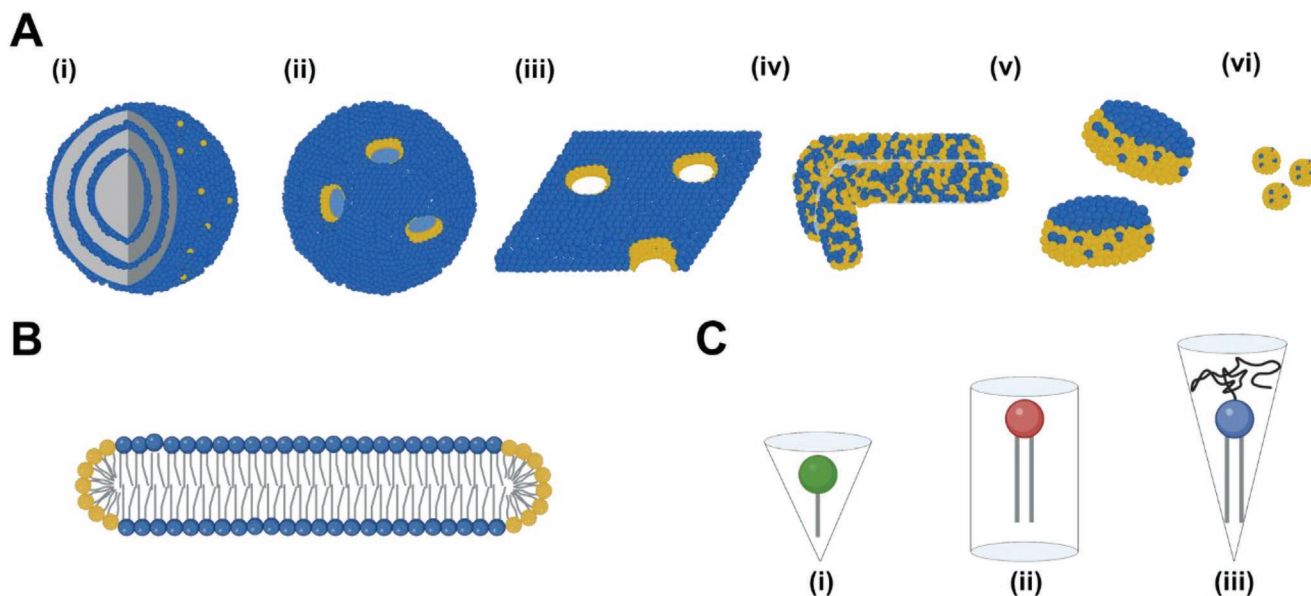


**Figure 9.** Lipid bicelle concept and molecular building blocks. A) Schematic illustrations of different bicelle morphologies that can form depending on molecular components and experimental conditions as follows: (i) multilamellar vesicles; (ii) toroidal pore complexes; (iii) extended lamellae; (iv) chiral nematic ribbons; (v) disk-shaped nanostructures; and (vi) spherical micelles. B) Cross-sectional view of a bicelle disk that is composed of long-chain and short-chain phospholipids. C) Molecular geometry of different molecular building blocks, including (i) detergents and short-chain phospholipids with cone-like geometries, (ii) long-chain phospholipids with cylinder-like geometries, and (iii) PEGylated phospholipids with cone-like geometries.

in such cases, PEGylated lipids can assume a more cone-like appearance than typical long-chain phospholipids and may locate in the edge and/or planar regions of a bicelle disk.<sup>[197]</sup>

There are also a few practical points to highlight: 1) the  $q$ -ratio must be within a certain range to form bicelle disks while other morphologies can form in different  $q$ -ratio ranges;<sup>[198]</sup> 2) the planar region of bicelle disks can present a membrane-mimicking environment, especially in cases where biologically relevant phospholipids are used. In certain cases, phospholipids and cholesterol can both be incorporated in the planar region and can form phase-separated domains in some cases;<sup>[199]</sup> 3) bicelle preparation should take place at a sufficiently high temperature so that all lipid components, especially the long-chain phospholipids, in the mixture are in the fluid phase.<sup>[194]</sup> The fabricated sample can then be cooled down afterward; and 4) the specific morphology of bicelles is highly sensitive to the specific phospholipids used in a mixture and the corresponding phase diagram must be carefully considered in each particular case. For example, including saturated or unsaturated lipids in bicelle compositions can cause wide variance in the phase diagram and possible morphologies<sup>[200]</sup> (for some compositions, the disk morphology is not possible), and similar attention must be placed on charged lipids which are sometimes added to enhance bicelle stability but can also affect possible morphologies.<sup>[201]</sup>

#### 4.1.2. Advanced Functionalization Strategies

There have been various functionalization strategies introduced into bicelle nanoarchitecture designs in order to improve performance and enable new application opportunities. One direction has focused on improving bicelle stability to prevent coalescence and to inhibit the structural transformation of bicellar disks into vesicles over time, especially at higher temperatures. Charged lipids such as negatively charged phosphatidylglycerols (PG) have often been incorporated into bicelles and prevent bicelle coalescence due to charge repulsion.<sup>[202]</sup> Inspired by other classes of lipid-based nanomedicines, researchers have also added PEGylated lipids such as distearoyl phosphoethanolamine-[methoxy (polyethyleneglycol)-2000] (DSPE-PEG2000) to further improve bicelle stability and reduce uptake by the reticuloendothelial system, potentially enabling increased circulation time in vivo. For example, it is possible to form disk-like bicelles in the presence of 5 mol% PEG2000-DSPE, which can enhance bicelle stability due to steric hindrance of the PEG chains.<sup>[203]</sup> While PEGylated lipids have a mainly cone-like geometry, more detailed structural studies have shown that a neutral PEGylated lipid (C16-PEG2000-ceramide) can distribute across both the planar region and rims of bicellar disk. Of note, there is indeed an approximately, two-fold greater density of PEGylated lipids in the rims,<sup>[197]</sup> however, it should also be noted that the broader distribution of the PEGylated lipid is advantageous for potential in vivo applications. In molecular dynamics simulations, it has also been shown that bicelles containing ligand-modified PEGylated lipids are more easily internalized by cells than similarly functionalized liposomes due to more favorable membrane energetics<sup>[204]</sup> (see also other examples of bicelles with improved cellular uptake properties over liposomes<sup>[205]</sup>).

Other efforts have explored how to create inorganic–organic hybrid bicelles based on mixing short-chain phospholipids and long-chain organoalkoxysilane lipids (termed cerasome-forming lipids, CFL).<sup>[206]</sup> After lipid hydration, the bicelles were incubated overnight at room temperature, during which time a sol-gel reaction occurs between the alkoxysilyl headgroups of the long-chain lipid molecules and results in a crosslinked siloxane network (a silica-like coating). The hybrid bicelles had typical diameters and heights of around 40 and 4 nm, respectively, and retained their structural morphology in the air environment upon drying. Whereas conventional bicelles transformed into vesicles at high temperature, the hybrid bicelles also maintained their disk-like nanostructures at high temperature.<sup>[207]</sup> Based on these advantageous properties, there have been efforts to develop partially silica-coated bicelles by mixing short-chain phospholipids with CFL and PEGylated lipids (DSPE-PEG2000). With increasing DSPE-PEG2000 lipid fraction, there was improved release of a small-molecule drug and the PEGylated bicelles also had improved biocompatibility and cellular uptake properties in vitro.<sup>[208]</sup> As such, there is increasing control over the functional properties of bicelles and these efforts have coincided with attempts to utilize bicelles for nucleic acid delivery.

## 4.2. Nucleic Acid Complexation

Currently, there are two main strategies to encapsulate nucleic acids within bicelles. The first strategy involves fabricating bicelles in the presence of nucleic acids while the second strategy focuses on bicelle fabrication initially, followed by mixing bicelles and nucleic acids in a lipoplex-type format. The merits and latest progress of both strategies, including structural and functional insights, are critically discussed below.

### 4.2.1. Coassembly of Lipids and Nucleic Acids

In the earliest example, the stacking of disk-like, cationic bicelles and negatively charged DNA was explored in order to form a new lipid nanoarchitecture for potential nucleic acid delivery applications.<sup>[209]</sup> The bicelles were composed of long-chain and short-chain lipids in a 3:1 molar ratio; the short-chain phospholipid was 1,2-diheptanoyl-*sn*-glycero-3-phosphocholine (diC<sub>7</sub>PC) while the long-chain phospholipid consisted of a mixture of 1,2-dihexadecanoyl-*sn*-glycero-3-phosphocholine (DPPC) lipid and a cationic lipid termed 3 $\beta$ -[*N*-(*N*',*N*'-dimethylaminoethane)-carbonyl] cholesterol hydrochloride (DC-Chol). The DNA strands had 700 or 2000 base pairs and the lipid-to-DNA molar ratio was from 0 to 3738 (0–40 mol% DC-Chol in the long-chain lipid population). An interesting point in the study was the simplicity of the fabrication approach. The dry lipid film was directly hydrated in an aqueous solution containing DNA molecules, followed by bath sonication at 30 °C. As such, the bicelles were directly formed in the presence of DNA, which is distinct from the lipoplex approach in which case liposomes are first formed before mixing with nucleic acids. It was determined that the DNA strands intercalate between the bicellar disk layers, and the number of layers increased at greater cationic lipid fractions in

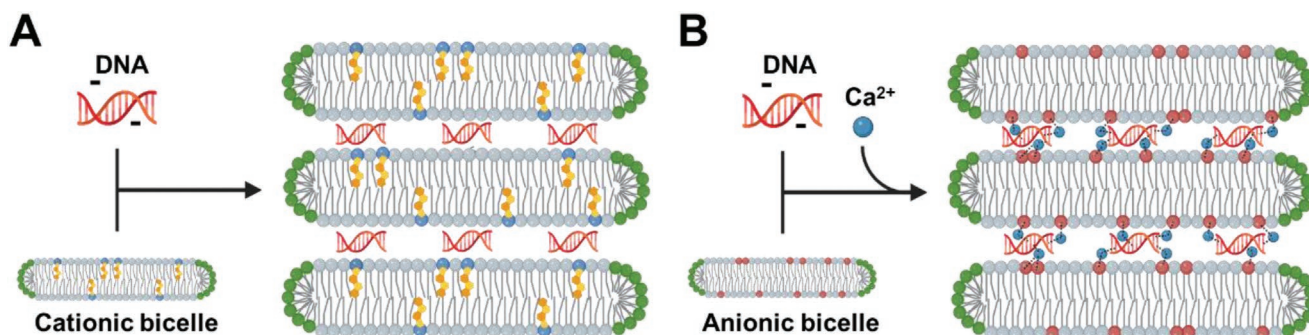


**Figure 10.** Nucleic acid interactions with lipid bicelles. A) Schematic illustration of a cationic bicelle–DNA complex. The interaction between cationic lipid bicelles and DNA molecules induced self-assembly of a multilamellar complex consisting of alternating layers of bicelles and DNA molecules. The complex formation was mediated by attractive electrostatic interactions between cationic lipids and negatively charged DNA. B) Schematic illustration of an anionic bicelle–DNA complex. The interaction between anionic lipid bicelles and DNA molecules is mediated by divalent  $\text{Ca}^{2+}$  ions and induces self-assembly of a multilamellar complex that consists of alternating layers of bicelles and DNA molecules.

the bicelles (Figure 10A). Accordingly, the size of the lipid–DNA nanostructures could be varied between  $\approx 50$ – $300$  nm and the ability to fabricate sub- $100$  nm nanostructures was highlighted as a potential merit compared to lipoplexes, which typically have  $>100$  nm diameter. It was further noted that the DNA–bicelle interactions were stable in acidic pH conditions and the fabrication approach was also applicable to other commonly used cationic lipids and surfactants such as 1,2-dioleoyl-3-trimethylammonium-propane (DOTAP) and hexadecyl-trimethyl-ammonium bromide (CTAB).

The bicelle–DNA stacking concept was further extended to anionic lipid bicelles by using the same basic design principles and fabrication approach as in the previous example and replacing the cationic lipid with an anionic lipid termed 1,2-dipalmitoyl-*sn*-glycero-3-phospho-(1'-*rac*-glycerol) (sodium salt) (DPPG) (15 mol% in the long-chain lipid population).<sup>[210]</sup> While cationic lipids can readily form complexes with nucleic acids and are effective transfection agents, they are cytotoxic, which prompted the exploration of anionic lipids as an alternative option. In order to promote bicelle–DNA interactions, divalent  $\text{Ca}^{2+}$  ions were incorporated into the system and a minimum  $\text{Ca}^{2+}$  concentration was needed to form stacked bicelle–DNA complexes (Figure 10B). Complex formation did not occur at  $1 \times 10^{-3}$  M  $\text{Ca}^{2+}$  concentration, whereas bicelle–DNA complexes did form at  $\geq 10 \times 10^{-3}$  M  $\text{Ca}^{2+}$  concentration and the interlayer spacing within the complexes did not depend on the  $\text{Ca}^{2+}$  concentration. At  $\geq 60 \times 10^{-3}$  M  $\text{Ca}^{2+}$  concentration, an additional lamellar phase of ion-lipid complexes also formed in cases of low DNA concentration, indicating that all three components—lipids, DNA, and ions—play an important role in driving the self-assembly process with controlled stoichiometry. The resulting bicelle–DNA complexes had typical dimensions around  $50$ – $100$  nm diameter and  $50$ – $150$  nm length.

In addition to DNA, there has also been exploration of utilizing bicelles to encapsulate peptide nucleic acids (PNAs) that target microRNA for potential gene editing and therapeutic purposes.<sup>[211]</sup> The bicelles had a lipid composition of around 70 mol% DPPC, 25 mol% DHPC, 3 mol% charged lipid (anionic DPPG or cationic DOTAP), and 2 mol% DSPE-PEG2000, and were prepared using a combination of vortexing, temperature cycling (between  $25^\circ\text{C}$  and  $70^\circ\text{C}$ ), and subsequent

room-temperature dilution—all steps were conducted in the presence of PNAs at a PNA:lipid molar ratio between 1:200 and 1:2500. The control bicelles without PNAs had an  $\approx 18$  nm diameter radius, while PNA-loaded anionic bicelles had an  $\approx 30$  nm diameter and disk-like appearance. In marked contrast, PNA-loaded cationic bicelles underwent extensive aggregation due to electrostatic attraction, resulting in large vesicles. By optimizing the PNA:lipid molar ratio, encapsulation efficiencies as high as 92% could be achieved with anionic bicelles, which also demonstrated superior cellular uptake properties in vitro compared to cationic bicelles and a polymeric nanoparticle control. The PNA-loaded anionic bicelles also had negligible cell cytotoxicity in vitro. Mechanistic studies further revealed that the PNA-loaded anionic bicelles were internalized by HeLa cells by an endocytic mechanism and the delivered PNAs were functionally active to inhibit a target microRNA.

#### 4.2.2. Mixing Prefabricated Bicelles with Nucleic Acids

Anecdotally, there have also been reports of bicelle–nucleic acid complexes that were developed using other fabrication protocols and were evaluated in terms of structural properties and in vitro transfection efficiency. For example, lipid mixtures consisting of gel-phase DPPC helper lipid and one of two cationic lipids (malonic acid diamides) were prepared using thin-film hydration followed by shaker incubation at  $45^\circ\text{C}$  and bath sonication, and were noted to form heterogeneous, disk-like bicelle aggregates with  $\approx 30$  nm height and  $\approx 100$  nm diameter (1:2 molar ratio of cationic lipid to helper lipid).<sup>[212]</sup> The cationic lipid bicelles were then mixed with negatively charged plasmid DNA (pDNA:  $\approx 1.5$  to 4 N/P ratios) using a lipoplex-type protocol at room temperature before attempting to transfect human lung carcinoma (A549) cells. It was noted that the bicelle–pDNA complexes had low transfection efficiency, which was attributed to poor mixing and phase separation, whereas liposome–pDNA complexes formed using other helper lipids such as fluid-phase DOPC had effective lipoplex-type transfection. A follow-up study characterized the interactions between DPPC/cationic lipid mixtures (1:1 molar ratio) and mainly double-stranded DNA ( $\approx 4$  N/P ratio), and noted that the bicelle–DNA complexes

retained disk-like nanostructures with a condensed lamellar phase.<sup>[213]</sup> In addition, using a similar preparation protocol, lipid mixtures consisting of DMPC helper lipid and a three-chain cationic lipid (DiTT4; another malonic acid diamide) were reported to form disk-like bicelles when the DiTT4 molar fraction was around 50–80 mol% and had  $\approx 50$ –100 nm diameters.<sup>[214]</sup> In that case, a lipoplex-type protocol was again followed to mix the DiTT4/DMPC bicelles with pDNA ( $\approx 1.5$  to 4 N/P ratio) and the resulting bicelle–pDNA complexes demonstrated efficient transfection of A549 cells, including in the presence of 10% serum. There is also evidence that the DiTT4 lipid by itself can self-assemble into disk-like nanostructures that can be useful for transfection.<sup>[215]</sup>

In another study, bicelles composed of CFL, DOTAP, and DHPC along with ligand-modified DSPE-PEG2000 or DHPE-PEG2000 were prepared for gene delivery applications.<sup>[216]</sup> The base bicelle composition was CFL, DOTAP, and DHPC in an approximately 6:1:2 molar ratio and, in some cases, ligand-modified DSPE-PEG2000 or DHPE-PEG2000 was included too. The conceptual idea was that ligand-modified DSPE-PEG2000 would present the ligand (i.e., cRGD peptide that binds to integrin receptors) on the main plane of the bicellar disk, whereas the ligand-modified DHPE-PEG2000 would present cRGD peptide on the bicellar edge instead. In general, the bicelles were initially prepared by hydrating a dry lipid film at 55 °C, followed by ultrasonication for 10 min and then overnight incubation at room temperature to induce sol–gel formation on the bicellar surface due to the presence of the CFL lipid. Afterward, using a lipoplex-type protocol, the bicelles were incubated for 20 min at 4 °C with small interfering RNA (siRNA) at a bicelle:siRNA molar ratio of  $\approx 64:1$ . The resulting bicelles had typical height and diameter values of  $\approx 6$  and  $\approx 50$  nm, respectively, while it was noted that the siRNA-loaded bicelles tended to be slightly larger. Notably, when bicelles with edge-located cRGD had superior siRNA loading capacity compared to bicelles with plane-located cRGD, in which case it was suggested that the ligand location diminishes bicelle–siRNA interactions. Moreover, the siRNA-loaded bicelles with edge-located cRGD showed greater performance to inhibit a cellular signaling pathway in vivo along with improved antitumor activities. The performance differences were attributed to the tailored, orthogonal functionalities afforded by the bicelle nanoarchitecture, whereby the targeting ligands were located on the bicelle edges while the cationic lipids (DOTAP) were located in the plane region to facilitate bicelle–siRNA interactions.

Together, these findings highlight how multiple strategies are being implemented to encapsulate and deliver nucleic acids using bicelles while the field evolves from fundamental structural studies to early application contexts where feasibility and utility are being demonstrated. Concurrently, efforts are being made to explore new ways of producing bicelles that can support the translation of these innovations from laboratory concepts to real-life applications.

### 4.3. Bicelle Manufacturing Considerations

While lipid bicelles are typically made by the thin-film hydration method as described above, the method has practical

limitations to advance beyond the laboratory scale. Here, we begin by briefly introducing the method in more detail before critically discussing the latest progress in developing more advanced bicelle production strategies.

For the thin-film hydration method, lipids in organic solvent are first mixed together and the solvent is evaporated in order to form a dry lipid film.<sup>[217]</sup> The film is then hydrated and the aqueous lipid suspension is subjected to multiple rounds of freeze-thaw-vortex cycling. The freezing step often involves immersing the sample in liquid nitrogen (0 °C or below) and the heating step is usually done in a water bath with  $\approx 40$ –60 °C temperature. Other variations with different temperature cycles are also possible to some extent. However, in all cases, the method is limited to batch production and the harsh processing conditions can potentially denature biological components such as proteins and nucleic acids. As such, to enhance translational prospects, there have been ongoing efforts to develop more suitable bicelle fabrication methods that are efficient and scalable.

#### 4.3.1. Semispontaneous Method

One pioneering example is adoption of the semispontaneous method to easily prepare bicelles from affordable lipids and surfactants.<sup>[218]</sup> The method was first demonstrated using soybean lecithin and poly(oxyethylene) sorbitan monooleate (Tween 80), which were initially dissolved in a water-soluble organic solvent, 1,3-butanediol in this case (and dipropylene glycol in some other cases), followed by water dilution; the temperature during the processing steps was fixed at 70 °C (other studies have used up to  $\approx 100$  °C). The lipid/surfactant mixture was then subjected to tip ultrasonication as the final processing step. Dynamic light scattering (DLS) and transmission electron microscopy (TEM) characterization of the aqueous suspension identified the formation of disk-like bicelles at a 2:1 molar ratio of lecithin to Tween 80. The typical diameter and thickness values of the bicelles were around 20 and 5 nm, respectively, and remained physically stable for at least 180 d. One recent mechanistic study discussed how two-tail lecithin molecules constitute the disk body while one-tail Tween 80 molecules form the disk rim.<sup>[219]</sup> The semi-spontaneous method has also been utilized to fabricate disk-like bicelles from other compositions, including using a polyglycerol-type nonionic surfactant with two asymmetrical tails<sup>[220]</sup> and mixtures of lecithin and poly(oxyethylene) cholesteryl ethers by themselves<sup>[221]</sup> or in combination with up to 33 mol% cholesterol in the liquid-ordered phase.<sup>[222]</sup>

#### 4.3.2. Microfluidic Production

In addition to the semispontaneous method that focuses on batch processing, there have been recent efforts to develop a continuous bicelle production method by utilizing microfluidic-based hydrodynamic flow focusing, which additionally does not require heating or cooling.<sup>[223]</sup> A schematic outline of the microfluidic chip is presented in **Figure 11A** and involves mixing tangential streams of long-chain phospholipids dispersed in an organic solvent such as methanol or ethanol with short-chain phospholipids dispersed in aqueous

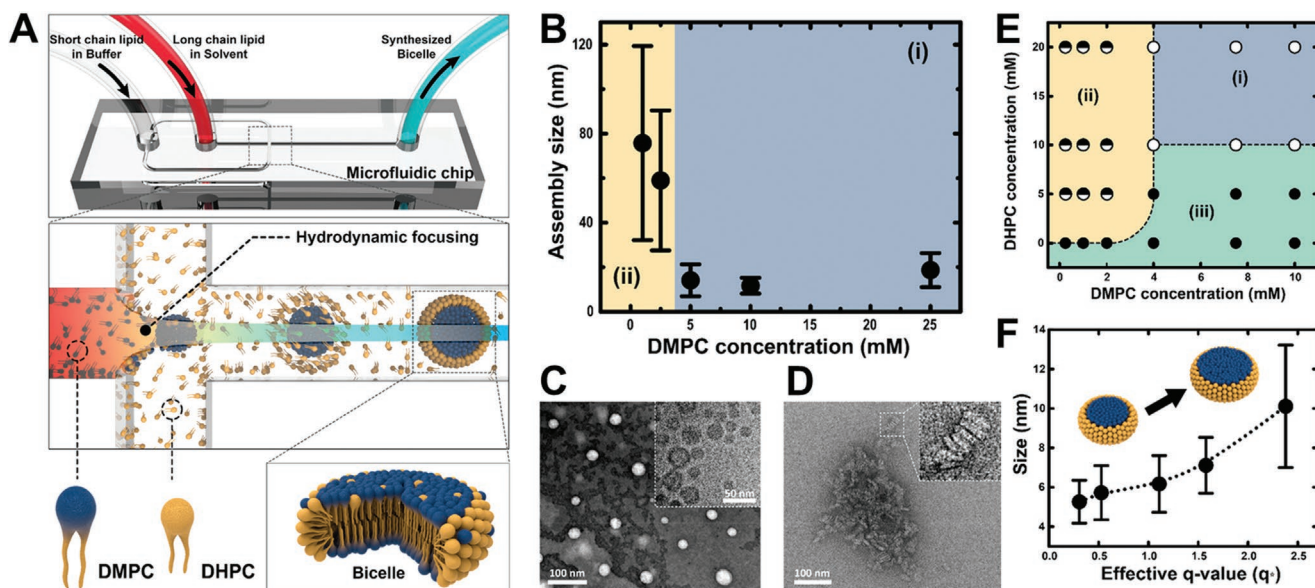


**Figure 11.** Microfluidic production of lipid bicelles. A) Schematic illustration of microfluidic setup whereby long-chain and short-chain phospholipids are dispersed in organic solvent and aqueous buffer, respectively, and mix to form lipid bicelles according to the hydrodynamic focusing concept. In this example, DMPC and DHPC are model long-chain and short-chain phospholipids, respectively. B) Effect of long-chain phospholipid (DMPC) concentration on the size of lipid nanoparticles. At low DMPC concentration, the size distribution indicates formation of heterogeneous vesicles (indicated by label ii), whereas bicelle formation (indicated by label i) occurred at higher DMPC concentrations. C) Transmission electron microscopy (TEM) image of microfluidic-fabricated vesicles and inset corresponds to a cryo-TEM image of the vesicles. D) TEM image of microfluidic-fabricated bicelles. E) Morphology of microfluidic-fabricated lipid nanoparticles depending on long-chain phospholipid (DMPC) and short-chain phospholipid (DHPDC) concentrations. i–iii) Bicelles, heterogeneous vesicles, and homogenous vesicles, respectively. F) Size of microfluidic-fabricated bicelles depending on the effective  $q$ -ratio of long-chain phospholipid to short-chain phospholipid concentrations. All panels are adapted with permission.<sup>[223]</sup> Copyright 2021, American Chemical Society.

buffer (pH 7.4). When the two streams merged, the long-chain and short-chain phospholipids mixed and self-assembled to form bicelles in a continuous manner while it was important to evaporate residual solvent in a low vacuum environment after sample collection from the microfluidic channel. Using 1,2-dimyristoyl-*sn*-glycero-3-phosphocholine (DMPC) and 1,2-dihexanoyl-*sn*-glycero-3-phosphocholine (DHPC) as model long-chain and short-chain phospholipids, respectively, it was found that the molar ratio ( $q$ -ratio) of DMPC to DHPC was an important determinant of the resulting lipid nanoparticle properties. When the DHPC concentration was fixed at  $20 \times 10^{-3}$  M, it was identified that heterogeneous vesicles formed at low DMPC concentrations ( $<5 \times 10^{-3}$  M; equivalent to  $q$ -ratio of less than 0.25) (Figure 11B). Conversely, bicelles formed at higher DMPC concentrations ( $\geq 5 \times 10^{-3}$  M; equivalent to  $q$ -ratio of equal to or greater than 0.25). The morphological structures in the different cases were confirmed by TEM imaging and it was further verified that the disk-like bicelle structures exhibited interfacial membrane properties that are characteristic of ordered bicelles (as opposed to those of mixed micelles<sup>[224]</sup>) (Figure 11C,D). Systematic experiments identified that heterogeneous vesicles, homogenous vesicles, or bicelles could be formed depending on the total lipid concentration and  $q$ -ratio, and that a sufficiently high total lipid concentration was needed to form bicelles (Figure 11E). The diffusional specifics of the solvent mixing process also influenced the self-assembly outcome while controlling the flow conditions along with the  $q$ -ratio enabled fine-tuning of the bicelle size (Figure 11F).

A follow-up study explored the general utility of the microfluidic chip based on hydrodynamic focusing to produce bicelles composed of DHPDC short-chain phospholipid with other long-chain phospholipids that have different gel-to-fluid phase transition temperatures ( $T_m$ ).<sup>[225]</sup> Interestingly, the effect of long-chain phospholipid concentration on lipid nanoparticle morphology varied depending on the specific type of long-chain phospholipid that was used in the microfluidic production process. While heterogeneous vesicles and bicelles were formed at low and high DMPC concentrations, respectively, replacing DMPC ( $T_m \approx 23$  °C) with 1-palmitoyl-2-oleoyl-*sn*-glycero-3-phosphocholine (POPC;  $T_m \approx -2$  °C) lipid led to a nearly opposite trend. In that case, bicelles were formed at low POPC concentrations, which was attributed to strong hydrophobic interactions between POPC molecules, whereas large vesicles were formed at high POPC concentrations. Additional experiments with 1,2-dipalmitoyl-*sn*-glycero-3-phosphocholine (DPPC;  $T_m \approx 41$  °C) lipid further revealed how lipid phase properties can affect self-assembly outcomes. When the microfluidic production process was carried out with DPPC at 20 °C, large vesicles were formed at all tested DPPC concentrations due to strong interactions between DPPC molecules, which is consistent with the gel-phase properties of DPPC at that temperature. In marked contrast, when the microfluidic production process was carried out with DPPC at 45 °C, DPPC was in the fluid-phase state during production and bicelles were formed at all tested DPPC concentrations. Of note, it was mentioned that the resulting DPPC/DHPC bicelles had high membrane

ordering after cooling down to ambient conditions, which is indicative of the gel-phase properties of DPPC in that temperature range. Together, these findings establish that microfluidic systems are capable of producing bicelles with diverse lipid compositions, and it is possible to rationally control bicelle size and lipid composition.

From a broader perspective, continued progress on the manufacturing side highlights how it is possible to produce bicelles using low-cost lipid and lipid-like materials and to shift from batch to continuous production methods. However, there is an outstanding need to expand efforts in this direction. Until now, such efforts have focused solely on producing lipid bicelles by considering short-chain and long-chain phospholipids and related surfactants, and it would be beneficial to also focus on how to fabricate bicelles containing nucleic acids based on the strategies described above along with adding other important components such as PEGylated lipids.

#### 4.4. Current Applications and Future Possibilities

Until now, there have been only a few cases that utilize nucleic-acid-loaded bicelles for applications. However, bicelles have emerged as a promising type of lipid nanoparticle for various biomedical applications due to their much smaller size than LNPs, liposomes, and lipoplexes so that they can effectively penetrate intercellular spaces (6-10 nm) and due to their unique morphological diversity depending on the lipid composition and molar ratio of components. Among numerous potential applications, bicelles are already known to reinforce the skin's biophysical properties and complement drug penetration. We critically review the latest progress in those fields, whereby particular focus is placed on advantageous features that could be useful for nucleic acid delivery applications in future work.

##### 4.4.1. Skin Repair and Delivery

Disk-like bicelles initially received attention for topical skin applications because they are smaller than liposomes (which cannot penetrate intracellular spaces of the stratum corneum (SC)),<sup>[226]</sup> which is the outermost layer of skin) and contain less irritating molecular components than micelles. Early studies verified that disk-like bicelles are useful for their permeability enhancing effects on skin while not causing irritation,<sup>[227]</sup> and can also penetrate the SC<sup>[228]</sup> and influence the lipid composition/phase there.<sup>[229]</sup> Follow-up studies revealed that adding specific molecular components such as cholesterol sulfate could improve the distribution and penetration of bicelles throughout the SC,<sup>[230]</sup> and such findings heightened interest in utilizing bicelles as lipid nanoparticles to improve skin properties and to deliver other medically useful molecules.<sup>[231]</sup> Indeed, continued research delineated how tuning bicelle morphology could expand the range of skin-related biological functionalities,<sup>[232]</sup> leading to the use of bicelles as dermal carriers and enhancers for treating impaired skin.

In terms of applying bicelles as carriers, it was reported that bicelle-encapsulated diclofenac diethylamine (DDEA) had lower skin penetration than aqueous DDEA suspensions.<sup>[233]</sup>

However, when skin was pretreated with empty bicelles prior to adding aqueous DDEA, the degree of skin penetration was enhanced. Similar retarding effects were observed when flufenamic acid was encapsulated in bicelles, which was suggested to be a potentially advantageous feature for safely delivering drugs that have otherwise rapid percutaneous absorption<sup>[234]</sup> (see also related structural studies<sup>[235]</sup>). Further investigation supported that bicelle-encapsulated DDEA can be delivered to damaged skin and help to repair SC barrier function while minimizing systemic side effects.<sup>[236]</sup>

While relevant application studies have been limited to small molecule drugs so far, there continues to be high interest in utilizing bicelles for dermal applications.<sup>[237]</sup> Several efforts have been made to evaluate the biophysical properties of healthy as well as irritated human skin *in vivo* before and after bicelle treatment.<sup>[227,238]</sup> While conventional bicelles composed of DMPC/DHPC increased transepidermal water loss, skin elasticity, and skin dehydration without affecting the phase behavior of SC lipidic microstructures in human subjects,<sup>[227]</sup> incorporation of long-chain lipids with longer alkyl chain lengths might tune the extent of skin reinforcement rather than penetrating into the SC lipid structures.<sup>[229b]</sup> Another study utilizing encapsulated bicelles in liposomes (bicosomes) to mimic epidermal lamellar bodies showed that treatment with bicosomes reinforced the skin barrier function in both healthy and irritated human skin, probably by reestablishing the lamellar lipid structure of the SC.<sup>[238]</sup>

Looking forward, there is an outstanding need to investigate how bicelle carriers might be useful carriers for delivering nucleic acids to the skin, especially in intradermal applications. Recent discussions have suggested that intradermal administration of RNA-based vaccines may reduce dose requirements and be possible with needle-free approaches.<sup>[239]</sup> In these respects, bicelles stand out among possible lipid nanoparticle carrier options because they have well-validated properties for skin delivery applications.

##### 4.4.2. Cancer Therapy

There has also been extensive interest in utilizing disk-like bicelles to deliver small-molecule and peptide drugs for anticancer therapy. For example, PEGylated lipid bicelles have been used to encapsulate the anticancer drug doxorubicin (DOX), with up to 96% encapsulation efficiency and >10-times longer circulation time in mice.<sup>[240]</sup> Compared to free DOX, the bicelle-encapsulated DOX was more effective at accumulating in tumors and the bicelles could be internalized by breast cancer cells. Anionic lipid bicelles have also been developed to co-encapsulate two anticancer drugs, paclitaxel (PTX) and parthenolide (PTL), for *in vivo* therapeutic treatment.<sup>[241]</sup> To improve tumor targeting, bicelles have been further functionalized with RGD peptides and this strategy was able to increase tumor penetration of bicelle-encapsulated melittin peptide compared to non-functionalized bicelles, which in turn improved antitumor activity *in vivo*.<sup>[242]</sup> Motivated by these early results, the field has continued to progress toward clinical applications, especially in terms of utilizing PEGylated lipids to enhance functional performance. In one case, the addition of a PEGylated lipid to

a disk-like bicelle composition triggered the formation of small, spherical micelles that, when loaded with the anticancer drug docetaxel (DTX), not only had superior stability and cell and tumor uptake properties compared to PEGylated liposomes, but also demonstrated improved antitumor activity *in vivo*.<sup>[243]</sup> There have also been other reports that show PEGylated lipids can help to sterically stabilize bicelles in order to enhance uptake and anticancer drug delivery to human cancer cells.<sup>[244]</sup>

Expanding on these concepts, there have also been efforts to utilize more durable, organic–inorganic hybrid bicelles for anticancer applications.<sup>[187]</sup> In one interesting example, DOX was loaded together with indocyanine green (ICG)—a fluorescent dye used for photothermal therapy—for temperature-regulated DOX release and photothermal-triggered cancer cell cytotoxicity, which could be achieved in the presence of near-infrared fluorescence light.<sup>[245]</sup> The bicelles exhibited high levels of tumor targeting and exhibited anticancer activity *in vivo*, which was superior to either the chemotherapy or photothermal therapy alone. Together with advances in developing partially silica-coated hybrid bicelles as described above,<sup>[208]</sup> such possibilities open the door to advanced cancer therapeutics and it has been suggested the hybrid bicelles could also be useful for gene delivery applications as well.<sup>[246]</sup> Indeed, one study utilizing hybrid bicelles for siRNA delivery has been reported for anticancer treatment *in vivo*<sup>[216]</sup> while highlighting the future opportunities that lie ahead to use various types of bicelles, including inorganic-organic hybrid bicelles, for nucleic acid delivery applications.

## 5. Conclusion and Outlook

The development of lipid-based nucleic acid delivery vehicles has increasingly gained traction over the past decade and shifted from innovative laboratory concepts to practically effective and scalable clinical technologies, most recently culminating in the large-scale manufacturing and worldwide distribution of mRNA–LNP vaccines to prevent COVID-19 infection. These advances have been largely enabled by rationally designing the LNP structure to achieve maximum performance based on the nanoarchitectonics concept along with utilizing microfluidic production technologies, which not only paved the way for production scale-up, but more importantly allowed precise control over production parameters to tune the nanoarchitecture features of manufactured LNPs in a precise and reproducible manner.

Along this line, there exist numerous opportunities to explore numerous combinations of lipid excipients and nucleic acid payloads, and the role of nanoarchitectonics-based research will become increasingly crucial to spur future innovation. We identify several key areas in which nanoarchitectonics is expected to play a central role. First, there is an opportunity to explore different routes of administration, especially by taking advantage of different lipid nanoarchitectures such as bicelles that can be potentially useful for intradermal applications. Secondly, there is an urgent demand to overcome challenges related to the *in vivo* behavior of LNPs, for example, due to issues related to the immune response. Specifically, recent efforts have been made to identify appropriate alternatives to PEG lipids. In doing so,

it is important to apply the concept of nanoarchitectonics to modulate interactions of the PEG lipid (or alternatives) with other lipid excipients and select appropriate candidates that will retain favorable interactions with the rest of the components.

Another area of interest is the expansion of microfluidic capabilities, especially to emerging classes of lipid-based nanoparticles such as bicelles for not only proof-of-concept demonstration as done so far but also for practical application (as in the LNP case). To date, improvements to microfluidic platforms have been achieved incrementally and are mostly aimed at obtaining better control over the physical properties of the resultant lipid-based vehicle (i.e., mainly size and size distribution). Enhancing the capability of microfluidic platforms to precisely control the morphology and architecture of the lipid-based delivery vehicle needs guidance from nanoarchitectonics and could help to improve nucleic acid encapsulation in tandem as well.

Finally, while clinically approved LNP-based drug and vaccines are composed of a single formulation (i.e., delivering a single type of nucleic acid payload) there is growing interest in multiple- or coformulations. For example, a recent study demonstrated successful *in vivo* CRISPR/Cas9 gene editing for the transthyretin gene in mice and rats using LNPs that were coformulated to include single guide RNA (sgRNA) and Cas9 mRNA.<sup>[247]</sup> Formulation optimization was performed for *in vitro* and *in vivo* gene editing with necessary modifications to incorporate sgRNA. The LNPs were formulated using microfluidics and they achieved >97% transthyretin protein knockdown for 12 months. This study highlights the need for nucleic acid LNPs to be carefully engineered to match their therapeutic applications; specifically, how optimized, co-formulated LNPs can be applied for cell engineering and genome editing. More notably, it emphasizes the vast potential of LNPs as nucleic acid delivery systems, which allows coformulations to be optimized with high efficiencies, paving the way for novel nucleic acid-based therapeutics for a wide range of diseases in the near future.

As a closing remark, we may also add that the three types of lipid-based nanoparticles covered herein were selected due to their distinct nanoarchitectures and breadth of development stages, spanning conceptual innovations to full-fledged commercial products. Across this spectrum, the nanoarchitectonics concept is a useful approach to analyze the progress and trends and to build a rational understanding of how to effectively design lipid-based nanoparticles for various biomedical applications. Until now, the impact of nanoarchitectonics on lipid-based nanoparticles for nucleic acid delivery applications had been largely implicit, but we foresee that nanoarchitectonics will play an increasingly prominent and visible role to drive forward future innovations both in terms of scientific discussion and research progress.

## Acknowledgements

A.R.F. and S.P. contributed equally to this work. This work was supported by the Ministry of Education (MOE) in Singapore under grant AcRF TIER1-2020-T1-002-032 (RG111/20) and by a sponsored research agreement from LUCA AICell Inc. (RCA- LUCA AICell REQ0239282 – LUCA), and by the National Research Foundation of Korea (NRF) grants funded by the Korean government (MSIT) (Nos. 2020R1C1C1004385

and 2021R1A4A1032782). In addition, this work was supported by the International Research & Development Program of the National Research Foundation of Korea (NRF) funded by the Ministry of Science and ICT (2020K1A3A1A39112724). This work was also supported by a grant of the Korea Health Technology R&D Project through the Korea Health Industry Development Institute (KHIDI), funded by the Ministry of Health & Welfare, Republic of Korea (Grant Number: HI19C1328). H.T. was supported by an SINGA graduate scholarship from the A\*STAR Graduate Academy, Singapore. Schematic illustrations were created with BioRender.com under an academic lab subscription.

## Conflict of Interest

N.-J.C. and J.A.J. are listed as coinventors on patents and patent applications that are related to lipid bilayer technologies. In addition, N.-J.C. is a founder of and J.A.J. is a scientific advisor to LUCA AICell Inc, which is developing lipid-related technologies. The other authors declare no conflict of interest.

## Keywords

drug delivery, lipid nanoparticle, microfluidics, nanoarchitectonics, vaccine

Received: March 31, 2022

Revised: May 9, 2022

Published online:

- [1] a) J. A. Kulkarni, D. Witzigmann, S. B. Thomson, S. Chen, B. R. Leavitt, P. R. Cullis, R. van der Meel, *Nat. Nanotechnol.* **2021**, *16*, 630; b) H. Yin, R. L. Kanasty, A. A. J. Vegas, J. R. Dorkin, D. G. Anderson, *Nat. Rev. Genet.* **2014**, *15*, 541.
- [2] S. Chesnoy, L. Huang, *Annu. Rev. Biophys. Biomol. Struct.* **2000**, *29*, 27.
- [3] P. Guo, *J. Nanosci. Nanotechnol.* **2005**, *5*, 1964.
- [4] Y. Eygeris, S. Patel, A. Jozic, G. Sahay, *Nano Lett.* **2020**, *20*, 4543.
- [5] Y. Zhang, H. Li, J. Sun, J. Gao, W. Liu, B. Li, Y. Guo, J. Chen, *Int. J. Pharm.* **2010**, *390*, 198.
- [6] E. Dolgin, *Nat. Biotechnol.* **2022**, *40*, 283.
- [7] P. F. McKay, K. Hu, A. K. Blakney, K. Samnuan, J. C. Brown, R. Penn, J. Zhou, C. R. Bouton, P. Rogers, K. Polra, *Nat. Commun.* **2020**, *11*, 3523.
- [8] C. Webb, S. Ip, N. V. Bathula, P. Popova, S. K. Soriano, H. H. Ly, B. Eryilmaz, V. A. Nguyen Huu, R. Broadhead, M. Rabel, *Mol. Pharmaceutics* **2022**, *19*, 1047.
- [9] a) K. S. Corbett, D. K. Edwards, S. R. Leist, O. M. Abiona, S. Boyoglu-Barnum, R. A. Gillespie, S. Himansu, A. Schäfer, C. T. Ziwawo, A. T. DiPiazza, *Nature* **2020**, *586*, 567; b) L. Schoenmaker, D. Witzigmann, J. A. Kulkarni, R. Verbeke, G. Kersten, W. Jiskoot, D. J. Crommelin, *Int. J. Pharm.* **2021**, *601*, 120586.
- [10] a) X. Hou, T. Zaks, R. Langer, Y. Dong, *Nat. Rev. Mater.* **2021**, *6*, 1078; b) R. Tenchov, R. Bird, A. E. Curtze, Q. Zhou, *ACS Nano* **2021**, *15*, 16982; c) B. Z. Igyártó, S. Jacobsen, S. Ndeupen, *Curr. Opin. Virol.* **2021**, *48*, 65; d) E. Kon, U. Elia, D. Peer, *Curr. Opin. Biotechnol.* **2022**, *73*, 329.
- [11] a) M. Aono, K. Ariga, *Adv. Mater.* **2016**, *28*, 989; b) K. Ariga, J. A. Jackman, N. J. Cho, S. H. Hsu, L. K. Shrestha, T. Mori, J. Takeya, *Chem. Rec.* **2019**, *19*, 1891; c) K. Ariga, Y. Yamauchi, *Chem.-Asian J.* **2020**, *15*, 718.
- [12] a) K. Ariga, S. Watanabe, T. Mori, J. Takeya, *NPG Asia Mater.* **2018**, *10*, 90; b) K. Ariga, M. Nishikawa, T. Mori, J. Takeya, L. K. Shrestha, J. P. Hill, *Sci. Technol. Adv. Mater.* **2019**, *20*, 51; c) K. Ariga, X. Jia, J. Song, J. P. Hill, D. T. Leong, Y. Jia, J. Li, *Angew. Chem., Int. Ed.* **2020**, *59*, 15424; d) K. Ariga, *Nanoscale Horiz.* **2021**, *6*, 364.
- [13] a) J. Geall Andrew, A. Verma, R. Otten Gillis, A. Shaw Christine, A. Hekele, K. Banerjee, Y. Cu, W. Beard Clayton, A. Brito Luis, T. Krucker, T. O'Hagan Derek, M. Singh, W. Mason Peter, M. Valiante Nicholas, R. Dormitzer Philip, W. Barnett Susan, R. Rappuoli, B. Ulmer Jeffrey, W. Mandl Christian, *Proc. Natl. Acad. Sci. USA* **2012**, *109*, 14604; b) E. Samaridou, J. Heyes, P. Lutwyche, *Adv. Drug Delivery Rev.* **2020**, *154-155*, 37; c) Y. Zhang, C. Sun, C. Wang, K. E. Jankovic, Y. Dong, *Chem. Rev.* **2021**, *121*, 12181.
- [14] a) A. C. Anselmo, S. Mitragotri, *Bioeng. Transl. Med.* **2016**, *1*, 10; b) A. C. Anselmo, S. Mitragotri, *Bioeng. Transl. Med.* **2019**, *4*, e10143; c) S. Yonezawa, H. Koide, T. Asai, *Adv. Drug Delivery Rev.* **2020**, *154-155*, 64.
- [15] a) T. T. Thi, E. J. A. Suys, J. S. Lee, D. H. Nguyen, K. D. Park, N. P. Truong, *Vaccines* **2021**, *9*, 359; b) B. N. Aldosari, I. M. Alfagih, A. S. Almurshedi, *Pharmaceutics* **2021**, *13*, 206; c) A. C. Anselmo, S. Mitragotri, *Bioeng. Transl. Med.* **2021**, *6*, e10246.
- [16] a) M. Cornebise, E. Narayanan, Y. Xia, E. Acosta, L. Ci, H. Koch, J. Milton, S. Sabnis, T. Salerno, K. E. Benenato, *Adv. Funct. Mater.* **2022**, *32*, 2106727; b) G. Basha, T. I. Novobrantseva, N. Rosin, Y. Y. C. Tam, I. M. Hafez, M. K. Wong, T. Sugo, V. M. J. Ruda, J. Qin, B. Klebanov, M. Ciufolini, A. Akinc, Y. K. Tam, M. J. Hope, P. R. Cullis, *Mol. Ther.* **2011**, *19*, 2186; c) N. Maurer, K. F. Wong, H. Stark, L. Louie, D. McIntosh, T. Wong, P. Scherrer, S. C. Semple, P. R. Cullis, *Biophys. J.* **2001**, *80*, 2310; d) S. C. Semple, S. K. Klimuk, T. O. Harasym, N. Dos Santos, S. M. Ansell, K. F. Wong, N. Maurer, H. Stark, P. R. Cullis, M. J. Hope, P. Scherrer, *Biochim. Biophys. Acta, Biomembr.* **2001**, *1510*, 152.
- [17] a) S. J. Shepherd, D. Issadore, M. J. Mitchell, *Biomaterials* **2021**, *274*, 120826; b) M. Maeki, S. Uno, A. Niwa, Y. Okada, M. Tokeshi, *J. Controlled Release* **2022**, *344*, 80.
- [18] a) K. Ward, Z. H. Fan, *J. Micromech. Microeng.* **2015**, *25*, 094001; b) C.-Y. Lee, C.-L. Chang, Y.-N. Wang, L.-M. Fu, *Int. J. Mol. Sci.* **2011**, *12*, 3263; c) M. J. W. Evers, J. A. Kulkarni, R. van der Meel, P. R. Cullis, P. Vader, R. M. Schiffelers, *Small Methods* **2018**, *2*, 1700375.
- [19] a) K. M. McMahon, M. P. Plebanek, C. S. Thaxton, *Adv. Funct. Mater.* **2016**, *26*, 7824; b) K. M. McMahon, R. K. Mutharasan, S. Tripathy, D. Veliceasa, M. Bobeica, D. K. Shumaker, A. J. Luthi, B. T. Helfand, H. Ardehali, C. A. Mirkin, O. Volpert, C. S. Thaxton, *Nano Lett.* **2011**, *11*, 1208; c) K. M. McMahon, C. S. Thaxton, *Expert Opin. Drug Delivery* **2014**, *11*, 231; d) J. Wang, A. E. Calvert, N. Kaplan, K. M. McMahon, W. Yang, K. Q. Lu, H. Peng, C. S. Thaxton, R. M. Lavker, *Adv. Ther.* **2020**, *3*, 2000138.
- [20] a) K. C. Vickers, B. T. Palmisano, B. M. Shoucri, R. D. Shamburek, A. T. Remaley, *Nat. Cell Biol.* **2011**, *13*, 423; b) F. Tabet, K. C. Vickers, L. F. Cuesta Torres, C. B. Wiese, B. M. Shoucri, G. Lambert, C. Catherinet, L. Prado-Lourenco, M. G. Levin, S. Thacker, P. Sethupathy, P. J. Barter, A. T. Remaley, K.-A. Rye, *Nat. Commun.* **2014**, *5*, 3292.
- [21] M. Ouimet, T. J. Barrett, E. A. Fisher, *Circ. Res.* **2019**, *124*, 1505.
- [22] a) K. C. Vickers, A. T. Remaley, *Curr. Opin. Lipidol.* **2012**, *23*, 91; b) K. C. Vickers, A. T. Remaley, *J. Lipid Res.* **2014**, *55*, 4; c) S. Nazir, V. Jankowski, G. Bender, S. Zewinger, K.-A. Rye, E. P. C. van der Vorst, *Adv. Drug Delivery Rev.* **2020**, *159*, 94.
- [23] X. Chen, L. S. Mangala, L. Mooberry, E. Bayraktar, S. K. Dasari, S. Ma, C. Ivan, K. A. Court, C. Rodriguez-Aguayo, R. Bayraktar, S. Raut, N. Sabnis, X. Kong, X. Yang, G. Lopez-Berestein, A. G. Lacko, A. K. Sood, *Oncogene* **2019**, *38*, 6095.
- [24] A. G. Lacko, N. A. Sabnis, B. Nagarajan, W. J. McConathy, *Front. Pharmacol.* **2015**, *6*, 247.
- [25] M. M. K. Shahzad, L. S. Mangala, H. D. Han, C. Lu, J. Bottsford-Miller, M. Nishimura, E. M. Mora, J.-W. Lee, R. L. Stone, C. V. Pecot, D. Thanappapras, J.-W. Roh, P. Gaur,



- M. P. Nair, Y.-Y. Park, N. Sabnis, M. T. Deavers, J.-S. Lee, L. M. Ellis, G. Lopez-Berestein, W. J. McConathy, L. Prokai, A. G. Lacko, A. K. Sood, *Neoplasia* **2011**, *13*, 309.
- [26] T. M. Allen, P. R. Cullis, *Adv. Drug Delivery Rev.* **2013**, *65*, 36.
- [27] a) J. S. Suk, Q. Xu, N. Kim, J. Hanes, L. M. Ensign, *Adv. Drug Delivery Rev.* **2016**, *99*, 28; b) Z. Wang, E. D. Hood, J. Nong, J. Ding, O. A. Marcos-Contreras, P. M. Glassman, K. M. Rubey, M. Zaleski, C. L. Espy, D. Gullipali, T. Miwa, V. R. Muzykantov, W.-C. Song, J. W. Myerson, J. S. Brenner, *Adv. Mater.* **2022**, *34*, 2107070.
- [28] M. Longmire, P. L. Choyke, H. Kobayashi, *Nanomedicine* **2008**, *3*, 703.
- [29] a) J. Lu, Y. Zhao, X. Zhou, J. H. He, Y. Yang, C. Jiang, Z. Qi, W. Zhang, J. Liu, *Biomacromolecules* **2017**, *18*, 2286; b) A. Orellana Esteban, S. Tennen, L. Rangasamy, L. T. Lyle, S. Low Philip, L. Kasinski Andrea, *Sci. Transl. Med.* **2017**, *9*, eaam9327.
- [30] a) C. Wolfrum, S. Shi, K. N. Jayaprakash, M. Jayaraman, G. Wang, R. K. Pandey, K. G. Rajeev, T. Nakayama, K. Charrise, E. M. Ndungo, T. Zimmermann, V. Koteliansky, M. Manoharan, M. Stoffel, *Nat. Biotechnol.* **2007**, *25*, 1149; b) M. Egli, M. Manoharan, *Acc. Chem. Res.* **2019**, *52*, 1036.
- [31] a) Y. Yang, J. Wang, H. Shigematsu, W. Xu, W. M. Shih, J. E. Rothman, C. Lin, *Nat. Chem.* **2016**, *8*, 476; b) Z. Zhang, Y. Yang, F. Pincet, M. C. Llaguno, C. Lin, *Nat. Chem.* **2017**, *9*, 653.
- [32] a) J. Guan, Q. Shen, Z. Zhang, Z. Jiang, Y. Yang, M. Lou, J. Qian, W. Lu, C. Zhan, *Nat. Commun.* **2018**, *9*, 2982; b) N. AlSawaftah, W. G. Pitt, G. A. Hussein, *ACS Pharmacol. Transl. Sci.* **2021**, *4*, 1028.
- [33] C. Kelly, C. Jefferies, S.-A. Cryan, *J. Drug Delivery* **2011**, *2011*, 727241.
- [34] a) P.-A. Monnard, T. Oberholzer, P. Luisi, *Biochim. Biophys. Acta, Biomembr.* **1997**, *1329*, 39; b) S. Dow, *Expert Opin. Drug Delivery* **2008**, *5*, 11; c) C. R. Safinya, K. K. Ewert, R. N. Majzoub, C. Leal, *New J. Chem.* **2014**, *38*, 5164.
- [35] A. A. Barba, G. Lamberti, C. Sardo, B. Dapas, M. Abrami, M. Grassi, R. Farra, F. Tonon, G. Forte, F. Musiani, M. Licciardi, G. Pozzato, F. Zanonati, B. Scaggiante, G. Grassi, G. Cavallaro, *Curr. Drug Metab.* **2015**, *16*, 427.
- [36] a) E. H. Pilkington, E. J. A. Suys, N. L. Trevaskis, A. K. Wheatley, D. Zukancic, A. Algarni, H. Al-Wassiti, T. P. Davis, C. W. Pouton, S. J. Kent, N. P. Truong, *Acta Biomater.* **2021**, *131*, 16; b) Y. Eygeris, M. Gupta, J. Kim, G. Sahay, *Acc. Chem. Res.* **2022**, *55*, 2.
- [37] N. R. Larson, G. Hu, Y. Wei, A. D. Tiesca, M. L. Forrest, C. R. Middaugh, *J. Pharm. Sci.* **2022**, *111*, 690.
- [38] A. Dilliard Sean, Q. Cheng, J. Siegwart Daniel, *Proc. Natl. Acad. Sci. USA* **2021**, *118*, e2109256118.
- [39] M. Schlich, R. Palomba, G. Costabile, S. Mizrahy, M. Pannuzzo, D. Peer, P. Decuzzi, *Bioeng. Transl. Med.* **2021**, *6*, e10213.
- [40] a) S. M. Lee, Q. Cheng, X. Yu, S. Liu, L. T. Johnson, D. J. Siegwart, *Angew. Chem., Int. Ed.* **2021**, *60*, 5848; b) M. Jayaraman, S. M. Ansell, B. L. Mui, Y. K. Tam, J. Chen, X. Du, D. Butler, L. Eltepu, S. Matsuda, J. K. Narayanannair, K. G. Rajeev, I. M. Hafez, A. Akinc, M. A. Maier, M. A. Tracy, P. R. Cullis, T. D. Madden, M. Manoharan, M. J. Hope, *Angew. Chem., Int. Ed.* **2012**, *51*, 8529; c) O. S. Fenton, K. J. Kauffman, R. L. McClellan, E. A. Appel, J. R. Dorkin, M. W. Tibbitt, M. W. Heartlein, F. DeRosa, R. Langer, D. G. Anderson, *Adv. Mater.* **2016**, *28*, 2939.
- [41] a) S. Liu, Q. Cheng, T. Wei, X. Yu, L. T. Johnson, L. Farbiak, D. J. Siegwart, *Nat. Mater.* **2021**, *20*, 701; b) N. Meng, D. Grimm, *Signal Transduction Targeted Ther.* **2021**, *6*, 206.
- [42] K. A. Hajj, R. L. Ball, S. B. Deluty, S. R. Singh, D. Strelkova, C. M. Knapp, K. A. Whitehead, *Small* **2019**, *15*, 1805097.
- [43] a) M. A. Maier, M. Jayaraman, S. Matsuda, J. Liu, S. Barros, W. Querbes, Y. K. Tam, S. M. Ansell, V. Kumar, J. Qin, X. Zhang, Q. Wang, S. Panesar, R. Hutabarat, M. Carioto, J. Hettinger, P. Kandasamy, D. Butler, K. G. Rajeev, B. Pang, K. Charisse, K. Fitzgerald, B. L. Mui, X. Du, P. Cullis, T. D. Madden, M. J. Hope, M. Manoharan, A. Akinc, *Mol. Ther.* **2013**, *21*, 1570; b) Y. Suzuki, K. Hyodo, T. Suzuki, Y. Tanaka, H. Kikuchi, H. Ishihara, *Int. J. Pharm.* **2017**, *519*, 34; c) H. Tanaka, T. Takahashi, M. Konishi, N. Takata, M. Gomi, D. Shirane, R. Miyama, S. Hagiwara, Y. Yamasaki, Y. Sakurai, K. Ueda, K. Higashi, K. Moribe, E. Shinsho, R. Nishida, K. Fukuzawa, E. Yonemochi, K. Okuwaki, Y. Mochizuki, Y. Nakai, K. Tange, H. Yoshioka, S. Tamagawa, H. Akita, *Adv. Funct. Mater.* **2020**, *30*, 1910575; d) H. Tanaka, T. Takahashi, M. Konishi, N. Takata, M. Gomi, D. Shirane, R. Miyama, S. Hagiwara, Y. Yamasaki, Y. Sakurai, *Adv. Funct. Mater.* **2020**, *30*, 1910575.
- [44] a) O. S. Fenton, K. J. Kauffman, R. L. McClellan, J. C. Kaczmarek, M. D. Zeng, J. L. Andresen, L. H. Rhym, M. W. Heartlein, F. DeRosa, D. G. Anderson, *Angew. Chem., Int. Ed.* **2018**, *57*, 13582; b) M. J. Carrasco, S. Alshetty, M.-G. Alameh, H. Said, L. Wright, M. Paige, O. Soliman, D. Weissman, T. E. Cleveland, A. Grishae, M. D. Buschmann, *Commun. Biol.* **2021**, *4*, 956.
- [45] F. Ding, H. Zhang, J. Cui, Q. Li, C. Yang, *Biomater. Sci.* **2021**, *9*, 7534.
- [46] M. Kim, M. Jeong, S. Hur, Y. Cho, J. Park, H. Jung, Y. Seo, H. A. Woo, K. T. Nam, K. Lee, H. Lee, *Sci. Adv.* **2021**, *7*, eabf4398.
- [47] a) S. Mochizuki, N. Kanegae, K. Nishina, Y. Kamikawa, K. Koivai, H. Masunaga, K. Sakurai, *Biochim. Biophys. Acta, Biomembr.* **2013**, *1828*, 412; b) J. A. Kulkarni, D. Witzigmann, J. Leung, Y. Y. C. Tam, P. R. Cullis, *Nanoscale* **2019**, *11*, 21733; c) R. Zhang, R. El-Mayta, T. J. Murdoch, C. C. Warzecha, M. M. Billingsley, S. J. Shepherd, N. Gong, L. Wang, J. M. Wilson, D. Lee, M. J. Mitchell, *Biomater. Sci.* **2021**, *9*, 1449; d) J. Kim, A. Jozic, G. Sahay, *Cell. Mol. Bioeng.* **2020**, *13*, 463.
- [48] S. Patel, N. Ashwanikumar, E. Robinson, Y. Xia, C. Mihai, J. P. Griffith, S. Hou, A. A. Esposito, T. Ketova, K. Welscher, J. L. Joyal, Ö. Almarsson, G. Sahay, *Nat. Commun.* **2020**, *11*, 983.
- [49] H. Tanaka, R. Miyama, Y. Sakurai, S. Tamagawa, Y. Nakai, K. Tange, H. Yoshioka, H. Akita, *Pharmaceutics* **2021**, *13*, 2097.
- [50] F. Sebastiani, M. Yanez Arteta, M. Lerche, L. Porcar, C. Lang, R. A. Bragg, C. S. Elmore, V. R. Krishnamurthy, R. A. Russell, T. Darwish, H. Pichler, S. Waldie, M. Moulin, M. Haertlein, V. T. Forsyth, L. Lindfors, M. Cárdenas, *ACS Nano* **2021**, *15*, 6709.
- [51] a) P. Sellaturay, S. Nasser, S. Islam, P. Gurugama, P. W. Ewan, *Clin. Exp. Allergy* **2021**, *51*, 861; b) A. Troelnikov, G. Perkins, C. Yuson, A. Ahamdie, S. Balouch, P. R. Hurtado, P. Hissaria, *J. Allergy Clin. Immunol.* **2021**, *148*, 91; c) M. Picard, J.-P. Drolet, M.-S. Masse, C. A. Fillion, F. Almuhihi, M. Fein, A. Copescu, G. A. C. Isabwe, M. Blaquière, M.-N. Primeau, *J. Allergy Clin. Immunol.: Pract.* **2022**, *10*, 620; d) J. A. Cahill, M. Kan, *Allergy* **2022**, *77*, 337; e) P. Sellaturay, P. Gurugama, V. Harper, T. Dymond, P. Ewan, S. Nasser, *Clin. Exp. Allergy* **2022**, *52*, 12.
- [52] B. Cabanillas, N. Novak, C. A. Akdis, *Allergy* **2021**, *76*, 1938.
- [53] a) A. Akinc, W. Querbes, S. De, J. Qin, M. Frank-Kamenetsky, K. N. Jayaprakash, M. Jayaraman, K. G. Rajeev, W. L. Cantley, J. R. Dorkin, J. S. Butler, L. Qin, T. Racie, A. Sprague, E. Fava, A. Zeigerer, M. J. Hope, M. Zerial, D. W. Y. Sah, K. Fitzgerald, M. A. Tracy, M. Manoharan, V. Koteliansky, A. d. Fougerolles, M. A. Maier, *Mol. Ther.* **2010**, *18*, 1357; b) S. Sabnis, E. S. Kumarasinghe, T. Salerno, C. Mihai, T. Ketova, J. J. Senn, A. Lynn, A. Bulychev, I. McFadyen, J. Chan, Ö. Almarsson, M. G. Stanton, K. E. Benenato, *Mol. Ther.* **2018**, *26*, 1509.
- [54] a) D. W. Lee, X. Banquy, K. Kristiansen, Y. Kaufman, J. M. Boggs, J. N. Israelachvili, *Proc. Natl. Acad. Sci. USA* **2014**, *111*, E768; b) A. H. Pande, S. Qin, S. A. Tatulian, *Biophys. J.* **2005**, *88*, 4084.
- [55] a) A. Wittrup, A. Ai, X. Liu, P. Hamar, R. Trifonova, K. Charisse, M. Manoharan, T. Kirchhausen, J. Lieberman, *Nat. Biotechnol.* **2015**, *33*, 870; b) J. Gilleron, W. Querbes, A. Zeigerer, A. Borodovsky, G. Marsico, U. Schubert, K. Manygoats, S. Seifert, C. Andree, M. Stöter, H. Epstein-Barash, L. Zhang, V. Koteliansky, K. Fitzgerald, E. Fava, M. Bickle, Y. Kalaidzidis, A. Akinc, M. Maier,

- M. Zerial, *Nat. Biotechnol.* **2013**, *31*, 638; c) G. Sahay, W. Querbes, C. Alabi, A. Eltoukhy, S. Sarkar, C. Zurenko, E. Karagiannis, K. Love, D. Chen, R. Zoncu, Y. Buganim, A. Schroeder, R. Langer, D. G. Anderson, *Nat. Biotechnol.* **2013**, *31*, 653.
- [56] a) N. Hartl, F. Adams, O. M. Merkel, *Adv. Ther.* **2021**, *4*, 2000092; b) P. Sabourian, G. Yazdani, S. S. Ashraf, M. Frounchi, S. Mashayekhan, S. Kiani, A. Kakkar, *Int. J. Mol. Sci.* **2020**, *21*, 8019.
- [57] R. Gaspar, F. Coelho, B. F. B. Silva, *Molecules* **2020**, *25*, 5006.
- [58] R. L. Ball, K. A. Hajj, J. Vizelman, P. Bajaj, K. A. Whitehead, *Nano Lett.* **2018**, *18*, 3814.
- [59] a) J. K. Watts, G. F. Deleavey, M. J. Damha, *Drug Discovery Today* **2008**, *13*, 842; b) N. J. Caplen, E. W. Alton, P. G. Middleton, J. R. Dorin, B. J. Stevenson, X. Gao, S. R. Durham, P. K. Jeffery, M. E. Hodson, C. Coutelle, *Nat. Med.* **1995**, *1*, 39.
- [60] a) B. Lewin, *Genes* 9, Jones & Bartlett Learning, Burlington, MA **2008**; b) B. Alberts, *Molecular Biology of the Cell*, Garland Science, New York **2004**.
- [61] A. Wu, Y. Peng, B. Huang, X. Ding, X. Wang, P. Niu, J. Meng, Z. Zhu, Z. Zhang, J. Wang, J. Sheng, L. Quan, Z. Xia, W. Tan, G. Cheng, T. Jiang, *Cell Host Microbe* **2020**, *27*, 325.
- [62] a) M. Yanez Arteta, T. Kjellman, S. Bartesaghi, S. Wallin, X. Wu, J. Kvist Alexander, A. Dabkowska, N. Székely, A. Radulescu, J. Bergholtz, L. Lindfors, *Proc. Natl. Acad. Sci.* **2018**, *115*, E3351; b) J. A. Kulkarni, M. M. Darjuan, J. E. Mercer, S. Chen, R. van der Meel, J. L. Thewalt, Y. Y. C. Tam, P. R. Cullis, *ACS Nano* **2018**, *12*, 4787.
- [63] Z. Hejdankova, V. Vanek, F. Sedlak, J. Prochazka, A. Diederichs, S. Kereiche, B. Novotna, M. Budesinsky, G. Birkus, K. Grantz Saskova, P. Cigler, *Adv. Funct. Mater.* **2021**, *31*, 2101391.
- [64] a) K. J. Kauffman, J. R. Dorkin, J. H. Yang, M. W. Heartlein, F. DeRosa, F. F. Mir, O. S. Fenton, D. G. Anderson, *Nano Lett.* **2015**, *15*, 7300; b) M. P. Lokugamage, D. Vanover, J. Beyersdorf, M. Z. C. Hatit, L. Rotolo, E. S. Echeverri, H. E. Peck, H. Ni, J.-K. Yoon, Y. Kim, P. J. Santangelo, J. E. Dahlman, *Nat. Biomed. Eng.* **2021**, *5*, 1059; c) S. C. Semple, A. Akinc, J. Chen, A. P. Sandhu, B. L. Mui, C. K. Cho, D. W. Y. Sah, D. Stebbing, E. J. Crosley, E. Yaworski, I. M. Hafez, J. R. Dorkin, J. Qin, K. Lam, K. G. Rajeev, K. F. Wong, L. B. Jeffs, L. Nechev, M. L. Eisenhardt, M. Jayaraman, M. Kazem, M. A. Maier, M. Srinivasulu, M. J. Weinstein, Q. Chen, R. Alvarez, S. A. Barros, S. De, S. K. Klimuk, T. Borland, et al., *Nat. Biotechnol.* **2010**, *28*, 172; d) M. M. Billingsley, N. Singh, P. Ravikumar, R. Zhang, C. H. June, M. J. Mitchell, *Nano Lett.* **2020**, *20*, 1578; e) T. Terada, J. A. Kulkarni, A. Huynh, S. Chen, R. van der Meel, Y. Y. C. Tam, P. R. Cullis, *Langmuir* **2021**, *37*, 1120.
- [65] K. T. Love, K. P. Mahon, C. G. Levins, K. A. Whitehead, W. Querbes, J. R. Dorkin, J. Qin, W. Cantley, L. L. Qin, T. Racie, M. Frank-Kamenetsky, K. N. Yip, R. Alvarez, D. W. Y. Sah, A. de Fougères, K. Fitzgerald, V. Kotliansky, A. Akinc, R. Langer, D. G. Anderson, *Proc. Natl. Acad. Sci. USA* **2010**, *107*, 1864.
- [66] a) R. A. Petros, J. M. DeSimone, *Nat. Rev. Drug Discovery* **2010**, *9*, 615; b) T. Nakamura, M. Kawai, Y. Sato, M. Maeki, M. Tokeshi, H. Harashima, *Mol. Pharmaceutics* **2020**, *17*, 944.
- [67] S. Chen, Y. Y. C. Tam, P. J. C. Lin, M. M. H. Sung, Y. K. Tam, P. R. Cullis, *J. Controlled Release* **2016**, *235*, 236.
- [68] A. U. Andar, R. R. Hood, W. N. Vreeland, D. L. DeVoe, P. W. Swaan, *Pharm. Res.* **2014**, *31*, 401.
- [69] K. J. Hassett, J. Higgins, A. Woods, B. Levy, Y. Xia, C. J. Hsiao, E. Acosta, Ö. Almarsson, M. J. Moore, L. A. Brito, *J. Controlled Release* **2021**, *335*, 237.
- [70] D. Chen, K. T. Love, Y. Chen, A. A. Eltoukhy, C. Kastrup, G. Sahay, A. Jeon, Y. Dong, K. A. Whitehead, D. G. Anderson, *J. Am. Chem. Soc.* **2012**, *134*, 6948.
- [71] K. Ariga, *Molecules* **2021**, *26*, 1621.
- [72] a) A. Tan, L. Hong, J. D. Du, B. J. Boyd, *Adv. Sci.* **2019**, *6*, 1801223; b) M. R. Molla, P. A. Levkin, *Adv. Mater.* **2016**, *28*, 1159; c) S. Banerjee, J. Pillai, *Expert Opin. Drug Metab. Toxicol.* **2019**, *15*, 499.
- [73] A. Wagner, K. Vorauer-Uhl, G. Kreismayr, H. Katinger, *J. Liposome Res.* **2002**, *12*, 259.
- [74] a) G. M. Whitesides, *Nature* **2006**, *442*, 368; b) J. Zhang, S. Yan, D. Yuan, G. Alici, N.-T. Nguyen, M. Ebrahimi Warkiani, W. Li, *Lab Chip* **2016**, *16*, 10.
- [75] a) T. A. Duncombe, A. M. Tentori, A. E. Herr, *Nat. Rev. Mol. Cell Biol.* **2015**, *16*, 554; b) S. Damiani, U. B. Kompella, S. A. Damiani, R. Kodzius, *Genes* **2018**, *9*, 103; c) Y. Bai, M. Gao, L. Wen, C. He, Y. Chen, C. Liu, X. Fu, S. Huang, *Biotechnol. J.* **2018**, *13*, 1700170; d) L. Zhang, Q. Chen, Y. Ma, J. Sun, *ACS Appl. Bio Mater.* **2020**, *3*, 107; e) M. Maeki, N. Kimura, Y. Sato, H. Harashima, M. Tokeshi, *Adv. Drug Delivery Rev.* **2018**, *128*, 84.
- [76] a) E. C. Jensen, B. P. Bhat, R. A. Mathies, *Lab Chip* **2010**, *10*, 685; b) B. Schuster, M. Junkin, S. S. Kashaf, I. Romero-Calvo, K. Kirby, J. Matthews, C. R. Weber, A. Rzhetsky, K. P. White, S. Tay, *Nat. Commun.* **2020**, *11*, 5271.
- [77] H. Wang, K. Liu, K.-J. Chen, Y. Lu, S. Wang, W.-Y. Lin, F. Guo, K.-i. Kamei, Y.-C. Chen, M. Ohashi, M. Wang, M. A. Garcia, X.-Z. Zhao, C. K. F. Shen, H.-R. Tseng, *ACS Nano* **2010**, *4*, 6235.
- [78] Y. Kim, B. Lee Chung, M. Ma, W. J. M. Mulder, Z. A. Fayad, O. C. Farokhzad, R. Langer, *Nano Lett.* **2012**, *12*, 3587.
- [79] P. M. Valencia, E. M. Pridgen, M. Rhee, R. Langer, O. C. Farokhzad, R. Karnik, *ACS Nano* **2013**, *7*, 10671.
- [80] P. M. Valencia, O. C. Farokhzad, R. Karnik, R. Langer, *Nat. Nanotechnol.* **2012**, *7*, 623.
- [81] M. D. Buschmann, M. J. Carrasco, S. Alishetty, M. Paige, M. G. Alameh, D. Weissman, *Vaccines* **2021**, *9*, 65.
- [82] C. M. Bailey-Hytholt, P. Ghosh, J. Dugas, I. E. Zarraga, A. Bandekar, *J. Visualized Exp.* **2021**, *168*, e62226.
- [83] a) M. T. Abrams, M. L. Koser, J. Seitzer, S. C. Williams, M. A. DiPietro, W. Wang, A. W. Shaw, X. Mao, V. Jadhav, J. P. Davide, P. A. Burke, A. B. Sachs, S. M. Stirdivant, L. Sepp-Lorenzino, *Mol. Ther.* **2010**, *18*, 171; b) T. S. Zimmermann, A. C. H. Lee, A. Akinc, B. Bramlage, D. Bumcrot, M. N. Fedoruk, J. Harborth, J. A. Heyes, L. B. Jeffs, M. John, A. D. Judge, K. Lam, K. McClintock, L. V. Nechev, L. R. Palmer, T. Racie, I. Röhl, S. Seiffert, S. Shanmugam, V. Sood, J. Soutschek, I. Toudjarska, A. J. Wheat, E. Yaworski, W. Zedalis, V. Kotliansky, M. Manoharan, H.-P. Vornlocher, I. MacLachlan, *Nature* **2006**, *441*, 111.
- [84] D. Stroock Abraham, K. W. Dertinger Stephan, A. Ajdari, I. Mezić, A. Stone Howard, M. Whitesides George, *Science* **2002**, *295*, 647.
- [85] S. J. Shepherd, C. C. Warzecha, S. Yadavali, R. El-Mayta, M.-G. Alameh, L. Wang, D. Weissman, J. M. Wilson, D. Issadore, M. J. Mitchell, *Nano Lett.* **2021**, *21*, 5671.
- [86] N. M. Belliveau, J. Huft, P. J. C. Lin, S. Chen, A. K. K. Leung, T. J. Leaver, A. W. Wild, J. B. Lee, R. J. Taylor, Y. K. Tam, C. L. Hansen, P. R. Cullis, *Mol. Ther.–Nucleic Acids* **2012**, *1*, e37.
- [87] A. Jahn, W. N. Vreeland, M. Gaitan, L. E. Locascio, *J. Am. Chem. Soc.* **2004**, *126*, 2674.
- [88] C. Webb, N. Forbes, C. B. Roces, G. Anderluzzi, G. Lou, S. Abraham, L. Ingalls, K. Marshall, T. J. Leaver, J. A. Watts, J. W. Aylott, Y. Perrie, *Int. J. Pharm.* **2020**, *582*, 119266.
- [89] N. Kimura, M. Maeki, Y. Sato, Y. Note, A. Ishida, H. Tani, H. Harashima, M. Tokeshi, *ACS Omega* **2018**, *3*, 5044.
- [90] K. Amreen, S. Goel, *ECS J. Solid State Sci. Technol.* **2021**, *10*, 017002.
- [91] a) J. B. Lee, K. Zhang, Y. Y. C. Tam, Y. K. Tam, N. M. Belliveau, V. Y. C. Sung, P. J. C. Lin, E. LeBlanc, M. A. Ciufolini, P. S. Rennie, P. R. Cullis, *Int. J. Cancer* **2012**, *131*, E781; b) S. Rietwyk, D. Peer, *ACS Nano* **2017**, *11*, 7572; c) Z. Liu, S. Wang, C. Tapeinos, G. Torrieri, V. Känkänen, N. El-Sayed, A. Python, J. T. Hirvonen, H. A. Santos, *Adv. Drug Delivery Rev.* **2021**, *174*, 576; d) A. del Pozo-Rodríguez, M. Á. Solinís, A. Rodríguez-Gascón, *Eur. J. Pharm. Biopharm.* **2016**, *109*, 184.
- [92] a) D. Bumcrot, M. Manoharan, V. Kotliansky, D. W. Y. Sah, *Nat. Chem. Biol.* **2006**, *2*, 711; b) R. L. Setten, J. J. Rossi, S.-p. Han, *Nat. Rev. Drug Discovery* **2019**, *18*, 421.

- [93] a) A. Fire, S. Xu, M. K. Montgomery, S. A. Kostas, S. E. Driver, C. C. Mello, *Nature* **1998**, 391, 806; b) D. M. Dykxhoorn, D. Palliser, J. Lieberman, *Gene Ther.* **2006**, 13, 541.
- [94] D. M. Dykxhoorn, J. Lieberman, *Annu. Rev. Biomed. Eng.* **2006**, 8, 377.
- [95] J. A. Kulkarni, D. Witzigmann, S. Chen, P. R. Cullis, R. van der Meel, *Acc. Chem. Res.* **2019**, 52, 2435.
- [96] V. Kumar, J. Qin, Y. Jiang, R. G. Duncan, B. Brigham, S. Fishman, J. K. Nair, A. Akinc, S. A. Barros, P. V. Kasperkovitz, *Mol. Ther.–Nucleic Acids* **2014**, 3, e210.
- [97] C. B. Roces, G. Lou, N. Jain, S. Abraham, A. Thomas, G. W. Halbert, Y. Perrie, *Pharmaceutics* **2020**, 12, 1095.
- [98] a) L. Schoenmaker, D. Witzigmann, J. A. Kulkarni, R. Verbeke, G. Kersten, W. Jiskoot, D. J. A. Crommelin, *Int. J. Pharm.* **2021**, 601, 120586; b) M. Gaviria, B. Kilib, *Nat. Biotechnol.* **2021**, 39, 546.
- [99] a) C. Wang, Y. Zhang, Y. Dong, *Acc. Chem. Res.* **2021**, 54, 4283; b) M. Qiu, Y. Li, H. Bloomer, Q. Xu, *Acc. Chem. Res.* **2021**, 54, 4001; c) L. R. Baden, H. M. El Sahly, B. Essink, K. Kotloff, S. Frey, R. Novak, D. Diemert, S. A. Spector, N. Rouphael, C. B. Creech, J. McGettigan, S. Khetan, N. Segall, J. Solis, A. Brosz, C. Fierro, H. Schwartz, K. Neuzil, L. Corey, P. Gilbert, H. Janes, D. Follmann, M. Marovich, J. Mascola, L. Polakowski, J. Ledgerwood, B. S. Graham, H. Bennett, R. Pajon, C. Knightly, et al., *New Engl. J. Med.* **2020**, 384, 403; d) F. P. Polack, S. J. Thomas, N. Kitchin, J. Absalon, A. Gurtman, S. Lockhart, J. L. Perez, G. Pérez Marc, E. D. Moreira, C. Zerbini, R. Bailey, K. A. Swanson, S. Roychoudhury, K. Koury, P. Li, W. V. Kalina, D. Cooper, R. W. Frenck, L. L. Hammitt, Ö. Türeci, H. Nell, A. Schaefer, S. Ünal, D. B. Tresnan, S. Mather, P. R. Dormitzer, U. Şahin, K. U. Jansen, W. C. Gruber, *New Engl. J. Med.* **2020**, 383, 2603.
- [100] a) D. Adams, A. Gonzalez-Duarte, W. D. O’Riordan, C.-C. Yang, M. Ueda, A. V. Kristen, I. Tournev, H. H. Schmidt, T. Coelho, J. L. Berk, K.-P. Lin, G. Vita, S. Attarian, V. Planté-Bordeneuve, M. M. Mezei, J. M. Campistol, J. Buades, T. H. Brannagan, B. J. Kim, J. Oh, Y. Parman, Y. Sekijima, P. N. Hawkins, S. D. Solomon, M. Polydefkis, P. J. Dyck, P. J. Gandhi, S. Goyal, J. Chen, A. L. Strahs, et al., *New Engl. J. Med.* **2018**, 379, 11; b) A. Akinc, M. A. Maier, M. Manoharan, K. Fitzgerald, M. Jayaraman, S. Barros, S. Ansell, X. Du, M. J. Hope, T. D. Madden, B. L. Mui, S. C. Semple, Y. K. Tam, M. Ciufolini, D. Witzigmann, J. A. Kulkarni, R. van der Meel, P. R. Cullis, *Nat. Nanotechnol.* **2019**, 14, 1084.
- [101] M. L. Guevara, F. Persano, S. Persano, *Front. Chem.* **2020**, 8, 963.
- [102] a) R. Hoffman, L. Margolis, L. Bergelson, *FEBS Lett.* **1978**, 93, 365; b) R. Fraley, S. Subramani, P. Berg, D. Papahadjopoulos, *J. Biol. Chem.* **1980**, 255, 10431.
- [103] F. Martinon, S. Krishnan, G. Lenzen, R. Magné, E. Gomard, J. G. Guillet, J. P. Lévy, P. Meulien, *Eur. J. Immunol.* **1993**, 23, 1719.
- [104] R. Fraley, D. Papahadjopoulos, *Trends Biochem. Sci.* **1981**, 6, 77.
- [105] P. Felgner, Y. Barenholz, J. Behr, S. Cheng, P. Cullis, L. Huang, J. Jessee, L. Seymour, F. Szoka, A. Thierry, *Hum. Gene Ther.* **1997**, 8, 511.
- [106] P. L. Felgner, T. R. Gadek, M. Holm, R. Roman, H. W. Chan, M. Wenz, J. P. Northrop, G. M. Ringold, M. Danielsen, *Proc. Natl. Acad. Sci. USA* **1987**, 84, 7413.
- [107] R. W. Malone, P. L. Felgner, I. M. Verma, *Proc. Natl. Acad. Sci. USA* **1989**, 86, 6077.
- [108] U. Sahin, P. Oehm, E. Derhovanessian, R. A. Jabulowsky, M. Vormehr, M. Gold, D. Maurus, D. Schwarck-Kokarakis, A. N. Kuhn, T. Omokoko, *Nature* **2020**, 585, 107.
- [109] a) T. Wang, L. M. Larcher, L. Ma, R. N. Veedu, *Molecules* **2018**, 23, 2564; b) X. Yu, X. Liang, H. Xie, S. Kumar, N. Ravinder, J. Potter, X. de Mollerat du Jeu, J. D. Chesnut, *Biotechnol. Lett.* **2016**, 38, 919; c) A. Masotti, G. Mossa, C. Cametti, G. Ortaggi, A. Bianco, N. Del Grosso, D. Malizia, C. Esposito, *Colloids Surf., B* **2009**, 68, 136.
- [110] a) F. Barthel, J.-S. Remy, J.-P. Loeffler, J.-P. Behr, *DNA Cell Biol.* **1993**, 12, 553; b) J. H. Felgner, R. Kumar, C. Sridhar, C. J. Wheeler, Y. J. Tsai, R. Border, P. Ramsey, M. Martin, P. L. Felgner, *J. Biol. Chem.* **1994**, 269, 2550.
- [111] a) F. Ponti, M. Campolungo, C. Melchiori, N. Bono, G. Candiani, *Chem. Phys. Lipids* **2021**, 235, 105032; b) D. Zhi, S. Zhang, S. Cui, Y. Zhao, Y. Wang, D. Zhao, *Bioconjugate Chem.* **2013**, 24, 487; c) D. Zhi, Y. Bai, J. Yang, S. Cui, Y. Zhao, H. Chen, S. Zhang, *Adv. Colloid Interface Sci.* **2018**, 253, 117.
- [112] M. L. Tilkins, P. Hawley-Nelson, P. Battista, *Focus* **1994**, 16, 117.
- [113] S. Guan, J. Rosenecker, *Gene Ther.* **2017**, 24, 133.
- [114] a) E. Galanis, E. Hersh, A. Stopeck, R. Gonzalez, P. Burch, C. Spier, E. Akporiaye, J. Rinehart, J. Edmonson, R. Sobol, *J. Clin. Oncol.* **1999**, 17, 3313; b) J. Buck, P. Grossen, P. R. Cullis, J. Huwyler, D. Witzigmann, *ACS Nano* **2019**, 13, 3754.
- [115] a) J.-S. Remy, C. Sirlin, P. Vierling, J.-P. Behr, *Bioconjugate Chem.* **1994**, 5, 647; b) D. A. Balazs, W. Godbey, *J. Drug Delivery* **2011**, 2011, 326497.
- [116] a) C. Srinivasan, D. J. Burgess, *J. Controlled Release* **2009**, 136, 62; b) E. Dodds, M. Dunckley, K. Naujoks, U. Michaelis, G. Dickson, *Gene Ther.* **1998**, 5, 542; c) B. Maiti, M. Kamra, A. A. Karande, S. Bhattacharya, *Org. Biomol. Chem.* **2018**, 16, 1983; d) J. Yang, L. Huang, *Gene Ther.* **1998**, 5, 380.
- [117] N. F. Boussein, C. S. McAllister, K. K. Ewert, C. E. Samuel, C. R. Safinya, *Biochemistry* **2007**, 46, 4785.
- [118] X. Gao, L. Huang, *Biochem. Biophys. Res. Commun.* **1991**, 179, 280.
- [119] a) S. Li, X. Gao, K. Son, F. Sorgi, H. Hofland, L. Huang, *J. Controlled Release* **1996**, 39, 373; b) C. Esposito, J. Generosi, G. Mossa, A. Masotti, A. C. Castellano, *Colloids Surf., B* **2006**, 53, 187.
- [120] N. J. Zuidam, Y. Barenholz, *Biochim. Biophys. Acta, Biomembr.* **1997**, 1329, 211.
- [121] D. Pozzi, C. Marchini, F. Cardarelli, F. Salomone, S. Coppola, M. Montani, M. E. Zabaleta, M. Dignum, E. Gratton, V. Colapicchioni, *Biochim. Biophys. Acta, Biomembr.* **2014**, 1838, 957.
- [122] a) Y. Tan, L. Huang, *J. Drug Targeting* **2002**, 10, 153; b) G. J. Nabel, E. G. Nabel, Z.-Y. Yang, B. A. Fox, G. E. Plautz, X. Gao, L. Huang, S. Shu, D. Gordon, A. E. Chang, *Proc. Natl. Acad. Sci. USA* **1993**, 90, 11307.
- [123] G. Settanni, W. Brill, H. Haas, F. Schmid, *Macromol. Rapid Commun.* **2021**, 2100683.
- [124] a) D. Habrant, P. Peuziat, T. Colombani, L. Dallet, J. Gehin, E. Goudeau, B. Evrard, O. Lambert, T. Haudebourg, B. Pitard, *J. Med. Chem.* **2016**, 59, 3046; b) L. Desigaux, M. Sainlos, O. Lambert, R. Chevre, E. Letrou-Bonneval, J.-P. Vigneron, P. Lehn, J.-M. Lehn, B. Pitard, *Proc. Natl. Acad. Sci. USA* **2007**, 104, 16534.
- [125] N. Tateshita, N. Miura, H. Tanaka, T. Masuda, S. Ohtsuki, K. Tange, Y. Nakai, H. Yoshioka, H. Akita, *J. Controlled Release* **2019**, 310, 36.
- [126] S. Akhter, M. Berchel, P.-A. Jaffrès, P. Midoux, C. Pichon, *Pharmaceutics* **2022**, 14, 581.
- [127] D. P. Vangasseri, Z. Cui, W. Chen, D. A. Hokey, L. D. Falojr, L. Huang, *Mol. Membr. Biol.* **2006**, 23, 385.
- [128] Z. Du, M. M. Munye, A. D. Tagalakis, M. D. Manunta, S. L. Hart, *Sci. Rep.* **2014**, 4, 7107.
- [129] H. Farhood, N. Serbina, L. Huang, *Biochim. Biophys. Acta, Biomembr.* **1995**, 1235, 289.
- [130] D. Simberg, D. Danino, Y. Talmon, A. Minsky, M. E. Ferrari, C. J. Wheeler, Y. Barenholz, *J. Biol. Chem.* **2001**, 276, 47453.
- [131] a) Y. Liu, L. C. Mounkes, H. D. Liggitt, C. S. Brown, I. Solodin, T. D. Heath, R. J. Debs, *Nat. Biotechnol.* **1997**, 15, 167; b) B. Sternberg, K. Hong, W. Zheng, D. Papahadjopoulos, *Biochim. Biophys. Acta, Biomembr.* **1998**, 1375, 23.
- [132] D. Pozzi, C. Marchini, F. Cardarelli, H. Amenitsch, C. Garulli, A. Bifone, G. Caracciolo, *Biochim. Biophys. Acta, Biomembr.* **2012**, 1818, 2335.
- [133] L. Xu, T. J. Anchordoquy, *Biochim. Biophys. Acta, Biomembr.* **2008**, 1778, 2177.
- [134] G. Caracciolo, D. Pozzi, A. L. Capriotti, C. Cavaliere, A. Laganà, *J. Nanopart. Res.* **2013**, 15, 1498.

- [135] R. Koynova, B. Tenchov, in *Nucleic Acid Transfection*, Vol. 296 (Eds: W. Bielke, C. Erbacher), Springer, Berlin **2010**, p. 51.
- [136] J. Wang, X. Guo, Y. Xu, L. Barron, F. C. Szoka, *J. Med. Chem.* **1998**, *41*, 2207.
- [137] M. Kang, H. Kim, C. Leal, *Curr. Opin. Colloid Interface Sci.* **2016**, *26*, 58.
- [138] S. Eastman, C. Siegel, J. Tousignant, A. Smith, S. Cheng, R. Scheule, *Biochim. Biophys. Acta, Biomembr.* **1997**, *1325*, 41.
- [139] C. R. Safinya, *Curr. Opin. Struct. Biol.* **2001**, *11*, 440.
- [140] J. O. Rädler, I. Koltover, T. Salditt, C. R. Safinya, *Science* **1997**, *275*, 810.
- [141] I. Koltover, T. Salditt, J. O. Rädler, C. R. Safinya, *Science* **1998**, *281*, 78.
- [142] A. J. Lin, N. L. Slack, A. Ahmad, C. X. George, C. E. Samuel, C. R. Safinya, *Biophys. J.* **2003**, *84*, 3307.
- [143] a) K. Ewert, A. Ahmad, H. M. Evans, C. R. Safinya, *Expert Opin. Biol. Ther.* **2005**, *5*, 33; b) G. Caracciolo, D. Pozzi, R. Caminiti, A. Congiu Castellano, *Eur. Phys. J.* **2003**, *10*, 331.
- [144] B. Ma, S. Zhang, H. Jiang, B. Zhao, H. Lv, *J. Controlled Release* **2007**, *123*, 184.
- [145] a) R. Koynova, L. Wang, R. C. MacDonald, *Proc. Natl. Acad. Sci. USA* **2006**, *103*, 14373; b) R. Hulst, I. Muizebelt, P. Oosting, C. van der Pol, A. Wagenaar, J. R. Mysterová, E. Bulten, C. Driessen, D. Hoekstra, J. B. Engberts, *Eur. J. Org. Chem.* **2004**, *2004*, 835.
- [146] B. M. Bruininks, P. C. Souza, H. Ingolfsson, S. J. Marrink, *eLife* **2020**, *9*, e2012.
- [147] K. K. Ewert, H. M. Evans, A. Zidovska, N. F. Boussein, A. Ahmad, C. R. Safinya, *J. Am. Chem. Soc.* **2006**, *128*, 3998.
- [148] a) H. Kim, C. Leal, *ACS Nano* **2015**, *9*, 10214; b) H. Kim, J. Sung, Y. Chang, A. Alfeche, C. Leal, *ACS Nano* **2018**, *12*, 9196.
- [149] M. Riaz, *Pak. J. Pharm. Sci.* **1996**, *9*, 65.
- [150] J. W. Meisel, G. W. Gokel, *Sci. Rep.* **2016**, *6*, 27662.
- [151] S. Sriwongsitanont, M. Ueno, *Open Colloid Sci. J.* **2010**, *4*, 1.
- [152] S. Batzri, E. D. Korn, *Biochim. Biophys. Acta, Biomembr.* **1973**, *298*, 1015.
- [153] P. Ross, S. Hui, *Gene Ther.* **1999**, *6*, 651.
- [154] M. R. Almofti, H. Harashima, Y. Shinohara, A. Almofti, W. Li, H. Kiwada, *Mol. Membr. Biol.* **2003**, *20*, 35.
- [155] a) Y. Maitani, S. Igarashi, M. Sato, Y. Hattori, *Int. J. Pharm.* **2007**, *342*, 33; b) S. Yang, J. Chen, D. Zhao, D. Han, X. Chen, *Int. J. Pharm.* **2012**, *434*, 155; c) I. Tranchant, B. Thompson, C. Nicolazzi, N. Mignet, D. Scherman, *J. Gene Med.* **2004**, *6*, S24.
- [156] K. Krienke, L. Kolb, E. Diken, M. Streuber, S. Kirchoff, T. Bukur, Ö. Akilli-Öztürk, L. M. Kranz, H. Berger, J. Petschenka, *Science* **2021**, *371*, 145.
- [157] a) V. Pector, J. Backmann, D. Maes, M. Vandenbranden, J.-M. Ruyschaert, *J. Biol. Chem.* **2000**, *275*, 29533; b) E. Pozharski, R. C. MacDonald, *Biophys. J.* **2003**, *85*, 3969.
- [158] S. Even-Chen, R. Cohen, Y. Barenholz, *Chem. Phys. Lipids* **2012**, *165*, 414.
- [159] J. Kim, J. Y. Kim, H. Kim, E. Kim, S. Park, K.-H. Ryu, E. G. Lee, *Int. J. Mol. Sci.* **2021**, *22*, 12344.
- [160] O. Zelphati, C. Nguyen, M. Ferrari, J. Felgner, Y. Tsai, P. Felgner, *Gene Ther.* **1998**, *5*, 1272.
- [161] M. T. Kennedy, E. V. Pozharski, V. A. Rakhmanova, R. C. MacDonald, *Biophys. J.* **2000**, *78*, 1620.
- [162] L. Wasungu, D. Hoekstra, *J. Controlled Release* **2006**, *116*, 255.
- [163] J. M. Barichello, T. Ishida, H. Kiwada, in *Liposomes: Methods and Protocols* (Ed: V. Weissig), Springer, Berlin **2010**, p. 461.
- [164] a) T. A. Balbino, N. T. Aoki, A. A. Gasperini, C. L. Oliveira, A. R. Azzoni, L. P. Cavalcanti, G. Lucimara, *Chem. Eng. J.* **2013**, *226*, 423; b) T. A. Balbino, A. R. Azzoni, L. G. de La Torre, *Colloids Surf., B* **2013**, *111*, 203; c) X. Liu, B. Bahloul, R. L. Kuen, K. Andrieux, C. Roques, D. Scherman, *Int. J. Pharm.* **2021**, *605*, 120772.
- [165] a) D. Llères, J. M. Weibel, D. Heissler, G. Zuber, G. Duportail, Y. Mély, *J. Gene Med.* **2004**, *6*, 415; b) T. A. Balbino, J. M. Serafin, A. A. Malfatti-Gasperini, C. L. de Oliveira, L. P. Cavalcanti, M. B. de Jesus, L. G. de La Torre, *Langmuir* **2016**, *32*, 1799; c) A. T.-H. Hsieh, N. Hori, R. Massoudi, P. J.-H. Pan, H. Sasaki, Y. A. Lin, A. P. Lee, *Lab Chip* **2009**, *9*, 2638.
- [166] V. Escriou, C. Ciolina, F. Lacroix, G. Byk, D. Scherman, P. Wils, *Biochim. Biophys. Acta, Biomembr.* **1998**, *1368*, 276.
- [167] P. Forozaandeh, A. A. Aziz, *Nanoscale Res. Lett.* **2018**, *13*, 339.
- [168] a) S. Grabbe, H. Haas, M. Diken, L. M. Kranz, P. Langguth, U. Sahin, *Nanomedicine* **2016**, *11*, 2723; b) J. C. Birchall, I. W. Kellaway, S. N. Mills, *Int. J. Pharm.* **1999**, *183*, 195.
- [169] L. M. Kranz, M. Diken, H. Haas, S. Kreiter, C. Loquai, K. C. Reuter, M. Meng, D. Fritz, F. Vascotto, H. Hefesha, *Nature* **2016**, *534*, 396.
- [170] a) A. Peletta, E. Prompetchara, K. Tharakhet, P. Kaewpang, S. Buranapraditkun, T. Techawiwattanaboon, T. Jbilou, P. Krangvichian, S. Sirivichayakul, S. Manopwisedjaroen, *Vaccines* **2021**, *9*, 874; b) Z. Heidari, J. S. Arora, D. Datta, V. T. John, N. Kumar, G. P. Bansal, *Pharm. Res.* **2017**, *34*, 1796.
- [171] Q. Cheng, T. Wei, L. Farbiak, L. T. Johnson, S. A. Dilliard, D. J. Siegwart, *Nat. Nanotechnol.* **2020**, *15*, 313.
- [172] A. K. Blakney, P. F. McKay, B. I. Yus, Y. Aldon, R. J. Shattock, *Gene Ther.* **2019**, *26*, 363.
- [173] T. A. Balbino, J. M. Serafin, A. Radaic, M. B. de Jesus, G. Lucimara, *Colloids Surf., B* **2017**, *152*, 406.
- [174] D. Simberg, S. Weisman, Y. Talmon, A. Faerman, T. Shoshani, Y. Barenholz, *J. Biol. Chem.* **2003**, *278*, 39858.
- [175] W.-Z. Zhou, D. Hoon, S. Huang, S. Fujii, K. Hashimoto, R. Morishita, Y. Kaneda, *Hum. Gene Ther.* **1999**, *10*, 2719.
- [176] A. De Beuckelaer, C. Pollard, S. Van Lint, K. Roose, L. Van Hoecke, T. Naessens, V. K. Udhayakumar, M. Smet, N. Sanders, S. Lienenklaus, *Mol. Ther.* **2016**, *24*, 2012.
- [177] K. Okumura, M. Nakase, M. Inui, S. Nakamura, Y. Watanabe, T. Tagawa, *J. Gene Med.* **2008**, *10*, 910.
- [178] L. Van Hoecke, K. Roose, M. Ballegeer, Z. Zhong, N. N. Sanders, S. De Koker, X. Saelens, S. Van Lint, *Mol. Ther.– Nucleic Acids* **2020**, *22*, 373.
- [179] W. De Haes, J. Rejman, C. Pollard, C. Merlin, M. Vekemans, E. Florence, S. C. De Smedt, J. Grooten, G. Vanham, S. De Koker, *Nanomedicine* **2013**, *8*, 77.
- [180] C. Pollard, J. Rejman, W. De Haes, B. Verrier, E. Van Gulck, T. Naessens, S. De Smedt, P. Bogaert, J. Grooten, G. Vanham, *Mol. Ther.* **2013**, *21*, 251.
- [181] D. Christensen, K. S. Korsholm, I. Rosenkrands, T. Lindström, P. Andersen, E. M. Agger, *Expert Rev. Vaccines* **2007**, *6*, 785.
- [182] T. R. Smith, A. Patel, S. Ramos, D. Elwood, X. Zhu, J. Yan, E. N. Gary, S. N. Walker, K. Schultheis, M. Purwar, Z. Xu, J. Walters, P. Bhojnagarwala, M. Yang, N. Chokkalingam, P. Pezzoli, E. Parzych, E. L. Reuschel, A. Doan, N. Tursi, M. Vasquez, J. Choi, E. Tello-Ruiz, I. Maricic, M. A. Bah, Y. Wu, D. Amante, D. H. Park, Y. Dia, A. R. Ali, et al., *Nat. Commun.* **2020**, *11*, 2601.
- [183] D. J. Crommelin, T. J. Anchordoquy, D. B. Volkin, W. Jiskoot, E. Mastrobattista, *J. Pharm. Sci.* **2021**, *110*, 997.
- [184] K. Kubota, K. Onishi, K. Sawaki, T. Li, K. Mitsuoka, T. Sato, S. Takeoka, *Int. J. Nanomed.* **2017**, *12*, 5121.
- [185] A. K. Blakney, P. Deletic, P. F. McKay, C. R. Bouton, M. Ashford, R. J. Shattock, A. Sabirsh, *J. Controlled Release* **2021**, *330*, 1250.
- [186] A. A. De Angelis, S. J. Opella, *Nat. Protoc.* **2007**, *2*, 2332.
- [187] L. Lin, X. Wang, Y. Guo, K. Ren, X. Li, L. Jing, X. Yue, Q. Zhang, Z. Dai, *RSC Adv.* **2016**, *6*, 79811.
- [188] T. N. Sut, E. R. Valle-González, B. K. Yoon, S. Park, J. A. Jackman, N.-J. Cho, *Appl. Mater. Today* **2021**, *22*, 100947.
- [189] a) K. Kolahdouzan, J. A. Jackman, B. K. Yoon, M. C. Kim, M. S. Johal, N.-J. Cho, *Langmuir* **2017**, *33*, 5052; b) J. A. Jackman, N.-J. Cho, *Langmuir* **2020**, *36*, 1387.
- [190] E. J. Dufourc, *Biochim. Biophys. Acta, Biomembr.* **2021**, *1863*, 183478.

- [191] a) N. E. Gabriel, M. F. Roberts, *Biochemistry* **1984**, *23*, 4011; b) C. R. Sanders, G. C. Landis, *Biochemistry* **1995**, *34*, 4030; c) R. R. Vold, R. S. Prosser, *J. Magn. Reson.* **1996**, *113*, 267.
- [192] C. R. Sanders, J. P. Schwonek, *Biochemistry* **1992**, *31*, 8898.
- [193] T. A. Harroun, M. Koslowsky, M.-P. Nieh, C.-F. de Lannoy, V. Raghunathan, J. Katsaras, *Langmuir* **2005**, *21*, 5356.
- [194] U. H. Dürr, R. Soong, A. Ramamoorthy, *Prog. Nucl. Magn. Reson. Spectrosc.* **2013**, *69*, 1.
- [195] a) N. L. Yamada, M. Hishida, N. Torikai, *Phys. Rev. E* **2009**, *79*, 032902; b) U. H. Dürr, M. Gildenberg, A. Ramamoorthy, *Chem. Rev.* **2012**, *112*, 6054.
- [196] S. Ghosh, A. Ray, N. Pramanik, *Biophys. Chem.* **2020**, *265*, 106429.
- [197] C.-H. Yang, T.-L. Lin, U.-S. Jeng, *Langmuir* **2019**, *35*, 9483.
- [198] L. van Dam, G. Karlsson, K. Edwards, *Biochim. Biophys. Acta, Biomembr.* **2004**, *1664*, 241.
- [199] H. S. Cho, J. L. Dominick, M. M. Spence, *J. Phys. Chem. B* **2010**, *114*, 9238.
- [200] M. N. Triba, P. F. Devaux, D. E. Warschawski, *Biophys. J.* **2006**, *91*, 1357.
- [201] M. Li, W. T. Heller, C.-H. Liu, C. Y. Gao, Y. Cai, Y. Hou, M.-P. Nieh, *Biochim. Biophys. Acta, Biomembr.* **2020**, *1862*, 183315.
- [202] J. Struppe, J. A. Whiles, R. R. Vold, *Biophys. J.* **2000**, *78*, 281.
- [203] Y. Liu, M. Li, Y. Yang, Y. Xia, M.-P. Nieh, *Biochim. Biophys. Acta, Biomembr.* **2014**, *1838*, 1871.
- [204] Z. Shen, H. Ye, M. Kröger, S. Tang, Y. Li, *Nanoscale* **2019**, *11*, 15971.
- [205] a) W. Aresh, Y. Liu, J. Sine, D. Thayer, A. Puri, Y. Huang, Y. Wang, M.-P. Nieh, *J. Biomed. Nanotechnol.* **2016**, *12*, 1852; b) X. Wang, L. Lin, R. Liu, M. Chen, B. Chen, B. He, B. He, X. Liang, W. Dai, H. Zhang, *Adv. Funct. Mater.* **2017**, *27*, 1700406.
- [206] K. Yasuhara, S. Miki, H. Nakazono, A. Ohta, J.-i. Kikuchi, *Chem. Commun.* **2011**, *47*, 4691.
- [207] K. Yasuhara, H. Hayashi, J.-i. Kikuchi, *Chem. Lett.* **2012**, *41*, 1223.
- [208] L. Lin, X. Wang, X. Li, Y. Yang, X. Yue, Q. Zhang, Z. Dai, *Bioconjugate Chem.* **2017**, *28*, 53.
- [209] P.-W. Yang, T.-L. Lin, T.-Y. Lin, C.-H. Yang, Y. Hu, U.-S. Jeng, *Soft Matter* **2013**, *9*, 11542.
- [210] P.-W. Yang, T.-L. Lin, Y. Hu, U.-S. Jeng, *Soft Matter* **2014**, *10*, 2313.
- [211] A. T. Rad, S. Malik, L. Yang, T. K. Oberoi-Khanuja, M.-P. Nieh, R. Bahal, *Nanoscale* **2019**, *11*, 12517.
- [212] C. Janich, C. Wölk, S. Taßler, S. Drescher, A. Meister, G. Brezesinski, B. Dobner, A. Langner, *Eur. J. Lipid Sci. Technol.* **2014**, *116*, 1184.
- [213] C. Janich, S. Taßler, A. Meister, G. Hause, J. Schäfer, U. Bakowsky, G. Brezesinski, C. Wölk, *Soft Matter* **2016**, *12*, 5854.
- [214] C. Wölk, C. Janich, A. Meister, S. Drescher, A. Langner, G. Brezesinski, U. Bakowsky, *Bioconjugate Chem.* **2015**, *26*, 2461.
- [215] C. Wölk, C. Janich, D. Pawlowska, S. Drescher, A. Meister, G. Hause, B. Dobner, A. Langner, G. Brezesinski, *ChemPhysChem* **2015**, *16*, 2115.
- [216] Q. Chen, G. Guan, F. Deng, D. Yang, P. Wu, S. Kang, R. Sun, X. Wang, D. Zhou, W. Dai, *Biomaterials* **2020**, *251*, 120008.
- [217] H. Zhang, in *Liposomes: Methods and Protocols* (Ed: V. Weissig), Springer, Berlin **2017**, p. 17.
- [218] Y. Watanabe, K. Aramaki, Y. Kadomatsu, K. Tanaka, Y. Konno, *Chem. Lett.* **2016**, *45*, 558.
- [219] I. K. Mkam Tsengam, M. Omarova, E. G. Kelley, A. McCormick, G. D. Bothun, S. R. Raghavan, V. T. John, *J. Phys. Chem. B* **2022**, *126*, 2208.
- [220] K. Aramaki, C. Iwata, J. Mata, T. Maehara, D. Aburano, Y. Sakanishi, K. Kitao, *Phys. Chem. Chem. Phys.* **2017**, *19*, 23802.
- [221] K. Aramaki, K. Adachi, M. Maeda, J. Mata, J. Kamimoto-Kuroki, D. Tsukamoto, Y. Konno, *Materials* **2020**, *13*, 3066.
- [222] J. Kamimoto-Kuroki, M. Yamashita, K. Tanaka, Y. Kadomatsu, D. Tsukamoto, K. Aramaki, K. Adachi, Y. Konno, *Colloids Surf., A* **2020**, *606*, 125418.
- [223] S. Choi, B. Kang, S. Taguchi, H. Umakoshi, K. Kim, M. K. Kwak, H.-S. Jung, *Langmuir* **2021**, *37*, 12255.
- [224] S. Taguchi, K. Suga, K. Hayashi, Y. Okamoto, H.-S. Jung, H. Nakamura, H. Umakoshi, *Colloids Interfaces* **2018**, *2*, 73.
- [225] S. Choi, B. Kang, T. Shimanouchi, K. Kim, H. Jung, *Micro Nano Syst. Lett.* **2021**, *9*, 7.
- [226] H. A. Benson, *Curr. Drug Delivery* **2005**, *2*, 23.
- [227] L. Barbosa-Barros, C. Barba, M. Cócera, L. Coderch, C. López-Iglesias, A. de la Maza, O. López, *Int. J. Pharm.* **2008**, *352*, 263.
- [228] L. Barbosa-Barros, A. De La Maza, J. Estelrich, A. Linares, M. Feliz, P. Walther, R. Pons, O. López, *Langmuir* **2008**, *24*, 5700.
- [229] a) G. Rodríguez, L. Barbosa-Barros, L. Rubio, M. Cocera, A. Diez, J. Estelrich, R. Pons, J. Caelles, A. D. I. Maza, O. Lopez, *Langmuir* **2009**, *25*, 10595; b) G. Rodríguez, L. Rubio, M. Cócera, J. Estelrich, R. Pons, A. de la Maza, O. López, *Langmuir* **2010**, *26*, 10578.
- [230] G. Rodríguez, M. Cócera, L. Rubio, C. Alonso, R. Pons, C. Sandt, P. Dumas, C. López-Iglesias, A. de la Maza, O. López, *Phys. Chem. Chem. Phys.* **2012**, *14*, 14523.
- [231] L. Barbosa-Barros, G. Rodríguez, C. Barba, M. Cócera, L. Rubio, J. Estelrich, C. López-Iglesias, A. de la Maza, O. López, *Small* **2012**, *8*, 807.
- [232] a) G. Rodríguez, M. Cocera, L. Rubio, C. Lopez-Iglesias, R. Pons, A. de la Maza, O. López, *Mol. Pharmaceutics* **2012**, *9*, 482; b) G. Rodríguez, L. Rubio, C. Barba, C. López-Iglesias, A. de la Maza, O. López, M. Cócera, *Eur. Biophys. J.* **2013**, *42*, 333.
- [233] L. Rubio, C. Alonso, G. Rodríguez, L. Barbosa-Barros, L. Coderch, A. De la Maza, J. Parra, O. López, *Int. J. Pharm.* **2010**, *386*, 108.
- [234] L. Rubio, C. Alonso, G. Rodríguez, M. Cócera, C. López-Iglesias, L. Coderch, A. De la Maza, J. Parra, O. López, *Int. J. Pharm.* **2013**, *444*, 60.
- [235] L. Rubio, G. Rodríguez, C. Alonso, C. Lopez-Iglesias, M. Cocera, L. Coderch, A. De la Maza, J. Parra, O. Lopez, *Soft Matter* **2011**, *7*, 8488.
- [236] L. Rubio, C. Alonso, G. Rodríguez, M. Cócera, L. Barbosa-Barros, L. Coderch, A. de la Maza, J. Parra, O. López, *Eur. J. Pharm. Biopharm.* **2014**, *86*, 212.
- [237] a) G. Rodríguez, L. Barbosa-Barros, L. Rubio, M. Cócera, F. Fernández-Campos, A. Calpena, E. Fernández, A. De La Maza, O. López, *J. Biomed. Nanotechnol.* **2015**, *11*, 282; b) M. S. Kapoor, S. GuhaSarkar, R. Banerjee, *Ther. Delivery* **2017**, *8*, 701.
- [238] V. Moner, E. Fernández, A. Del Pozo, G. Rodríguez, M. Cócera, A. de la Maza, O. López, *Contact Dermatitis* **2017**, *77*, 25.
- [239] G. Anderluzzi, G. Lou, S. Woods, S. T. Schmidt, S. Gallorini, M. Brazzoli, R. Johnson, C. W. Roberts, D. T. O'Hagan, B. C. Baudner, *J. Controlled Release* **2022**, *342*, 388.
- [240] W. Zhang, J. Sun, Y. Liu, M. Tao, X. Ai, X. Su, C. Cai, Y. Tang, Z. Feng, X. Yan, *Mol. Pharmaceutics* **2014**, *11*, 3279.
- [241] A. T. Rad, D. Hargrove, L. Daneshmandi, A. Ramsdell, X. Lu, M.-P. Nieh, *Adv. NanoBiomed Res.* **2022**, *2*, 2100080.
- [242] J. Gao, C. Xie, M. Zhang, X. Wei, Z. Yan, Y. Ren, M. Ying, W. Lu, *Nanoscale* **2016**, *8*, 7209.
- [243] P. E. Saw, M. Yu, M. Choi, E. Lee, S. Jon, O. C. Farokhzad, *Biomaterials* **2017**, *123*, 118.
- [244] V. M. Steffes, Z. Zhang, S. MacDonald, J. Crowe, K. K. Ewert, B. Carragher, C. S. Potter, C. R. Safinya, *ACS Appl. Mater. Interfaces* **2019**, *12*, 151.
- [245] L. Lin, X. Liang, Y. Xu, Y. Yang, X. Li, Z. Dai, *Bioconjugate Chem.* **2017**, *28*, 2410.
- [246] S. Hameed, P. Bhattarai, Z. Dai, *Front. Chem.* **2018**, *6*, 127.
- [247] J. D. Finn, A. R. Smith, M. C. Patel, L. Shaw, M. R. Youniss, J. van Heteren, T. Dirstine, C. Ciullo, R. Lescarbeau, J. Seitzer, R. R. Shah, A. Shah, D. Ling, J. Growe, M. Pink, E. Rohde, K. M. Wood, W. E. Salomon, W. F. Harrington, C. Dombrowski, W. R. Strapps, Y. Chang, D. V. Morrissey, *Cell Rep.* **2018**, *22*, 2227.



**Abdul Rahim Ferhan**, Ph.D. is a research fellow in the Translational Materials Innovation Group in the School of Materials Science and Engineering at Nanyang Technological University. He received his B.Eng. degree in Chemical and Biomolecular Engineering and Ph.D. degree in Biomedical Engineering from the School of Chemical and Biomedical Engineering at Nanyang Technological University. His research focuses on lipid membrane interactions and the incorporation of lipid membrane models within novel nanoplasmonic sensing platforms for fundamental investigations into biomacromolecular interaction processes.



**Soohyun Park**, Ph.D. is a research fellow in the School of Materials Science and Engineering, Nanyang Technological University. She earned her B.S. in Biomaterials Engineering from Seoul National University in 2016 and Ph.D. in Materials Science and Engineering from Nanyang Technological University in 2021. Her research interests include lipid membrane-targeting antiviral peptides, lipid nanoparticles, model lipid membranes, and biomaterials.



**Joshua A. Jackman**, Ph.D. is an assistant professor in the School of Chemical Engineering and Director of the Translational Nanobioscience Research Center at Sungkyunkwan University. He earned his B.S. degree in Chemistry from the University of Florida in 2010 and his Ph.D. degree in Materials Science and Engineering from Nanyang Technological University in 2015, and completed postdoctoral studies at the Stanford University School of Medicine. His research focuses on lipid membrane biotechnology, membrane biophysics, and the development of membrane-targeting strategies for infectious disease and cancer applications.



**Nam-Joon Cho**, Ph.D. is the MRS-Singapore Chair Professor in the School of Materials Science and Engineering at Nanyang Technological University. He earned his B.S. degree in Civil Engineering from the University of California, Berkeley in 1996 and his M.S. degree in Materials Science and Engineering and Ph.D. degree in Chemical Engineering from Stanford University in 2003 and 2007, respectively, and completed postdoctoral studies at the Stanford University School of Medicine. His research focuses on biomaterial strategies to develop new classes of anti-infective drugs, to engineer advanced lipid nanoparticle technology, and to create natural materials to replace plastics.